## ABSTRACT

TILLY, JOSEPH. Thermal and Photo-initiated Crosslinking of Network Polymers and Their Ultimate Film Properties (Under the direction of Dr. Saad A. Khan and Dr. Richard J. Spontak).

Network polymers are an interesting and diverse class of materials that have found applications in a number of different areas, from coatings to optical materials to bulky structural parts. These materials are typically formed through a process known as crosslinking, whereby at least one species within the material is able to interact with the other species (or itself) to form a three-dimensional network structure. This crosslinking process is typically initiated by exposure to heat or another type of radiation, such as ultraviolet radiation. Crosslinks can be reversible, although they are often irreversible. These systems can be filled or unfilled, and the ultimate properties of the network depend on the physical and chemical properties of the starting materials. The vast library of available chemical species from which network polymers can be formed allows for numerous potential applications of this class of materials, and understanding the aspects of network formation and ultimate network properties of a network is important when designing and considering a material for a specific application. Herein, we examine two different classes of materials; a thermosetting system with varied polymer backbone chemistry and its role on crosslinking and ultimate film thermomechanical properties, and a UV-crosslinkable system with and without fillers, in which we probe the effect of filler type and loading on the evolution of a network microstructure and some of the resulting film properties of the nanocomposite network.

Dynamic rheology and variable temperature Fourier-transform infrared spectroscopy are employed in order to elucidate the role of secondary hydroxyl content on the crosslinking behavior of a series of polyester polyol resins reacting with a polymerized aliphatic isocyanate in the presence of a tin catalyst and solvent at four different temperatures. We find that increasing

the level of secondary hydroxyl content not only increases the time required to achieve a crossover in the dynamic moduli, or the sol-gel transition, but it also increases the degree of chemical conversion required to achieve this transition. The apparent activation energies of gelation and average kinetic activation energies up to the crossover are in good agreement, confirming that the crosslinking reaction is indeed playing a critical role in microstructure evolution. The critical extents of conversion are compared with classical theories and are found to deviate substantially at high contents of secondary hydroxyls. A qualitative model is proposed which agrees with findings previously reported in the literature.

The same systems are then cured at two temperatures relevant to the automotive coatings industry and a suite of characterization techniques are utilized to determine the effect of polyester backbone composition on the films' ultimate thermomechanical and free volume properties. We find that the glass transition temperatures can be tailored by changing the diol content of the polyesters, along with the bulk and surface mechanical properties. Nanoindentation experiments show a strong dependence on backbone chemistry and cure condition on surface mechanical properties, and a phenomenon known as "pile-up" is observed. The sub-nanometer free volume of these films is also explored and is found to increase by ~9% as the chemical makeup of the polyester backbone is altered.

Finally, the UV-crosslinking behavior and ultimate film properties of a low molecular weight poly(dimethyl siloxane) with and without reactive and passive zirconia nanoparticle fillers is examined as a function of filler type and loading, as well as UV irradiation strength. We find that increasing filler content up to 85 wt% of solids increases the time required to achieve the sol-gel transition, and the type and loading of filler alters the ultimate film optical properties.

# Thermal and Photo-initiated Crosslinking of Network Polymers and Their Ultimate Film Properties

by
Joseph Tilly

A dissertation submitted to the Graduate Faculty of
North Carolina State University
in partial fulfillment of the
requirements for the degree of
Doctor of Philosophy

Chemical Engineering

Raleigh, North Carolina
2019

APPROVED BY:

| | |
|---|---|
| _____ | _____ |
| Dr. Saad A. Khan<br>Committee Co-chair | Dr. Richard J. Spontak<br>Committee Co-chair |
| _____ | _____ |
| Dr. Jan Genzer | Dr. Russell E. Gorga |
| _____ | |
| Dr. Erik E. Santiso | |

## DEDICATION

*I dedicate this dissertation to my parents, Jean and John Tilly, without whom I would not be where I am today. They have always been incredibly supportive of my personal and professional aspirations, and have taught me strength and to persevere. The curiosity that they have instilled in me has led me to become the person that I am today, and they constantly inspire me to be the best that I can be. I also dedicate this dissertation to my wife, Dr. Deepti Srivastava Tilly, who has stood by me, fostered my sense of adventure and pushed me to always be better. Her friendship and her support has been instrumental in shaping the person that I am today.*

*I am eternally grateful to them.*

## BIOGRAPHY

Joseph Tilly was born in Portsmouth, NH to his parents, John and Jean Tilly. He is the first of three sons, succeeded by his brothers John and Michael. He spent his first five years in Portsmouth, NH, where he enjoyed watching trains and learning about dinosaurs. Just before age 6, his family moved to Dudley, MA where Joseph attended the public schools. It was here that he first developed a love for math and science. Joseph attended high school at Shepherd Hill Regional High School, where his favorite classes were AP Chemistry with Ms. Lippold and AP Calculus with Mrs. Leach. From these two classes, Joseph learned that his passions would lead him to the discipline of chemical engineering.

In 2010, Joseph attended the University of Massachusetts Amherst for his undergraduate chemical engineering education. He was fortunate enough to study abroad in Wollongong, Australia, during his third semester there. Upon returning, Joseph completed his undergraduate chemical engineering degree. During his third summer and into his senior year, Joseph undertook an internship with Eastman Chemical Company (formerly Solutia), and it was here that Joseph realized his passion for research. During his senior year, he worked in the lab of Dr. Jonathan Rothstein in the Mechanical Engineering Department at UMass, studying the rheology of micelle solutions.

August 2014 marked the beginning of Joseph's graduate career at North Carolina State University in pursuit of a Ph.D. in chemical and biomolecular engineering. After his first semester he joined the research groups of Drs. Saad Khan and Richard Spontak, and he is eternally grateful to both of his advisors for the guidance that he received and their support of his professional goals. In the summer after his third year of graduate school, Joseph was given the opportunity to undertake an internship with Eastman Chemical Company under the direction of

Dr. Geoffrey Webster in Kingsport, TN, where he further honed his research skills with Dr. Webster's guidance and support.

In graduate school Joseph met his wife, Dr. Deepti Srivastava Tilly, a fellow Ph.D. student at NC State, and her Labrador dog, Ace the Bat Hound. Joseph enjoys playing a variety of sports and traveling in his spare time.

## ACKNOWLEDGMENTS

First and foremost, I would like to thank my advisors, Dr. Saad Khan and Dr. Richard Spontak, for supporting me financially over these past five years and for the helpful guidance that they provided along the way. I am grateful to you both for letting me explore research areas tangential to my main projects and for encouraging me to experience new things, whether that was the A2i Industry Immersion Week or a summer internship at Eastman Chemical Company. I want to thank you both for all of the great brainstorming meetings, and for all of your tireless efforts that have gone into helping prepare me to write and defend this dissertation. Words cannot express my gratitude. I would also like to thank the various members of their respective research groups over the years, and for the guidance, assistance and camaraderie that you all offered. I am truly lucky to have been a member of these two research groups.

I would also like to thank my committee members. Dr. Genzer, I am thankful for the time that you have taken out these past five years to not only help me figure out how to approach several different research problems, but also to talk hockey and life in general. Dr. Gorga, I really appreciate the guidance with DMA that you have been able to provide over the course of this work, and for taking the time to sit on my Ph.D. committee. Dr. Santiso, I have enjoyed our time working together and I am very grateful for all of the ideas and guidance you have been able to provide on the Polyol Project.

I would like to acknowledge the Eastman Chemical Company Center of Excellence for funding much of this work, and the friendly, knowledgeable and helpful staff there for all of their guidance and support with the different projects. I would specifically like to acknowledge Dr. Andrew Detwiler at Eastman Chemical Company for helping steward the work presented in the

first two chapters, as well as Dr. Geoffrey Webster for serving as an exceptional mentor during my internship.

Finally, I would like to thank my parents, Jean and John Tilly; my brothers, Pat and Mike Tilly; and my loving wife, Dr. Deepti Srivastava Tilly. The words on this page cannot do justice to how grateful I am for all you, and for your love and support. Deepti, thank you for being my rock when I struggled, and for reminding me to not take life too seriously. Thank you for putting up with the late nights in lab for weeks on end, and for pushing me to be my best self.

## TABLE OF CONTENTS

## LIST OF TABLES

## LIST OF FIGURES

# CHAPTER 1: INTRODUCTION

## 1.1. Fundamentals of Polymers

The term "polymer" refers to a large molecule consisting of many repeat units, or monomers, in a chain. These repeat units can all be the same, creating homopolymers, or can be a mixture of different constituents, creating copolymers. Copolymers can have the various substituents randomly distributed along the backbone, they can blocky (i.e. different statistical compositions at different points along the backbone), or they can have more complex architectures, such as grafted, dendritic or star polymers. Post-polymerization, these materials have vastly different properties from their monomeric constituents, opening up a host of new potential applications. These polymers can be crystalline, semi-crystalline or amorphous, and each type of polymer has unique properties that make it suited for different applications.

Polymers are ubiquitous in our everyday lives, from rubber to paint to grocery bags, and are also present in nature, such as cellulose in biomass. These types of materials also find uses within more advanced stimuli-responsive applications, such as sensing[1] and electroactive materials[2].

Synthetic polymers are a subset of polymers that are deliberately created, and have wide-ranging properties that are dependent upon the chemistry of the monomers and the size and architecture of the chains. Synthetic polymers can be further subdivided into two categories; thermoplastics and thermosets, or more generally network polymers. Thermoplastics are polymers that can be re-shaped by heating above their melting point or glass transition temperature, whereas thermosets are irreversibly cross-linked to form an infusible polymer network. As a more general rule, network polymers can be formed with reversible crosslinks,[3] however these are beyond the scope of this dissertation. Both thermoplastic and network polymers have a plethora of uses; for instance, thermoplastics are often used in bulky parts and

membranes, and network polymers often find uses in applications such as coatings, where a dense network structure is required for mechanical integrity and barrier properties. Some network polymers, such as poly(dimethylsiloxane) also find applications in materials known as elastomers, which are able to achieve very high strains and regain their original microstructure upon return to an unstrained state.

The properties of polymers may be altered or enhanced by introducing additional species into the network. Previous works have looked at the effect of high-modulus fillers in polymer systems.[4] These fillers can be carbonaceous nanomaterials,[5] organic nanomaterials such as nanocellulose,[6] or inorganic molecules or nano/microstructures.[7] There is also significant previous work investigating larger-scale fillers, such as glass fibers, in polymeric matrices for enhanced mechanical performance.[8] By including fillers in a polymeric system, it is possible to enhance the material's thermal, barrier or mechanical properties or even introduce new functionality into the system. The compatibility of the filler with the polymer matrix, as well as its dispersion throughout the matrix, both play an important role in how the composite material functions.[9] The architecture of the polymer (length of chain, thermoplastic vs. network) can also play a role in how well the material is incorporated within the system. The discussions contained within this dissertation will focus primarily on network polymers, with and without fillers.

### 1.2. Network Polymers – Synthesis and Applications

Under the proper reaction conditions, monomers and polymers can both undergo network formation via crosslinking reaction. Most crosslinking reactions require at least one multi-functional species ($n > 2$), sometimes referred to as a crosslinking agent, in order to achieve a percolated three-dimensional network structure. These cross-linking reactions have been heavily studied in the past, both experimentally and computationally, for reactive systems containing a

number of different functionalities and average degrees of functionality.[10–14] Crosslinking reactions can be achieved in a few different ways: they can be thermally-induced (via addition of heat, i.e. epoxides or alcohol-isocyanate reactions)[15], or they can be induced by some sort of radiation, such as ultraviolet radiation (i.e. thiol-ene "click" chemistry or acrylates).[16,17] Many of these reactions require a catalyst of sorts, or in the case of UV-crosslinking a photoinitiator to accelerate the reaction process. These catalysts can take many different forms, although two common catalysts are dibutyltin dilaurate for the thermally crosslinked isocyanate-alcohol reaction[18], and 2,2-dimethoxy-2-phenylacetophenone. (DMPA), for UV radiation-induced crosslinking[19]. Of course there are other "catalyst" choices for different chemistries, however these are the two that are utilized extensively throughout this body of work.

Network polymers find applications in a number of different areas, from coatings[20,21] and elastomeric parts[22] to adhesives[23] and optical devices[24]. Recently, network polymers have garnered significant research interests in 3D printing[25], self-healing materials[26] and biomedical applications.[27] What makes this class of materials attractive for these applications is their infusible network, ability to be swollen in solvent and their highly tailorable physical and chemical properties based on materials selection. For instance, epoxy-based networks tend to form materials with good protective properties and find uses in coatings applications, but tend to have far too high moduli to be used in soft robotics.[28] Poly(dimethyl siloxane)-based networks, on the other hand, tend to be softer and have excellent oxygen permeability which makes them good candidates for materials such as soft contact lenses, but not necessarily for protective coatings, where a high modulus is desired.[29]

The diversity in polymer network building blocks brings us to an important point: it is imperative that materials be designed specifically for the application in which they are intended

for use. It does not make sense using a soft, rubbery material as a protective coating for the body of a car that must endure physical abrasion, and it does not make sense to design a soft robot based upon a material that is too rigid for deformation under minor stressors that are favorable to soft robotics applications. When designing a material for an end-use application, it is important to not only consider the final properties of the material, but also how the material achieves its final form. In the following section, a few different techniques for monitoring cross-linking will be described in the next section, as well as some popular techniques used to interrogate the final properties of a polymer network.

## 1.3. Characterizing Polymeric Systems

### *1.3.1. Crosslinking Behavior – Theory and Experiment*

A number of theories exist which seek to describe polymer network formation, or gelation, in systems involving at least one species with an average functionality of n > 2. The first of these theories to gain popularity originated with Carothers' description of stoichiometrically balanced condensation polymers.[30] This work defined the extent of conversion *p* as 1/(1-x), where x is the degree of polymerization. In order to pinpoint the extent of conversion required to achieve a polymer of infinite molecular weight (gelation), the expression for p becomes 2/*f*, where *f* is the average functionality of the system. For systems containing only bifunctional reactants, the extent of conversion where the molecular weight would become infinite is 1, which is not physically possible to achieve; therefore, gelation will not occur within a system containing only bifunctional reactants. As the average functionality of the system increases, the critical extent for conversion decreases. Pinner expanded the definition of average functionality to systems that contain nonstoichiometric amounts of reactants, allowing the theory to be extended to these systems.[31] Flory and Stockmayer further expanded upon this theory with

a statistical treatment that included those systems with stoichiometric and nonstoichiometric amounts of reactants.[32,33] Both of these classical theories are still in use today, and a number of new theories have emerged as well to describe crosslinking behavior in systems that do not necessarily adhere to either of the theories of Carothers or Flory and Stockmayer, such as the one posited by Miller and Macosko.[34] While the theoretical treatment of network formation within polymeric systems can provide an expectation of how crosslinking will occur, it is still necessary to measure the phenomenon experimentally in order to validate the theories.

There exist different techniques that can be used to monitor the cross-linking of a polymeric system. One such technique is differential scanning calorimetry, through which the heat generated (exothermic reaction) or consumed (endothermic reaction) throughout a reaction is monitored. This technique can be used for both thermally and UV-induced cross-linking reactions, and the heats of reactions are generally used to fit data to empirical models.[35,36] This technique is widely used, however it does not provide any explicit information regarding the chemical kinetics or the microstructural build-up as the reaction proceeds. Another technique that widely used is Fourier-transform infrared spectroscopy (FTIR). By using FTIR, it is possible to follow a reaction's progress by monitoring the consumption or generation of chemical species by observing the chemical bonds within the system.[18,37] This technique is used for coating systems that rely on isocyanate crosslinking agents, wherein the consumption of the isocyanate group is traced as a function of time.[38] From this technique, chemical kinetics for the reaction can be easily obtained, however it does not provide any direct information regarding the changing microstructure as the reaction proceeds.

A third common technique for following cross-linking reactions within polymeric systems is dynamic shear rheology. Dynamic shear rheology is the study of the deformation of a

material under oscillatory shear stress or strain. If a small enough oscillatory deformation is performed then it is possible to probe a material's mechanical response without disrupting or destroying its microstructure, a method known as small amplitude oscillatory shear rheometry. Dynamic shear rheology enables the study of a system's mechanical response as a microstructure forms and can provide insights into the nature of that response, i.e., is the input energy stored elastically or is it dissipated through viscous losses? At early times in a cross-linking reaction, materials often exhibit much more of a viscous response than an elastic response. As the reaction proceeds and a microstructure forms, the material response begins to become more elastic in character, and often times a material will exhibit an increase of multiple orders of magnitude after crosslinking. While rheology does not provide any explicit information about the chemical kinetics or heat evolution associated with the crosslinking reaction, it does provide valuable insight into the evolution of mechanical properties as the reaction proceeds.

All three of the techniques described above are useful in monitoring crosslinking reactions, however each is somewhat limited in the information it can provide. When used in parallel, however, these techniques become much more powerful and are able to elucidate significantly more information about the crosslinking reaction. For instance, data obtained from FTIR can give information about how much of the reaction must occur before a sample-spanning crosslinked network is able to develop, and dynamic rheology can provide information as to what the mechanical behavior of a system is going to be at any point along the reaction coordinate. These two techniques have been used in concert in previous works[39,40], and have been shown to provide a comprehensive understanding of the chemical and mechanical changes that occur during crosslinking of polymeric systems. This type of multi-pronged approach to the analysis of network formation in polymers is a practical and powerful way to gain additional

insight into crosslinking that a single technique cannot provide. Once a polymer network is formed, it is imperative to evaluate its ultimate properties in order to determine its utility for a given application.

### *1.3.2. Experimental Analysis of Final Film Properties*

While developing a comprehensive understanding of crosslinking behavior is one important step in fully understanding a polymeric material, it is not the only important consideration. Once a polymer system is crosslinked, there are a host of properties which need to be studied that are critical to understanding the potential end-uses of the material. From thermal stability to thermomechanical characteristics, there are a number of material properties which can be measured via experimental techniques that play a major role in which applications a material is suited for.

Thermal stability is critical when considering a material's use in high-temperature applications. Thermogravimetric analysis (TGA) is a technique by which the thermal stability can be studied; this technique involves subjecting a sample to varying temperatures and measuring mass loss. The mass lost within these types of experiments can be traced to chemical reactions that are degrading the material, as well as the volatilization of additives. In either case the observed change in mass can relate back to changes in the overall composition, which can have a profound impact on the material's performance. The maximum operating temperature of a material can be determined in this manner, depending upon the prescribed requirements of the application. Once the thermal stability has been understood, the thermomechanical properties need to be studied in order to determine ultimate film performance.

One important thermomechanical property of network polymers is the glass transition temperature. The glass transition is a second-order phase transition that does not constitute a

traditional phase change, which are typically first-order and require a specific enthalpy, such as melting or crystallization. However, the transitions from a glassy to a rubbery state and vice versa are accompanied by a significant change in the material properties of a polymeric system. There exist extensive previous works on the molecular nature of the glass transition and its effect on macroscopic properties[41–43]. Below the glass transition temperature, or $T_g$ materials behave in a solid-like fashion, with the constituents of their microstructure locked in place by nearest neighbors. Polymers in the glassy state tend to be more brittle but also exhibit higher moduli than their rubbery counterparts, making them favorable materials in applications such as protective coatings. Cross-linked polymers in the rubbery state tend to exhibit higher compliance under applied stress and often find applications in materials such as rubber for car tires. In either case, the identification of the glass transition temperature is a key element in determining what potential end-uses exist for a polymeric material. One technique for identifying the glass transition temperature is differential scanning calorimetry, which is a thermal technique by which the transition is identified by a second-order transition in the heat flow curve. The glass transition can also be determined by a few different measures using mechanical testing; two possible techniques for doing so are dynamic rheology and dynamic mechanical thermal analysis (DMTA). The glass transition temperature can be identified as either the storage modulus onset (the point at which it begins a precipitous decrease), the primary loss modulus peak or the peak in the loss tangent curve, $\tan\delta$.

The mechanical properties of a crosslinked polymeric system must be understood in order to determine how it will perform in a given situation. There are a number of ways in which the mechanical response of a material can be probed, depending on the anticipated application. In order to understand how a bulk material responds to small deformations at a variety of

temperatures, dynamic rheology or DMTA can be used. Two common material properties that are used to describe the material response are the storage and loss modulus (G' (storage), G'' (loss) and E' (storage) and E'' (loss) for dynamic shear rheology and DMTA, respectively). The physical significance of these two measures is discussed in the dynamic rheology section. Different classes of materials can have vastly different bulk mechanical properties; for instance, rubbers such as poly(dimethyl siloxane) might have a storage modulus on the order of 1-100 MPa at room temperature (depending on crosslink density), whereas stiffer glassy polymer networks might exhibit storage moduli upwards of 1 GPa at room temperature.

Applications such as protective coatings and lenses, which have a relatively large exposed surface, might place emphasis on not only the bulk thermomechanical properties, but also the surface mechanical properties. It is prudent to specifically study the surface because a material's surface can have very different mechanical properties from the bulk material. One popular method for examining surface mechanical properties is through a technique known as nanoindentation, whereby a tip with a known geometry contacts and subsequently indents a material to a certain load or displacement and then releases.[44] From this type of experiment, quantities such as the elastic modulus of the surface and the indentation hardness can be determined. These material properties can provide insight into the mechanical response upon surface stresses.

Free volume is often a sub-nanometer characteristic of a material that can have significant impact on macroscopic properties. "Free volume" is a volume element within a substance that does not have any molecule or atom occupant. In polymeric materials, this free volume is then available for polymer chains to move into via reptation and diffusion, or penetrant molecules to occupy via diffusion. There exist a number of theories that suggest correlations

between the free volume and directly observable macroscopic properties, such as the glass transition.[45]

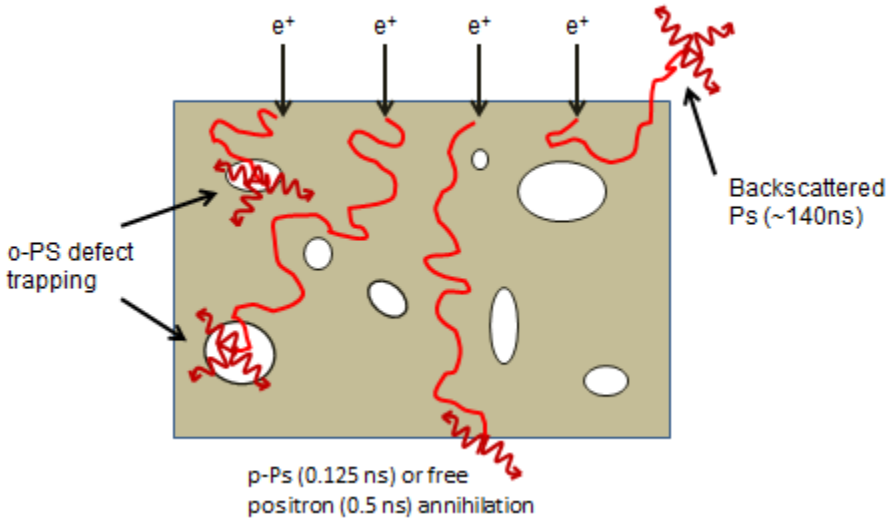


**Figure 0.1.** Cartoon representation of positrons (e+) and positronium (Ps) embedding in and subsequently annihilating within a polymeric matrix.

One method to probe the free volume of a substance is via a technique called positron annihilation lifetime spectroscopy (PALS). A cartoon representation of positrons interacting with a polymeric matrix is given in **Figure 1.1**. This technique relies upon a radioactive source such as $^{22}$Na to decay and produce positrons, the antiparticles of electrons, and impregnate the sample of interest with them. The positrons will localize to areas of low electron density, where they will interact with the edges of the free volume pore in a process known as "pick-off annihilation."[46] The nature of this annihilation event depends upon whether or not the positron pairs with an electron to form positronium (abbreviated Ps, similar size as hydrogen atom but about 1000 times lighter), as well as the relative spins of the paired particles. In the case where the electron and positron have the parallel spins, para-positronium (p-Ps) is formed; in the case of anti-parallel spins, ortho-positronium is formed (o-Ps). The ratio of o-Ps:p-Ps formation is 3:1,

indicating that 3 o-Ps are generated for every 1 p-Ps. Upon annihilation, free positrons and p-Ps generate 2 gamma rays; these two particles have very short lifetimes (on the order of a few nanoseconds in vacuum and significantly less in condensed matter), they are not particularly useful in probing free volume within polymeric materials. Instead, we look to the annihilation of o-Ps to probe free volume within polymeric materials. Upon annihilation, o-Ps produces 3 gamma rays and has a lifetime on the order of a few nanoseconds in condensed matter (a few hundred ns in vacuum) , which makes it practical to study polymeric materials.[47] This technique will be discussed in more detail in Chapter 3.

This section was meant to provide a brief and wide-ranging introduction for the work presented in this dissertation. Each chapter of this dissertation also contains its own in-depth literature review, which will provide further context for the results and discussions in each chapter.

## 1.4. Research Agendas and Techniques Used

### *1.4.1. Analysis of Crosslinking Behavior in Model Polyester Polyol-based Systems*

A thorough analysis of the cross-linking behavior in a set of model polyester polyol-based systems is presented in Chapter 2. The crosslinking reaction studied herein is the alcohol-isocyanate reaction, achieved by reacting the polyol's hydroxyl end groups with a polyisocyanate and resulting in the formation of a urethane linkage. Urethanes have found uses in an extensive number of applications, from biomedical materials to protective coatings. Specifically, we are interested in the use of these model materials to understand crosslinking in terms of protective coating formation and the effect of processing conditions and material chemistry on the crosslinking process. In this work, the backbone chemistry of the polyester polyols is varied in a ladder series of 5 polyester polyol resins, which in turn varies the nature of the reactive hydroxyl

moieties. One of the backbone monomers, 2,2,4,4-tetramethyl-1,3-cyclobutanediol (TMCD), has a secondary hydroxyl and its inclusion within the polyester backbone (along with the theoretical secondary hydroxyl content available for urethane formation) is varied by replacing the control monomer neopentane glycol (NPG, has a primary hydroxyl) with TMCD to varying degrees across the five resins. The primary focus of this chapter is to understand the effect of theoretical secondary hydroxyl content on the crosslinking behavior of these systems.

Dynamic shear rheology is utilized to track the microstructural evolution of the crosslinking system through *in-situ* monitoring of the dynamic moduli (storage modulus, G', and loss modulus, G'') as a function of time. As mentioned in a previous section of this chapter, this technique can allow for the identification of the onset of gelation, a process by which a material's mechanical response begins to be dominated by the elastic component and it behaves more as a solid than a liquid. As a complementary technique to the dynamic rheology experiments, the reaction progress is followed *in-situ* as a function of time at multiple temperatures that are relevant to some protective coating processes. This is achieved via variable temperature Fourier-transform infrared spectroscopy (VT-FTIR), which allows for *in-situ* monitoring of the disappearance of the isocyanate group as it is consumed in the urethane-forming crosslinking reaction. These two techniques used in parallel allow for simultaneous understanding of the role of network formation and chemical reaction progress on the time required to achieve a material that exhibits solid-like behavior. After developing this understanding, then it is prudent to try and understand how these same polyester polyol systems behave after being allowed to fully cure into model coating systems, which is the topic of Chapter 3.

### *1.4.2. Role of TMCD Content and Crosslinking Conditions in the Final Film Thermomechanical and Free Volume Properties of Model Coating Systems*

A discussion of the role of TMCD and the processing conditions under which a film is crosslinked on the final film thermomechanical and free volume properties comprises Chapter 3. Two cure temperatures are examined for all films and, upon completion of the crosslinking reactions, films were tested with a number of techniques in order to develop an understanding of processing conditions and TMCD content on a host of different properties critical to coating performance. The glass transition temperature was measured using DSC as well as DMTA for all TMCD contents at both cure temperatures. As was mentioned previously, this is an important material characteristic for protective coatings, as their performance can be drastically reduced if they are utilized above their glass transition temperature.

The mechanical properties of the films containing all levels of TMCD are also a subject of discussion within this chapter. Two specific types of mechanical properties are discussed within this chapter; bulk mechanical properties and surface mechanical properties. The differences between the two are discussed briefly earlier, as are some common techniques for measuring the bulk and surface mechanical characteristics. In this chapter, the primary engine for generating bulk mechanical property information is DMTA, and for surface mechanical property data it is nanoindentation. The motivation behind studying the bulk mechanical properties is the desire to understand how TMCD affects the final performance of the entirety of the coating film. Because the surface of a polymeric film may tend to have different mechanical properties than the bulk (and mechanical integrity of the surface can play a significant role in coating performance), it is important to consider that portion of the film as well. Additionally, it is possible to draw some insights as to the plasticity of the surface and the ability of the material to

recover from small surface deformations, providing additional motivation for examining surface mechanical properties, specifically with nanoindentation.

As discussed in a previous section, many of the bulk thermomechanical properties of a polymeric material can be attributed to their free volume, which can be measured using PALS. Due to the desire to understand the crosslinked polymer networks at a fundamental level with respect to the role of TMCD and processing conditions, it follows that one of the fundamental properties of a material, its free volume, be probed for the materials examined in Chapter 3. The free volumes associated with films containing different TMCD contents and prepared under different processing conditions, when combined with the thermal characterization provided by DSC/DMTA and the mechanical insights gained through DMTA and nanoindentation, allow for a fully developed understanding of the role of TMCD content and processing conditions on some of the various material properties important to network polymer coatings.

### *1.4.3. Rheology of UV-crosslinkable Polymer Nanocomposites Based on Poly(dimethyl siloxane) (PDMS) and Zirconia Nanoparticles: Role of Reactive vs. Passive Fillers*

In Chapters 2 and 3, the focus has been on more rigid polymer networks crosslinked upon heating. In Chapter 4 of this dissertation, a different type of polymer is examined with a different mechanism of crosslinking. The polymer examined within this chapter is a low molecular weight PDMS which is end-capped with a functional group that is curable when exposed to UV irradiation in the presence of a radical photoinitiator (in this case 2,2-dimethoxy-2-phenylacetophenone, or DMPA). Chapter 4 not only includes an analysis of a UV-crosslinkable polymer system, but also contains significant work and a lengthy discussion on the role of reactive and passive nanofillers and the role they play in network formation and the ultimate gel

strength and optical properties of systems filled with up to 85 wt% nanofiller on solids content (systems are 50 wt% solids).

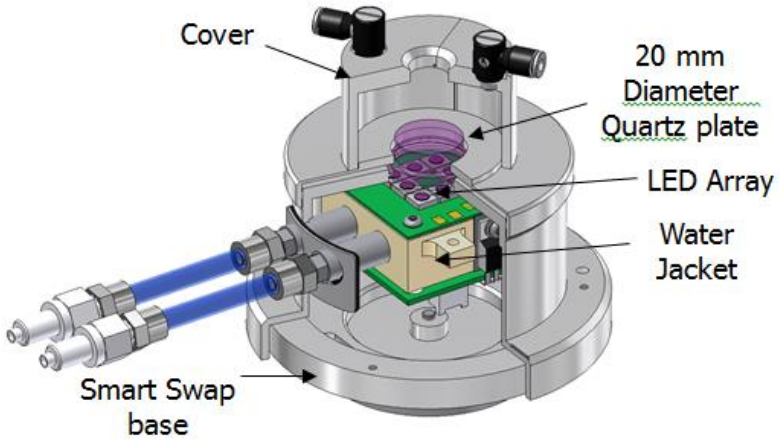


**Figure 0.2.** Schematic of 365nm UV LED accessory for DHR-3 rheometer used to monitor crosslinking reactions in Chapter 4 of this dissertation. Image courtesy of TA Instruments.

To date, there has not been substantial previous work on the rheology of polymeric systems undergoing UV-induced crosslinking in the presence of reactive and nonreactive fillers. As the field of polymer nanocomposites grows and the potential applications broaden, the need to understand how these fillers affect network formation persists. As was mentioned in previous sections, dynamic shear rheology can allow for the study of these phenomena. A schematic illustration, provided by TA Instruments, is given in **Figure 1.2**. Chapter 4 seeks to add a fundamental understanding of how reactive and passive fillers can not only affect the gelation of UV-crosslinking polymeric systems, but also their final film properties.

### 1.5. Scope of this Dissertation

The previous sections in this work have sought to identify a motivation for the work undertaken in this dissertation and provide some background information as to not only the breadth of network-forming polymers that are of interest to the greater scientific community, but

also some practical applications in which they might be utilized. At this point, it is prudent to pose some fundamental questions that this work attempts to shed clarity on. In Chapter 2, the primary questions that are addressed are:

- How does varying the statistical secondary hydroxyl content in thermally-induced polyester polyol systems affect the chemical and rheological crosslinking kinetics of the systems?
- Why do systems with high statistical secondary hydroxyl content ( > 25% ) begin to show increasing deviations from classical gelation theories?

Chapter 3 provides an extension of the analysis of the same systems studied in Chapter 2, although instead of interrogating network formation, the final crosslinked networks are probed after being subjected to two different crosslinking conditions. The primary questions that are addressed in Chapter 3 are:

- How does increasing TMCD content in a polyester polyol backbone affect the glass transition temperature of the polyester resin pre-crosslinking and the resulting crosslinked films?
- What is the effect of an incremental increase in TMCD content on the ultimate bulk and surface mechanical properties of films cured under two different conditions?
- How is the average free volume hole size within the crosslinked network affected by the amount of TMCD in the polyester backbone?

Chapter 3 wraps up the discussion of thermally cured TMCD-based polymer networks in this dissertation. In Chapter 4, the topic deviates slightly to UV-crosslinkable PDMS-based networks with nanofillers, one of which is reactive under UV irradiation and one of which is not.

The characteristics of both types of fillers at loadings of up to 85 wt% solids content are elucidated, with an emphasis on answering the following questions:

- What is the effect of fillers, regardless of functionality, on the rheological mechanism of crosslinking?
- How does filler type and loading affect the time required to achieve modulus crossover, as well as the magnitude of the crossover?
- What is the effect of both types of fillers on the ultimate network strength?
- What role does nanofiller functionality play in the ultimate film optical properties? How well are both types of filler retained within the matrix after swelling?

In addition to addressing the above questions, each chapter contains its own introduction and literature review, followed by a materials and methods section which describes the specific experimental setups utilized in detail. Afterwards, an in-depth analysis and discussion of results, as well as a conclusion of the findings presented within the chapter are followed by specific acknowledgements and references cited within the chapter. The final chapter summarizes all of the findings from the preceding 3 chapters and provides recommendations on future work that might build upon the research presented herein to increase the breadth and depth of knowledge in the field of network polymers.

## 1.6. References


(1) Adhikari, B.; Majumdar, S. *Prog. Polym. Sci.* **2004**, *29* (7), 699–766.

(2) Biggs, J.; Danielmeier, K.; Hitzbleck, J.; Krause, J.; Kridl, T.; Nowak, S.; Orselli, E.; Quan, X.; Schapeler, D.; Sutherland, W.; Wagner, J. *Angew. Chemie Int. Ed.* **2013**, *52* (36), 9409–9421.

(3) Roberts, M. C.; Hanson, M. C.; Massey, A. P.; Karren, E. A.; Kiser, P. F. *Adv. Mater.* **2007**, *19* (18), 2503–2507.

(4) Jordan, J.; Jacob, K. I.; Tannenbaum, R.; Sharaf, M. A.; Jasiuk, I. *Mater. Sci. Eng. A* **2005**, *393* (1–2), 1–11.

(5) Moniruzzaman, M.; Winey, K. I. *Macromolecules* **2006**, *39* (16), 5194–5205.

(6) Kargarzadeh, H.; Mariano, M.; Huang, J.; Lin, N.; Ahmad, I.; Dufresne, A.; Thomas, S. *Polymer (Guildf).* **2017**, *132*, 368–393.

(7) Perez, E. V.; Balkus, K. J.; Ferraris, J. P.; Musselman, I. H. *J. Memb. Sci.* **2009**, *328* (1–2), 165–173.

(8) DiBenedetto, A. T. *Mater. Sci. Eng. A* **2001**, *302* (1), 74–82.

(9) Schadler, L. S.; Kumar, S. K.; Benicewicz, B. C.; Lewis, S. L.; Harton, S. E. *MRS Bull.* **2007**, *32* (04), 335–340.

(10) Wang, R.; Lin, T.-S.; Johnson, J. A.; Olsen, B. D. *ACS Macro Lett.* **2017**, *6*, 1414–1419.

(11) Higham, A. K.; Garber, L. A.; Latshaw, D. C.; Hall, C. K.; Pojman, J. A.; Khan, S. A. *Macromolecules* **2014**, *47*, 821–829.

(12) Narayan, R.; Chattopadhyay, D. K.; Sreedhar, B.; Raju, K. V. S. N. *J. Mater. Sci.* **2002**, *37* (22), 4911–4918.

(13) Yousefi, A.; Lafleur, P. G.; Gauvin, R. *Polym. Compos.* **1997**, *18* (2), 157–168.

(14) Kiil, S. *Prog. Org. Coatings* **2011**, *70* (4), 192–198.

(15) Tillet, G.; Boutevin, B.; Ameduri, B. *Prog. Polym. Sci.* **2011**, *36* (2), 191–217.

(16) Higham, A. K.; Bonino, C. A.; Raghavan, S. R.; Khan, S. A. *Soft Matter* **2014**, *10* (27), 4990–5002.

(17) Ha, H.; Kim, S. C.; Ha, K. *Macromol. Res.* **2010**, *18* (7), 674–679.

(18) Burel, F.; Feldman, A.; Bunel, C. *Polymer (Guildf).* **2005**, *46*, 15–25.

(19) Goswami, K.; Daugaard, A. E.; Skov, A. L. *RSC Adv.* **2015**, *5* (17), 12792–12799.

(20) Sørensen, P. A.; Kiil, S.; Dam-Johansen, K.; Weinell, C. E. *J. Coatings Technol. Res.* **2009**, *6*, 135–176.

(21) Chattopadhyay, D. K.; Raju, K. V. S. N. *Prog. Polym. Sci.* **2007**, *32* (3), 352–418.

(22) Yu, L.; Skov, A. L. *RSC Adv.* **2017**, *7* (72), 45784–45791.

(23) Lee, S. H.; Kim, S. W.; Kang, B. S.; Chang, P.-S.; Kwak, M. K. *Soft Matter* **2018**, *14* (14), 2586–2593.

(24) Lee, S.-W.; Park, J.-W.; Kwon, Y.-E.; Kim, S.; Kim, H.-J.; Kim, E.-A.; Woo, H.-S.; Swiderska, J. *Int. J. Adhes. Adhes.* **2012**, *38*, 5–10.

(25) Patel, D. K.; Sakhaei, A. H.; Layani, M.; Zhang, B.; Ge, Q.; Magdassi, S. *Adv. Mater.*

**2017**, *29* (15), 1606000.

(26) Cao, S.; Li, S.; Li, M.; Xu, L.; Ding, H.; Xia, J.; Zhang, M.; Huang, K. *Polym. J.* **2017**, *49* (11), 775–781.

(27) Miguel, S. P.; Ribeiro, M. P.; Brancal, H.; Coutinho, P.; Correia, I. J. *Carbohydr. Polym.* **2014**, *111*, 366–373.

(28) Bajat, J. B.; Mišković-Stanković, V. B. *Prog. Org. Coatings* **2004**, *49*, 183–196.

(29) Efron, N.; Morgan, P. B.; Cameron, I. D.; Brennan, N. a; Goodwin, M. *Optom. Vis. Sci.* **2007**, *84* (4), 328–337.

(30) Carothers, W. H. *Trans. Faraday Soc.* **1936**, *32*, 39–49.

(31) Pinner, S. H. *J. Polym. Sci.* **1956**, *21*, 153–157.

(32) Flory, P. J. *J. Am. Chem. Soc.* **1941**, *63*, 3083–3090.

(33) Stockmayer, W. H. *J. Chem. Phys.* **1944**, *12*, 125–131.

(34) Miller, D. R.; Macosko, C. W. *Macromolecules* **1978**, *11*, 656–662.

(35) Belder, E. G.; Rutten, H. J. J.; Perera, D. Y. *Prog. Org. Coatings* **2001**, *42*, 142–149.

(36) Mohseni, M.; Bastani, S.; Jannesari, A. *Prog. Org. Coatings* **2014**, *77* (7), 1191–1199.

(37) Li, F.; Zhou, S.; You, B.; Wu, L. *J. Appl. Polym. Sci.* **2006**, *99* (4), 1429–1436.

(38) Li, S.; Vatanparast, R.; Lemmetyinen, H. *Polymer (Guildf).* **2000**, *41*, 5571–5576.

(39) Lucio, B.; de la Fuente, J. L. *Thermochim. Acta* **2014**, *596*, 6–13.

(40) Fu, X.; Fan, X. *J. Therm. Anal. Calorim.* **2016**, *125* (2), 977–982.

(41) Paul, W. In *Polymer*; 2004; Vol. 45, pp 3901–3905.

(42) Koo, B.; Liu, Y.; Zou, J.; Chattopadhyay, A.; Dai, L. L. *Model. Simul. Mater. Sci. Eng.* **2014**, *22* (6), 065018.

(43) Trachenko, K. *J. Non. Cryst. Solids* **2008**, *354*, 3903–3906.

(44) Skaja, A.; Fernando, D.; Croll, S. *J. Coatings Technol. Res.* **2006**, *3*, 41–51.

(45) White, R. P.; Lipson, J. E. G. *Macromolecules* **2016**, *49* (11), 3987–4007.

(46) Yoshinori, K.; Kenji, H.; Yoshinori, K.; Shigeru, H. *Bull. Chem. Soc. Jpn.* **1992**, *65* (1), 160–163.

(47) Sharma, S. K.; Pujari, P. K. *Prog. Polym. Sci.* **2017**, *75*, 31–47.

# CHAPTER 2: SPECTROSCOPIC AND RHEOLOGICAL CROSS-ANALYSIS OF POLYESTER POLYOL CURE BEHAVIOR: ROLE OF SECONDARY HYDROXYL CONTENT

## 2.1. Introduction

Polymeric systems are employed in a wide range of applications from precisely-shaped 3D parts to protective film coatings on various substrates.[1–5] For numerous coating technologies, thermosetting polymers are often particularly attractive due to their inherent ability to form densely cross-linked networks that impart a favorable combination of mechanical, barrier and chemical-resistance properties.[2,6–8] Such coating systems can take the form of dry powders[9–11] or variable-viscosity liquids (water-borne[12,13] or solvent-borne[14]) and can be applied as aerosol sprays, brushed finishes or rolled laminates onto a solid substrate prior to curing. Nearly all polymeric coatings are broadly divided into two categories: one-component (1K) and two-component (2K) systems.[8] Most of these polymers are acrylic-, alkyd- or polyester-based, and they react in the presence of a cross-linking agent to form dense molecular networks. Polyester-based urethane systems are popular 2K systems due to their versatility, desirable barrier/ mechanical properties and good weathering capability.[15] Understanding their cure behavior is crucial for designing such multicomponent polymers for coatings applications. In these systems, a polyol/catalyst/solvent mixture is typically combined with an isocyanate cross-linking agent, and the resulting mixture is sprayed or painted onto a substrate. While properties for transparent coatings must adhere to quality standards that vary with application,[16] coating viscosities must be compatible with the deposition method and associated crosslinking behavior must be acceptable for industrially relevant cure conditions, as well as for favorable film properties once cured.

The monomer 2,2,4,4-tetramethyl 1,3-cyclobutanediol (TMCD) has been previously investigated[15] in thermoplastic polyester systems and has been successfully commercialized as part of the Tritan® copolyester manufactured by Eastman Chemical Company. Prior efforts have demonstrated that TMCD improves the impact resistance of polyester-based systems while maintaining good thermal properties.[17] However, studies describing how the incorporation of TMCD in a polyester backbone affects cure behavior in 2K thermosetting polyesters remain lacking. Chemical conversion and accompanying thermomechanical property evolution constitute two vital characteristics of a coating system when considering the cure behavior of any 2K thermosetting coating. Previous efforts in this vein have relied on thermal calorimetry to monitor reaction kinetics and the corresponding evolution of the glass transition temperature ($T_g$), dynamic rheology to identify the sol-gel transition (also known as the gel point) and spectroscopy to measure the time-dependent chemical conversion at various temperatures.[18–25] These analytical techniques provide useful insights when used independently, but are especially valuable when used in parallel, as is the case here and in previous works.[26,27] In this work, we seek to exploit the individual benefits of dynamic rheology and variable-temperature IR spectroscopy by varying polyester backbone chemistry and directly relating the network evolution of TMCD-containing resins in 2K polyester-urethane systems to chemical conversion during the cure process at different industrially relevant temperatures.

## 2.2. Experimental

### *2.2.1. Materials*

Polyester resins were supplied by Eastman Chemical Company and used as-received. **Figure 2.1** depicts the chemical structures of all the monomers employed in the synthesis of the polyester resins. The cross-linking agent was hexamethylene diisocyanurate (HDI trimer),

purchased from Covestro (Desmodur 3390 BA/SN) and also pictured in **Figure 2.1**. Dibutyltin dilaurate (95%) obtained from Sigma Aldrich and urethane-grade methyl amyl ketone (MAK) supplied by the Eastman Chemical Company were both used without further purification.

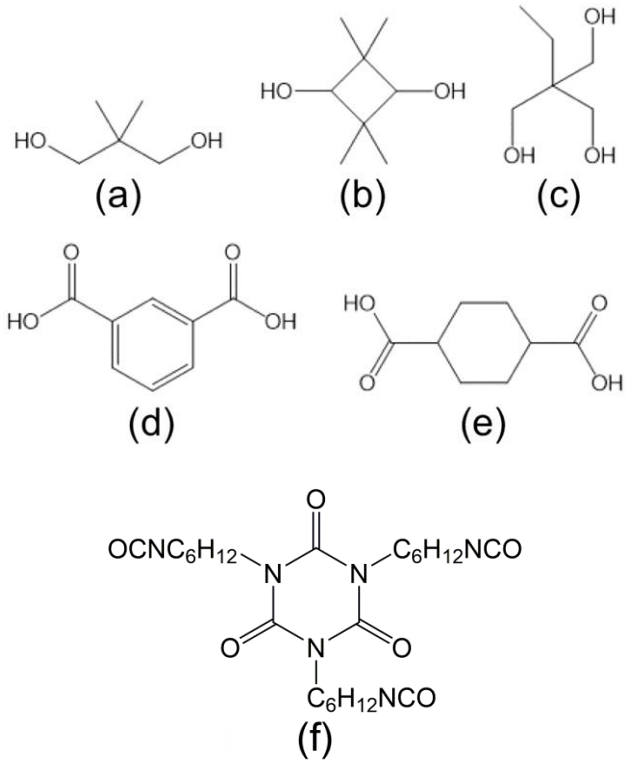


Figure 0.3. Chemical structures of the monomers used to synthesize polyester-polyol are shown in (a-e). (a) neopentane glycol (NPG), (b) 2,2,4,4-tetramethyl 1,3-cyclobutanediol (TMCD), (c) trimethylolpropane (TMP), (d) isophthalic acid (IPA), and (e) 1,4-cyclohexanediacid (CHDA). The chemical structure of the HDI crosslinking agent is shown in (f).

### *2.2.2. Methods*

#### 2.2.2.1. Specimen Preparation

Gel permeation chromatography with polystyrene standards was conducted in an Agilent Series 1260 liquid chromatograph with a UV/Vis detector to measure the number-average molecular weight ($M_n$) and polydispersity index (Đ), of each resin, the composition and

properties of which are listed in **Table 2.1.** The dibutyltin dilaurate catalyst was mixed with MAK to produce a 1 wt% catalyst solution, which was added at 2.5 wt% (relative to the total solids) to a known quantity of polyester resin in MAK. This catalyst/polyester/solvent mixture, hereafter referred to as component "A," was then agitated in the presence of a magnetic stir bar in a 20 mL glass scintillation vial until the polymer was fully dissolved (~8 h). A predetermined quantity of component A was added to a 10 mL glass scintillation vial, and the cross-linking agent (component "B") was added dropwise under agitation to achieve a NCO:OH stoichiometric ratio of 1.10 ± 0.02:1 at a constant solids content of 60 ± 2%. This mixture was then placed on a stir plate for 5 min at ambient temperature before analysis.

#### 2.2.2.2. Rheological Analysis

Dynamic oscillatory shear rheology was conducted to monitor the cross-linking reaction of each polyester in the presence of the HDI trimer. All rheological measurements were performed on a TA Instruments Discovery Series Hybrid Rheometer HR-3, outfitted with a Peltier plate temperature-control system and operated with 40 mm aluminum parallel plates and a solvent trap. Each experiment commenced after sample equilibration for 5 min at the reaction temperature. Reaction progress was followed *in-situ* as a function of time at a fixed strain amplitude within the linear viscoelastic regime of the sample at an angular frequency of 1 rad/s. Measured shear stresses were used to calculate the dynamic storage (G') and loss (G") moduli. To identify the temperature dependence of the gel point, times required for G'-G" crossover were evaluated at four different temperatures for each resin. We further discuss this gel-point criterion in subsequent sections.

**Table 0.1.** Compositions and selected properties of polyester-polyol resins.[a]

| | Diol composition (%) | | | Diacid composition (%) | | | | | |
|---|---|---|---|---|---|---|---|---|---|
| Resin Designation | NPG | TMCD | TMP | CHDA | IPA | $M_n$ (Da) | Đ | OH # | Secondary hydroxyl content[b] (mol%) |
| 0T | 93.35 | — | 6.65 | 50 | 50 | 1562 | 1.68 | 113 | 0.00 |
| 25T | 71.63 | 21.68 | 6.65 | 50 | 50 | 1616 | 1.76 | 111 | 21.67 |
| 50T | 46.65 | 46.65 | 6.65 | 50 | 50 | 1590 | 1.75 | 102 | 46.67 |
| 75T | 21.68 | 71.63 | 6.65 | 50 | 50 | 1707 | 1.78 | 97 | 71.67 |
| 100T | — | 93.35 | 6.65 | 50 | 50 | 1799 | 1.77 | 91 | 93.33 |

[a] All monomer species listed here are defined in **Figure 1.**

[b] Calculated on the basis of initial monomer compositions.

#### 2.2.2.3. Variable-temperature Spectroscopy

Variable-temperature Fourier-transform infrared (FTIR) spectroscopy was performed in attenuated total reflectance (ATR) mode on specimens with a Bio-Rad Excalibur Series spectrometer equipped with a germanium crystal and a PIKE Technologies heating stage. Approximately 0.05 g of each sample were placed on the crystal and heating stage, and a solvent trap was placed over the sample to prevent drying. The reaction clock began when the sample was placed on the stage, and spectra were collected as a function of time at each reaction temperature. A zero-point spectrum was collected 5 min after the sample was loaded to allow for

excess $CO_2$ to be flushed out of the spectrometer. Following the collection of FTIR spectra, baseline corrections were performed using the Win-IR Pro software package from Bio-Rad. Peak areas were calculated with Origin.

## 2.3. Results and Discussion

### *2.3.1. Gelation and Dynamic Rheology*

Small-amplitude dynamic rheology identifies the time required to achieve G'-G" crossover at 1 rad/s for all samples. This time, referred to as $t_c$, is an estimate of the gel point at which a contiguous network forms within a specimen. Networks are ubiquitous and important physical phenomena in polymers, as they are responsible for generating not only dense thermosets but also stretchy elastomers. Moreover, networks can be either chemically cross-linked, as is the case here, or they can be physically cross-linked in the case of, for instance, multiblock copolymers.[28] Once $t_c$ is reached, G' (a measure of elastic behavior) becomes equal to and subsequently greater than G" (a measure of viscous behavior). Therefore, at this point in time, the sample begins to exhibit more solid-like behavior. According to the Winter-Chambon rheological criterion for gelation, the true gel point occurs when tan □ (= G"/G') becomes independent of frequency.[29,30] The systems examined here do not strictly adhere to the Winter-Chambon criterion over the temperature range examined, so a true gel point is not possible to identify. Therefore, defining $t_c$ as the transition from viscous- to solid-like behavior at a single frequency is considered sufficient for the purpose of this study. A representative time sweep is presented in **Figure 2.2** for resin 0T at 45°C and clearly reveals the existence of G'-G" crossover at $t_c \approx 130$ min. Data such as these are employed to construct **Figure 2.3a**, which displays the average time for moduli crossover for all five resins examined at four different temperatures. An important observation in this figure is that resins possessing higher levels of secondary hydroxyl

content due to the presence of TMCD require appreciably longer times for network formation. We attribute this result to the TMCD secondary hydroxyl groups, which make the monomer more sterically hindered than NPG or TMP with primary hydroxyl groups (see **Figure 2.1**).

In addition, the time required for modulus crossover is seen to increase systematically with decreasing reaction temperature, a feature that is consistent with the behavior of a thermally-activated process. This expectation is confirmed by the linear trends evident in **Figure 2.3b**, which is an Arrhenius-style representation of the data provided in **Figure 2.3a**. Due to the thermally-activated nature of the gelation process, previous studies[31–34] of related systems have used an Arrhenius expression to extract values of the apparent activation energy ($E_a$) of gelation, *viz*.,

$$t_c = t_{c,0} exp\left(\frac{E_a}{RT}\right) \tag{2.1}$$

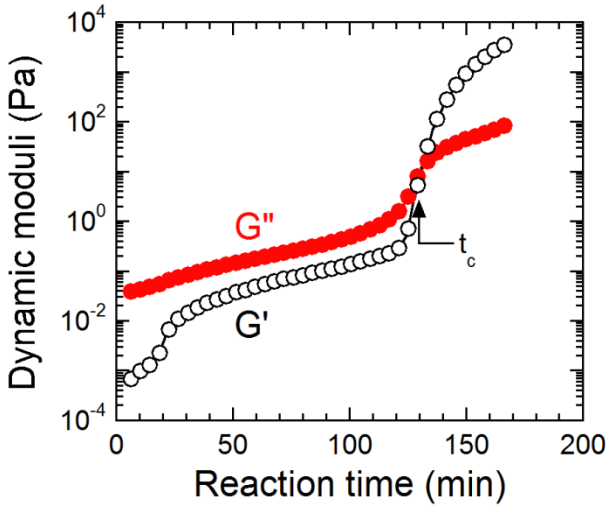


**Figure 0.4.** Variation of the dynamic moduli (G', □, and G", □) with reaction time during the cure of resin 0T at 45°C. The gel point at t c is identified at the G'-G" crossover. The solid lines serve to connect the data.

where $t_{c,0}$ is a constant, R is the universal gas constant and T denotes absolute temperature.

Values of $E_a$ calculated from the slopes of the lines in **Figure 2.3b** according to **Equation 2.1** are compiled in **Table 2.2** for each resin. In general, resins with a higher secondary hydroxyl content exhibit higher $E_a$ values. It is interesting that values of $E_a$ ascertained for 0T and 25T are similar, while those for 50T, 75T and 100T are likewise comparable. These groupings can be explained by considering the Flory-Stockmayer theory for gelation in conjunction with the difference in reactivity between primary and secondary hydroxyls.[35,36] For all the resin systems examined, the theoretical conversion of the total alcohol functionality is approximately 50% at the gel point. Since the reactivity of the secondary hydroxyls differs substantially from primary hydroxyls in the presence of dibutyltin dilaurate catalyst,[37] the secondary hydroxyls do not necessarily need to participate fully in network formation at concentration levels below ~50% (*e.g.*, samples 0T and 25T). Thus, the apparent activation energies reported here do not reflect the chemical kinetics governing the cross-linking reaction, but rather afford insight into network formation and the thermal process governing it.

Another classical network theory, proposed by Carothers,[38] has been expanded to include nonstoichiometric monomer mixtures by Pinner.[39] This theory and its subsequent expansion predict significantly higher critical extents of conversion to achieve gelation in polymeric systems than those given by Flory and Stockmayer.[35,36,40] We return to discuss this topic further in following sections.

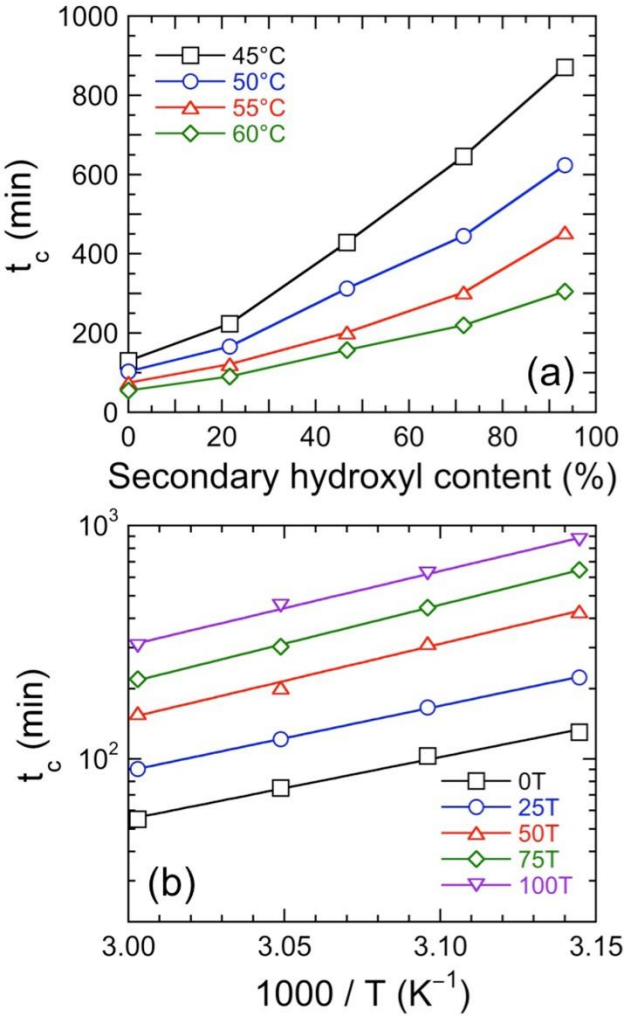


**Figure 0.5.** (a) Values of tc extracted from moduli crossover times (see Figure 2.2) as functions of resin composition (secondary hydroxyl content) and temperature (in °C): 45(□), 50 (□), 55 (r), and 60 (□). The color-matched solid lines serve to connect the data. (b) Arrhenius-style representation of $t_c$ as a function of reciprocal temperature for five different polyester-polyol resins: 0T (□), 25T (○), 50T (r), 75T (◇), and 100T (▽). The solid lines are linear regressions to the data, and the apparent activation energy values extracted from the slopes are listed in Table 2.2.

**Table 0.2.** Apparent activation energies from rheological and spectroscopic analyses.[a]

| Resin Designation | Apparent gelation $E_a$ (kJ/mol) | Apparent kinetic $E_a$ (kJ/mol) |
|---|---|---|
| 0T | 50.98 ± 2.886 | 62.89 ± 8.370 |
| 25T | 53.33 ± 0.6299 | 58.31 ± 12.79 |
| 50T | 60.84 ± 4.022 | 61.64 ± 5.586 |
| 75T | 63.81 ± 1.335 | 71.03 ± 18.51 (40.42) |
| 100T | 60.96 ± 2.672 | 79.58 ± 10.55 (65.74) |

[a] Parenthetical values exclude the kinetic rate constants at the lowest temperature examined.

*2.3.2. Reactivity from Chemical Spectroscopy*

Variable-temperature FTIR permits tracking the time-dependent intensity of the isocyanate peak for the five resins examined at four temperatures (45, 50, 55, and 60°C). Examples of overlaid FTIR spectra collected from one resin (100T) at one temperature (55°C) are displayed at several reaction times in **Figure 2.4**. To determine the concentration of the isocyanate functional group as a function of time, we first measure the area below the isocyanate stretch peak located at ~2260 $cm^{-1}$ and then normalize the result with respect to the area below the C-H stretch peaks between ~2840 and ~3050 $cm^{-1}$. The conversion of the isocyanate functional group ($p$) at any given time ($t$) is then calculated from

$$p = 1 - \frac{A_t}{A_0} \tag{2.2}$$

where $A_t$ is the normalized area under the isocyanate peak at $t$, and $A_0$ is the normalized area under the isocyanate peak at $t$ = 5 min. [The true zero time was not used because excess $CO_2$ had to be flushed from the spectrometer once the sample was loaded.] The same procedure has been followed for all five resins, and the conversion of the isocyanate peak has been monitored as

functions of both time and temperature, as illustrated in **Figure 2.5a** for resin 100T. These results confirm that the reaction reaches full conversion faster at higher temperatures and that full conversion appears to be achieved in less than 20 h over the temperature range examined here.

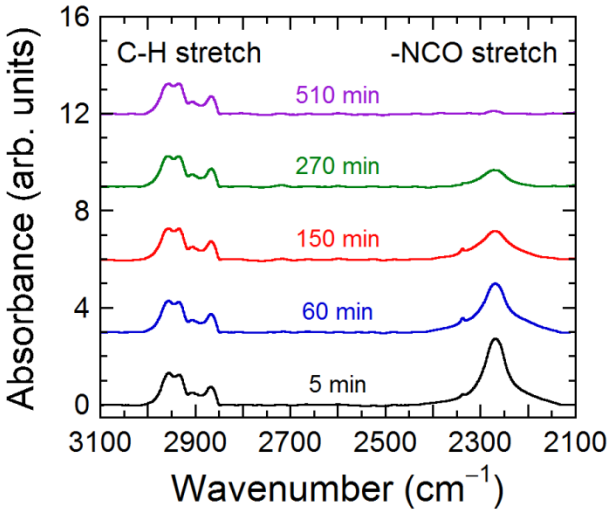


**Figure 0.6.** Representative FTIR spectra acquired at different reaction times (labeled and color-coded) from the 100T resin at 55°C. Disappearance of the isocyanate peak at 2260 cm$^{-1}$ (identified), normalized with respect to the C-H stretch peak (identified), is used to determine the reaction kinetics.

By assuming first-order reaction kinetics, the data presented in **Figure 2.5a** can be analyzed to extract kinetic rate constant (k) values. In this scenario, $p$ can be written as

$$p = 1 - exp(kt) \tag{2.3}$$

Algebraic rearrangement of **Equation 2.3** yields

$$ln(1 - p) = kt \tag{2.4}$$

in which case a plot of $(1 - p)$ versus $t$ on semi-logarithmic coordinates is expected to yield a linear trend, which is clearly observed in **Figure 2.5b**. The results displayed in **Figure 2.5b** are consistent with first-order reaction kinetics with respect to the isocyanate group for all five resin systems. To confirm the existence of first-order kinetics and rule out other possibilities, we have

also examined the conversion data for all five systems in the context of second-order kinetics with respect to the isocyanate group. The linear trends obtained from first-order kinetics agree much more closely with the measured conversions. The slopes of the curves in **Figure 2.5b** afford the first-order rate constants for resin 100T over the four temperatures examined. For consistency with the rheological analysis, we have elected to include data points from the beginning of the reaction to the time corresponding to the modulus crossover in our rheological tests. As such, the rate constants obtained from conversion-time plots such as the one shown in **Figure 2.5b** constitute average rate constants for the reaction between $t = 5$ min and $t \approx t_c$.

First-order kinetic rate constants discerned for the five resin systems are provided as functions of secondary hydroxyl content and temperature in **Figure 2.6**. As anticipated, the rate constants generally increase with increasing temperature for all five resin systems examined and decrease with increasing secondary hydroxyl content. To relate the temperature dependence of these first-order rate constants to the secondary hydroxyl content, **Figure 2.7** plots the data acquired for each resin in Arrhenius form. In accord with our earlier analysis employing this representation (*cf*. **Figure 2.5**), the slope of each line is used to extract the apparent kinetic activation energy of each resin up to $t_c$. These apparent activation energies are included for comparison with the apparent activation energies of gelation in **Table 2.2**. In **Figure 2.7**, the linearity of the data corresponding to the TMCD-rich resin systems (75T and 100T) appears to deviate at the lowest temperature examined (45°C).

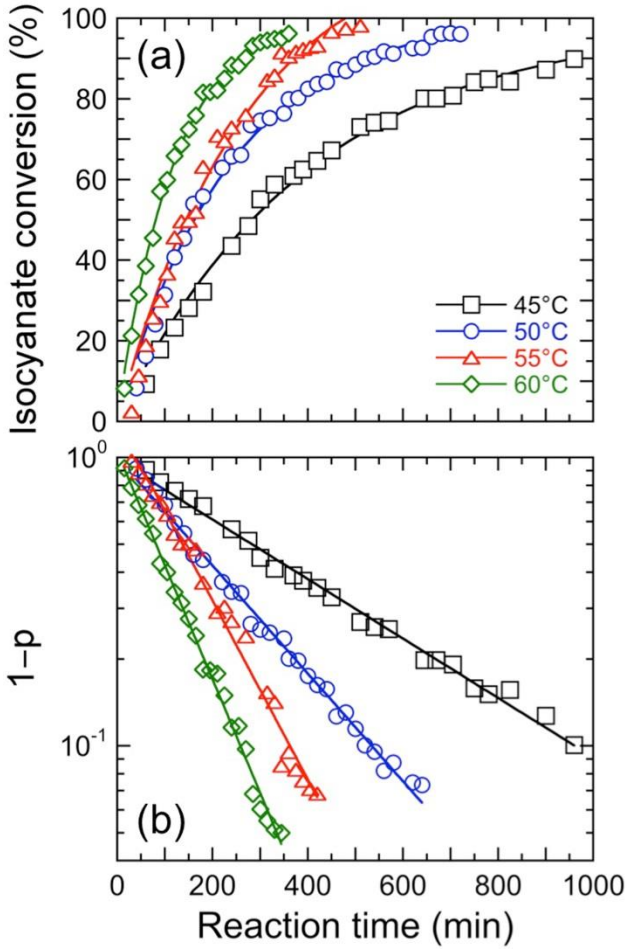


**Figure 0.7.** (a) Isocyanate conversion (*p*) calculated for resin 100T from **Equation 2.2** in the text and presented as a function of reaction time at four different temperatures (in °C): 45 (□), 50 (○), 55 (r), and 60 (◇). The color-matched solid lines serve to guides for the eye. (b) Isocyanate conversion for resin 100T presented as a function of reaction time according to first-order kinetics (see **Equation 2.4**) at four different temperatures (in °C): 45 (□), 50 (○), 55 (r), and 60 (◇). The color-matched solid lines are linear regressions to the data, and the slopes yield the kinetic rate constants.

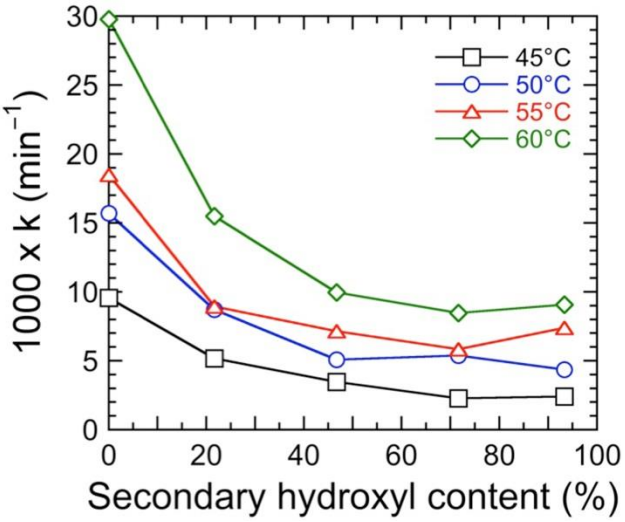


**Figure 0.8.** Dependence of the first-order kinetic rate constants calculated from plots such as the one provided in Figure 2.8 on composition at four different temperatures (in °C): 45 (□), 50 (○), 55 (r), and 60 (◇). The color-matched solid lines serve to connect the data.

To take this deviation into account, the apparent activation energies tabulated in **Table 2.2** for these two resins are calculated with and without the datum point measured at 45°C. This deviation at low temperature might be indicative of nontrivial diffusion limitations within the system as it cures. All the apparent kinetic activation energy values reported here naturally involve some degree of complex interplay between reaction and diffusion limitations because they are derived from average kinetic rate constants from the initial time (when the system behaves highly Newtonian) to the modulus crossover time (when the system begins to exhibit more solid- than viscous-like behavior). Another important consideration is that an increase in secondary hydroxyl content due to TMCD incorporation induces chain stiffening of the polyester resin. The impact of this phenomenon is discussed further below.

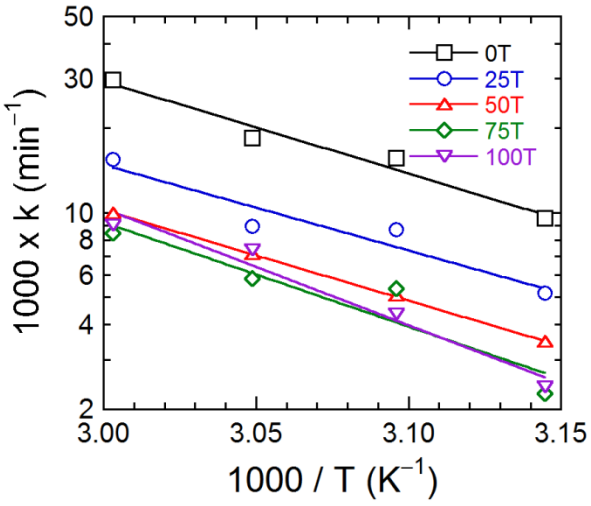


**Figure 0.9.** Arrhenius-style representation of the kinetic rate constants as a function of reciprocal temperature for five different polyester-polyol resins: 0T (□), 25T (○), 50T (r), 75T (◇), and 100T (▽). The solid lines are linear regressions to the data, and the apparent activation energy values extracted from the slopes are included in **Table 2.2**.

The apparent activation energies of gelation, measured by dynamic rheology, and the apparent kinetic activation energy, measured by VT-FTIR, are compared in **Figure 2.8**. While this comparison does not include the activation energies for the 75T and 100T resins calculated by omitting the rate constants measured at 45°C, we note that these activation energy values are consistently lower than those determined by considering all the data. The error bars included in **Figure 2.8** correspond to the standard error in the slope of the Arrhenius-style representations used to ascertain $E_a$ for each resin system. It is comforting that the measured apparent kinetic activation energies and apparent activation energies of gelation are relatively close and, in most cases, equal within experimental error. Such agreement does not, however, have to be the case. Since gelation is undoubtedly a thermally-activated process, it can be modeled as an Arrhenius phenomenon. With this expectation notwithstanding, the activation energy does not take into account the molecular-level phenomena accompanying a physical phase transition, but is rather a

measure of the temperature dependence of a mechanical property. In contrast, the apparent kinetic activation energies provide insight into the chemical changes occurring within the resins due to the cross-linking reaction, and can be used in conjunction with measured reaction times to determine the relative reactivity of the different hydroxyl-containing constituents. As we have measured it here, the apparent kinetic activation energy constitutes an average activation energy from the beginning of the reaction to the modulus crossover time, and provides information not only on the chemical nature of the reactive system as the cross-linked network develops, but also on how the hydroxyl reactivities change along the reaction coordinate.

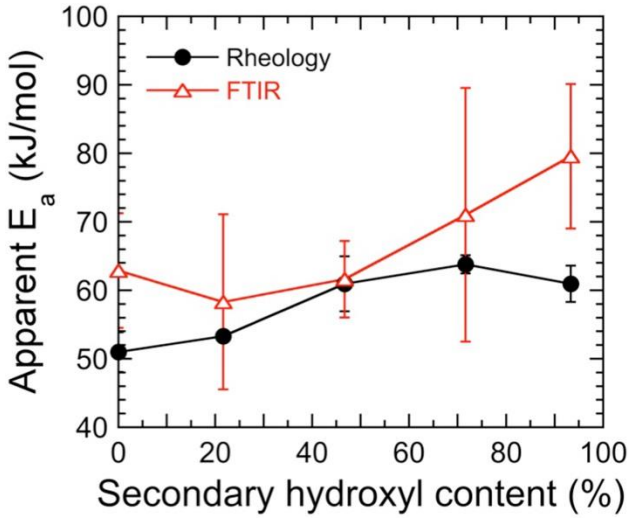


**Figure 0.10.** Comparison of apparent activation energies of gelation (●) and reaction (r) as determined by rheological and spectroscopic analyses, respectively. The error bars correspond to the standard error, and the color-matched solid lines serve to connect the data.

*2.3.3.Critical Extent of Conversion*

Another important metric of the present thermosetting resins is the critical extent of isocyanate conversion calculated at the time required for modulus crossover, as discerned by dynamic rheology. This critical conversion evaluated at $t_c$ is presented in **Figure 2.9**. Two important observations are immediately evident in this figure. The first is that the critical

conversion gradually increases from ~71 to 93% with increasing secondary hydroxyl content. Moreover, for all the resins examined, the critical conversion at $t_c$ deviates significantly from predictions afforded by the Flory-Stockmayer theory[35,36]. According to this theory, all reactive moieties in a chain possess the same reactivity that does not change as the reaction proceeds and microstructure develops. These results also deviate from Carothers' theory under non-stoichiometric conditions when the statistical secondary hydroxyl content is above 50%.[38–40] Moreover, these theories do not take into account any reactions that form network defects, such as intramolecular cyclization. Deviation from these theories increases further as the secondary hydroxyl content approaches 100%. Similar deviations of theoretical gel points reported in previous studies have been explained by such phenomena as intramolecular cyclization, intramolecular cross-linking, microgelation, and excluded volume effects especially at high molecular weights.[41–44] We attribute such deviation in the present work to two different reasons. One is the catalyst choice, since dibutyltin dilaurate catalyzes the isocyanate reaction with primary hydroxyls and water much more effectively than it catalyzes the reaction of isocyanate with secondary hydroxyls.[37] Although these resins are presumed to be dry, residual water from either the atmosphere or the solvent can react with the isocyanate to form urea. If present, every water molecule will react with two isocyanate functionalities to form a urea linkage.[45]

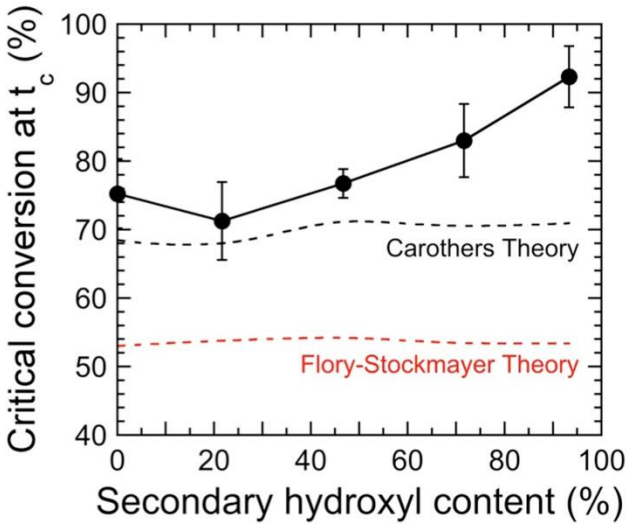


**Figure 0.11.** Critical isocyanate conversion levels evaluated by VT-FTIR spectroscopy at the G'-G" crossover as a function of resin composition. Corresponding predictions from the Flory-Stockmayer theory[35,36] and Carothers' theory[38–40] are also included for comparison (red and black dashed lines, respectively), and the solid line serves to connect the data.

A more significant and related consideration is the unequal reactivity between different types of hydroxyl groups, and the resulting change in $T_g$. The effect of TMCD addition on the $T_g$ of comparable films is the subject of a companion study. These differences are believed to be responsible for heterogeneous cross-linking and corresponding network fluctuations within the system, as confirmed previously by both experimental and computational studies.[46–50] Isocyanate groups on the cross-linking agent react much more rapidly with primary hydroxyls than with secondary hydroxyls. As a result, nearly all the primary hydroxyls react first, creating cross-linked microenvironments possessing a high cross-link density. Due to their size and irregular shape, these fluctuation regions diffuse more slowly and ultimately take a longer time to encounter one another and undergo further cross-linking. In the meantime, however, they continue to react within their local environments, thereby forming larger volumes of more highly cross-linked chains without the formation of a space-filling (percolated) network. Within these

local environments, network defects that do not promote network elasticity development and therefore do not contribute to mechanical properties measured by dynamic rheology up to $t_c$. The chemical reaction continues to proceed, leading to a phenomenon previously reported as gel-point suppression.[51,52] Resultant network defects take the form of loops (which behave as single-anchored polymer tails) instead of bridges (which serve as connecting units during network formation).[28] The existence of loops has been recently quantified using experimental and computational techniques for several chemically cross-linked polymer systems.[51,53–55] The propensity of loop defects is exacerbated by reaction medium concentration, as demonstrated[56] for tetrafunctional reactants. With the presence of ~40 wt% MAK in the present systems, we propose that such defects become increasingly prevalent as the TMCD content is increased, as evidenced by the results displayed in **Figure 2.9**. Fluctuations continue to grow until they ultimately encounter one another, at which time they can react to form a space-filling network.

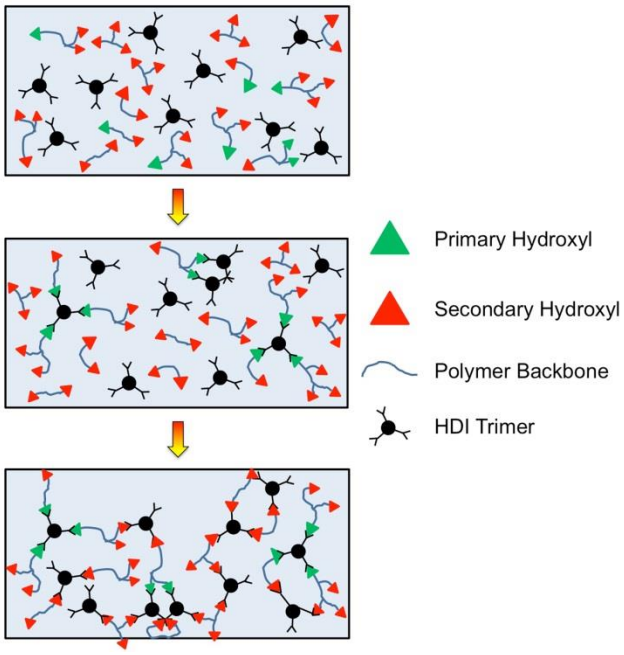


**Figure 0.12**. Schematic representation of the cross-linking reaction of polyester-polyols composed of monomer species with primary and secondary hydroxyl groups (labeled).

## 2.4. Conclusions

In this work, the cross-linking behavior of model polyester-urethane systems has been investigated by both mechanical and chemical means, and the two characterization techniques have been used in conjunction to systematically identify material changes as the systems cross-link and ultimately reach the sol-gel transition. We have established that an incremental increase in the secondary hydroxyl content in the backbone (due to incorporation of TMCD) serves to increase both the reaction time and the critical conversion (measured by VT-FTIR) at the modulus crossover time (measured by dynamic rheology). Although the present resins do not strictly adhere to the Winter-Chambon criterion for gelation,[29,30] the G'-G" crossover is identified here as the effective gel point at which the resins undergo their sol-gel transition. Values of the effective activation energies of gelation and reactivity are in favorable quantitative agreement (within experimental error), directly confirming that the isocyanate reaction is coupled to the growing network. A conceptual rationalization has been proposed to explain deviations from theoretical models (such as Carothers' theory[38–40] and classic Flory-Stockmayer theory[35,36]) that do not consider heterogeneities in cross-linking behavior or loop formation during cure. It lies at the intersection of two competing molecular-level processes: chemical cross-linking and chain vitrification. As the secondary hydroxyl content is increased in the present resins, the stiffness of the backbone also increases due to the sterically hindered nature of the TMCD monomer relative to NPG. This increased stiffness reduces chain mobility and increases cross-linking heterogeneity. Groups of chains are more likely to react with those functional groups in closer proximity, leading to the formation of loops as opposed to branches in the network. **Figure 10** is a schematic illustration of this process. While computer simulations are unavailable to elucidate the conditions responsible for the formation of defects during cure, this explanation is consistent

with previous studies that have identified heterogeneous network formation and loop formation within network-forming polymers.[54,55,57–59] The cure behavior reported in this study provides useful mechano-chemical insight into the cure process of polyester-polyol resins and can be used to design and synthesize multicomponent resins for specific coating applications.

## 2.5. Acknowledgements

This work was supported by the Eastman Chemical Center of Excellence at NC State University. We thank Professor Stefan Franzen in the Department of Chemistry at NC State University for the use of the VT-FTIR spectrometer, as well as Dr. Amulya Pervaje for her assistance in running some FTIR experiments. We also thank Dr. Andrew Detwiler of Eastman Chemical Company for his guidance with this work and for many fruitful discussions regarding its technical content.

## 2.6. References


(1) Garcés, J. M.; Moll, D. J.; Bicerano, J.; Fibiger, R.; McLeod, D. G. Polymeric Nanocomposites for Automotive Applications. *Adv. Mater.* **2000**, *12*, 1835–1839.

(2) Chattopadhyay, D. K.; Raju, K. V. S. N. Structural engineering of polyurethane coatings for high performance applications. *Prog. Polym. Sci.* **2007**, *32*, 352–418.

(3) Yang, Y.; Yu, G.; Cha, J. J.; Wu, H.; Vosgueritchian, M.; Yao, Y.; Bao, Z.; Cui, Y. Improving the Performance of Lithium–Sulfur Batteries by Conductive Polymer Coating. *ACS Nano* **2011**, *5*, 9187–9193.

(4) Twite, R. L.; Bierwagen, G. P. Review of alternatives to chromate for corrosion protection of aluminum aerospace alloys. *Prog. Org. Coatings* **1998**, *33*, 91–100.

(5) Arora, A.; Padua, G. W. Review: Nanocomposites in Food Packaging. *J. Food Sci.* **2010**, *75*, R43–R49.

(6) Raquez, J.-M.; Deléglise, M.; Lacrampe, M.-F.; Krawczak, P. Thermosetting (bio)materials derived from renewable resources: A critical review. *Prog. Polym. Sci.* **2010**, *35*, 487–509.

(7) Bajat, J. B.; Mišković-Stanković, V. B. Protective properties of epoxy coatings electrodeposited on steel electrochemically modified by Zn–Ni alloys. *Prog. Org. Coatings* **2004**, *49*, 183–196.

(8) Sørensen, P. A.; Kiil, S.; Dam-Johansen, K.; Weinell, C. E. Anticorrosive coatings: a review. *J. Coatings Technol. Res.* **2009**, *6*, 135–176.

(9) Belder, E. G.; Rutten, H. J. J.; Perera, D. Y. Cure characterization of powder coatings. *Prog. Org. Coatings* **2001**, *42*, 142–149.

(10) Ramis, X.; Cadenato, A.; Morancho, J. M.; Salla, J. M. Curing of a thermosetting powder coating by means of DMTA, TMA and DSC. *Polymer*. **2003**, *44*, 2067–2079.

(11) Misev, T. A.; van der Linde, R. Powder coatings technology: new developments at the turn of the century. *Prog. Org. Coatings* **1998**, *34*, 160–168.

(12) Decker, C.; Masson, F.; Schwalm, R. Dual-Curing of Waterborne Urethane-Acrylate Coatings by UV and Thermal Processing. *Macromol. Mater. Eng.* **2003**, *288*, 17–28.

(13) Xu, H.; Qiu, F.; Wang, Y.; Wu, W.; Yang, D.; Guo, Q. UV-curable waterborne polyurethane-acrylate: preparation, characterization and properties. *Prog. Org. Coatings* **2012**, *73*, 47–53.

(14) Jones, F. N.; Nichols, M. E.; Pappas, S. P. *Organic coatings : Science and Technology, 4th Ed.*; John Wiley & Sons: Hoboken, NJ, 2017.

(15) Marsh, S. Raising Polyester Performance with TMCD Glycol. In *The Waterborne Symposium : Proc. 39th Ann. Int. Waterborne, High-Solids, Powder Coatings Symp.*; DEStech Publications: Lancaster Penn., 2012; pp. 263–276.

(16) Weiss, K. D. Paint and coatings: A mature industry in transition. *Prog. Polym. Sci.* **1997**, *22*, 203–245.

(17) Kelsey, D. R.; Scardino, B. M.; Grebowicz, J. S.; Chuah, H. H. High Impact, Amorphous Terephthalate Copolyesters of Rigid 2,2,4,4-Tetramethyl-1,3-cyclobutanediol with Flexible Diols. *Macromolecules* **2000**, *33*, 5810–5818.

(18) Li, S.; Vatanparast, R.; Lemmetyinen, H. Cross-linking kinetics and swelling behaviour of aliphatic polyurethane. *Polymer* **2000**, *41*, 5571–5576.

(19) Li, S.; Vatanparast, R.; Vuorimaa, E.; Lemmetyinen, H. Curing kinetics and glass-transition temperature of hexamethylene diisocyanate-based polyurethane. *J. Polym. Sci. B: Polym. Phys.* **2000**, *38*, 2213–2220.

(20) Fernandez d'Arlas, B.; Rueda, L.; Stefani, P. M.; de la Caba, K.; Mondragon, I.; Eceiza, A. Kinetic and thermodynamic studies of the formation of a polyurethane based on 1,6-hexamethylene diisocyanate and poly(carbonate-co-ester)diol. *Thermochim. Acta* **2007**, *459*, 94–103.

(21) Lipshitz, S. D.; Macosko, C. W. Rheological changes during a urethane network polymerization. *Polym. Eng. Sci.* **1976**, *16*, 803–810.

(22) Macosko, C. W. Rheological changes during crosslinking. *Br. Polym. J.* **1985**, *17*, 239–245.

(23) Kim, D. S.; Macosko, C. W. Reaction kinetics and chemorheology of a highly reactive PU system. *Korea Polym. J.* **1996**, *4*, 54–60.

(24) Burel, F.; Feldman, A.; Bunel, C. Hydrogenated hydroxy-functionalized polyisoprene (H-HTPI) and isocyanurate of isophorone diisocyanates (I-IPDI): reaction kinetics study using FTIR spectroscopy. *Polymer* **2005**, *46*, 15–25.

(25) Maji, P. K.; Bhowmick, A. K. Influence of number of functional groups of hyperbranched polyol on cure kinetics and physical properties of polyurethanes. *J. Polym. Sci. A: Polym. Chem.* **2009**, *47*, 731–745.

(26) Lucio, B.; de la Fuente, J. L. Kinetic and chemorheological modelling of the polymerization of 2,4- Toluenediisocyanate and ferrocene-functionalized hydroxyl-terminated polybutadiene. *Thermochim. Acta* **2014**, *596*, 6–13.

(27) Fu, X.; Fan, X. Curing reaction kinetics of HTPE polymer studied by simultaneous rheometry and FTIR measurements. *J. Therm. Anal. Calorim.* **2016**, *125*, 977–982.

(28) Tuhin, M. O.; Ryan, J. J.; Sadler, J. D.; Han, Z.; Lee, B.; Smith, S. D.; Pasquinelli, M. A.; Spontak, R. J. Microphase-Separated Morphologies and Molecular Network Topology in Multiblock Copolymer Gels. *Macromolecules* **2018**, *51*, 5173–5181.

(29) Winter, H. H.; Chambon, F. Analysis of Linear Viscoelasticity of a Crosslinking Polymer at the Gel Point. *J. Rheol.* **1986**, *30*, 367–382.

(30) Chambon, F.; Winter, H. H. Linear Viscoelasticity at the Gel Point of a Crosslinking PDMS with Imbalanced Stoichiometry. *J. Rheol.* **1987**, *31*, 683–697.

(31) Chiou, B.-S.; English, R. J.; Khan, S. A. Rheology and Photo-Cross-Linking of Thiol−Ene Polymers. *Macromolecules* **1996**, *29*, 5368–5374.

(32) Raghavan, S. R.; Chen, L. A.; McDowell, C.; Khan, S. A.; Hwang, R.; White, S. Rheological study of crosslinking and gelation in chlorobutyl elastomer systems. *Polymer* **1996**, *37*, 5869–5875.

(33) Weng, L.; Chen, X.; Chen, W. Rheological characterization of in situ crosslinkable hydrogels formulated from oxidized dextran and N-carboxyethyl chitosan. *Biomacromolecules* **2007**, *8*, 1109–1115.

(34) Madbouly, S. A.; Xia, Y.; Kessler, M. R. Rheological Behavior of Environmentally Friendly Castor Oil-Based Waterborne Polyurethane Dispersions. *Macromolecules* **2013**, *46*, 4606–4616.

(35) Flory, P. J. Molecular Size Distribution in Three Dimensional Polymers. I. Gelation. *J. Am. Chem. Soc.* **1941**, *63*, 3083–3090.

(36) Stockmayer, W. H. Theory of Molecular Size Distribution and Gel Formation in Branched Polymers II. General Cross Linking. *J. Chem. Phys.* **1944**, *12*, 125–131.

(37) Rand, L.; Thir, B.; Reegen, S. L.; Frisch, K. C. Kinetics of alcohol–isocyanate reactions with metal catalysts. *J. Appl. Polym. Sci.* **1965**, *9*, 1787–1795.

(38) Carothers, W. H. Polymers and polyfunctionality. *Trans. Faraday Soc.* **1936**, *32*, 39–49.

(39) Pinner, S. H. Functionality of non-equivalent mixtures. *J. Polym. Sci.* **1956**, *21*, 153–157.

(40) Odian, G. G. *Principles of Polymerization, 4th ed*.; John Wiley & Sons: New York, 2004.

(41) Matsumoto, A.; Okuno, S.; Aota, H. Actual evaluation of flory-stockmayer gelation theory in free-radical monovinyl-divinylcopolymerization. *Macromol. Symp.* **1995**, *93*, 1–10.

(42) Dotson, N. A.; Macosko, C. W.; Tirrell, M. *Synthesis, Characterization, and Theory of Polymeric Networks and Gels*; Plenum Press, 1992.

(43) Anseth, K. S.; Bowman, C. N. Kinetic Gelation model predictions of crosslinked polymer network microstructure. *Chem. Eng. Sci.* **1994**, *49*, 2207–2217.

(44) Naghash, H. J.; Okay, O. Formation and Structure of Polyacrylamide Gels. *J. Appl. Polym. Sci.* **1996**, *60*, 971–979.

(45) Ni, H.; Nash, H. A.; Worden, J. G.; Soucek, M. D. Effect of catalysts on the reaction of an aliphatic isocyanate and water. *J. Polym. Sci. A: Polym. Chem.* **2002**, *40*, 1677–1688.

(46) Miller, D. R.; Macosko, C. W. Average Property Relations for Nonlinear Polymerization with Unequal Reactivity. *Macromolecules* **1978**, *11*, 656–662.

(47) Krakovský, I.; Bubeníková, Z.; Urakawa, H.; Kajiwara, K. Inhomogeneous structure of polyurethane networks based on poly(butadiene)diol: 1. The effect of the poly(butadiene)diol content. *Polymer* **1997**, *38*, 3637–3643.

(48) Tanaka, Y.; Stanford, J. L.; Stepto, R. Interpretation of Gel Points of an Epoxy-Amine System Including Ring Formation and Unequal Reactivity: Measurements of Gel Points and Analyses on Ring Structures. *Macromolecules* **2012**, *45*, 7197–7205.

(49) Elliott, J. E.; Bowman, C. N. Kinetics of Primary Cyclization Reactions in Cross-Linked Polymers: An Analytical and Numerical Approach to Heterogeneity in Network Formation. *Macromolecules* **1999**, *32*, 8621–8628.

(50) Dušek, K. In *Epoxy Resins and Composites III*; Springer-Verlag: Berlin/Heidelberg, 1986; pp. 1–59.

(51) Wang, R.; Lin, T.-S.; Johnson, J. A.; Olsen, B. D. Kinetic Monte Carlo Simulation for Quantification of the Gel Point of Polymer Networks. *ACS Macro Lett.* **2017**, *6*, 1414–1419.

(52) Yan, M.; Huang, Y.; Lu, M.; Lin, F.-Y.; Hernández, N. B.; Cochran, E. W. Gel Point Suppression in RAFT Polymerization of Pure Acrylic Cross-Linker Derived from Soybean Oil. *Biomacromolecules* **2016**, *17*, 2701–2709.

(53) Wang, R.; Johnson, J. A.; Olsen, B. D. Odd–Even Effect of Junction Functionality on the Topology and Elasticity of Polymer Networks. *Macromolecules* **2017**, *50*, 2556–2564.

(54) Kawamoto, K.; Zhong, M.; Wang, R.; Olsen, B. D.; Johnson, J. A. Loops versus Branch Functionality in Model Click Hydrogels. *Macromolecules* **2015**, *48*, 8980–8988.

(55) Zhong, M.; Wang, R.; Kawamoto, K.; Olsen, B. D.; Johnson, J. A. Quantifying the impact of molecular defects on polymer network elasticity. *Science* **2016**, *353*, 1264–1268.

(56) Lin, T.-S.; Wang, R.; Johnson, J. A.; Olsen, B. D. Topological Structure of Networks Formed from Symmetric Four-Arm Precursors. *Macromolecules* **2018**, *51*, 1224–1231.

(57) Wang, J.; Lin, T.-S.; Gu, Y.; Wang, R.; Olsen, B. D.; Johnson, J. A. Counting Secondary Loops Is Required for Accurate Prediction of End-Linked Polymer Network Elasticity. *ACS Macro Lett.* **2018**, *7*, 244–249.

(58) Dušek, K.; Galina, H.; Mikeš, J. Features of network formation in the chain crosslinking (co)polymerization. *Polym. Bull.* **1980**, *3*, 19–25.

(59) Mayne, J. E. O.; Scantlebury, J. D. Ionic conduction in polymer films: II. Inhomogeneous structure of varnish films. *Br. Polym. J.* **1970**, *2*, 240–243.

# CHAPTER 3: THERMOMECHANICAL AND FREE-VOLUME PROPERTIES OF POLYESTER POLYOL FILMS FOR COATINGS APPLICATIONS: ROLE OF DIOL COMPOSITION*

## 3.1. Introduction

Thermosetting polymers constitute a popular material of choice for numerous applications, extending from coatings and adhesive films to bulk structural parts.[1–9] These systems are highly attractive primarily because of their inherent ability to form irreversible and densely cross-linked networks under a variety of temperature and/or radiation conditions, as well as the physical properties that the networks impart.[10–13] Such materials generally possess a wide range of mechanical properties that are dictated by the backbone chemistry in conjunction with a material/ process-tunable degree of cross-linking. In this class of polymers, polyurethanes have developed a particularly versatile niche due to their broadly accessible physical properties, which makes them especially attractive for multiple coatings applications including waterborne, self-healing and textile applications.[14–21] In general, the thermomechanical properties for coatings must adhere to quality standards uniquely established for each application,[22] in which case it is critically important to design the polymer backbone so that it satisfies the requirements of the target application. In the case of a backbone composed of multiple constituent species specifically chosen to endow the resultant macromolecule with desired properties, monomer selection can be greatly expedited through the use of emerging combinatorial[23,24] and computational[25,26] methods, as recently evidenced by reasonably accurate prediction of the glass transition temperature ($T_g$) for designer polyester polyols from monomer properties alone.[27]

Previously, we have investigated the temperature-dependent chemical conversion (from time-resolved Fourier-transform infrared spectroscopy) and gelation behavior (from dynamic

strain-controlled rheology) of a series of polyester polyols that systematically incorporate 2,2,4,4-tetramethyl 1,3-cyclobutanediol (TMCD). This relatively uncommon monomer has been successfully incorporated[28] into thermoplastic polyesters and commercialized as part of the Tritan® copolyester line manufactured by the Eastman Chemical Company. Results from prior efforts[29,30] have demonstrated that TMCD improves the mechanical properties of polyester-based systems by delivering an excellent balance of hardness and flexibility. It also promotes good outdoor weathering capability in polyester systems, and its incorporation in a polyester backbone has been observed[28–30] to improve both thermal stability and mechanical properties while ensuring optical transparency. Although TMCD has been routinely introduced into thermoplastic polyesters, studies investigating its use in thermosetting polymer systems are few. In light of the potential benefits TMCD can introduce into such polymers, we investigate a series of model polyester polyols to elucidate the relationship between polymer composition, cure condition and film properties, such as thermal, mechanical and free-volume. More specifically, the work described herein affords a systematic interrogation of the effect of TMCD loading on property development in films cured under two different thermal conditions.

## 3.2. Experimental

### *3.2.1. Materials*

Polyester resins were kindly supplied by the Eastman Chemical Company (Kingsport, TN) and used as-received. **Figure 3.1** depicts the chemical structures of all the monomers used in the synthesis of the polyester resins. The cross-linking agent was hexamethylene diisocyanurate (HDI trimer), purchased from Covestro (Desmodur 3390 BA/SN) and is included in **Figure 3.1**. Dibutyltin dilaurate (95%) was obtained from Sigma-Aldrich (St. Louis, MO), whereas urethane-grade methyl amyl ketone (MAK) was also provided by the Eastman Chemical

Company. Both were likewise used without further purification.

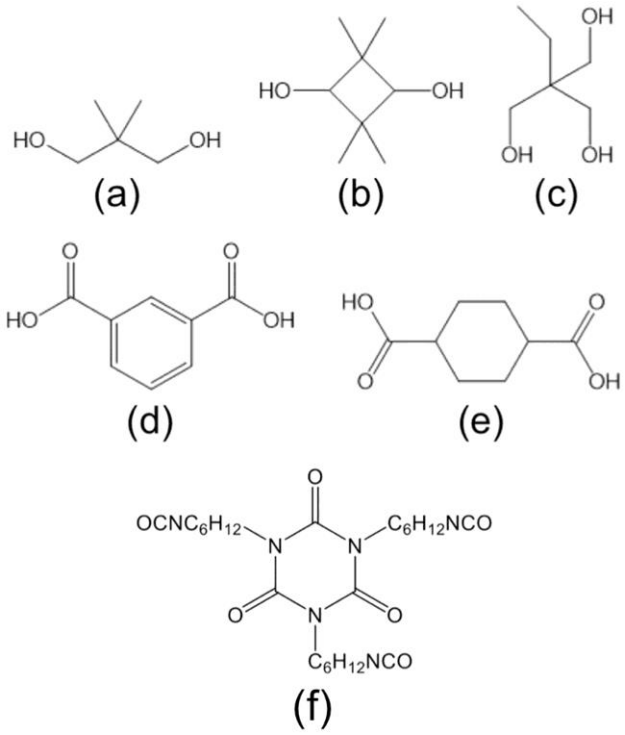


**Figure 0.13**. Chemical structures of the monomers used to synthesize the present polyester-polyol resins: (a) neopentane glycol (NPG), (b) 2,2,4,4-tetramethyl 1,3-cyclobutanediol (TMCD), (c) trimethylolpropane (TMP), (d) isophthalic acid (IPA), and (e) 1,4-cyclohexanediacid (CHDA). The chemical structure of the HDI trimer cross-linking agent is included in (f).

### *3.2.2. Methods*

#### 3.2.2.1. Specimen Preparation

Gel permeation chromatography (GPC) was conducted in the same manner as our previous work[31]. The composition and properties of the resins employed in this study are listed in **Table 3.1**. The dibutyltin dilaurate catalyst was mixed with MAK to yield a 1 wt% catalyst solution, which was added at 2.5 wt% (relative to the total solids) to a known

**Table 0.3.** Compositions and select molecular characteristics of polyester-polyol resins.

| | Diol (wt%) | | | Diacid (wt%) | | | | | |
|---|---|---|---|---|---|---|---|---|---|
| Specimen Designation | NPG | TMCD | TMP | CHDA | IPA | $M_n$ (Da) | Đ | OH # | TMCD[a] (wt%) |
| 0T | 93.35 | — | 6.65 | 50 | 50 | 1562 | 1.68 | 113 | 0 |
| 25T | 71.63 | 21.68 | 6.65 | 50 | 50 | 1616 | 1.76 | 111 | 25 |
| 50T | 46.65 | 46.65 | 6.65 | 50 | 50 | 1590 | 1.75 | 102 | 50 |
| 75T | 21.68 | 71.63 | 6.65 | 50 | 50 | 1707 | 1.78 | 97 | 75 |
| 100T | — | 93.35 | 6.65 | 50 | 50 | 1799 | 1.77 | 91 | 100 |

[a] Relative to the diol content.

quantity of polyester resin in anhydrous MAK. This catalyst/polyester/solvent mixture was then agitated in the presence of a magnetic stir bar in a 20 mL glass scintillation vial until the polymer was fully dissolved (~8 h). A predetermined quantity of the resultant solution was added to a 10 mL glass scintillation vial, and the cross-linking agent was added dropwise under agitation to achieve a NCO:OH stoichiometric ratio of 1.10 ± 0.02:1 at a constant solids content of 60 ± 2%. This mixture was then placed on a stir plate for 5 min at ambient temperature prior to film casting. Films were cast on three different substrates with a Gardco® multiple clearance square applicator at a wet film thickness of 76.2 □m. The substrates included Teflon®-coated aluminum (for dynamic mechanical analysis, DMA, and differential scanning calorimetry, DSC), aerospace-grade aluminum (for nanoindentation, NI) and Kapton® polyimide film (for positron annihilation lifetime spectroscopy, PALS). Immediately following casting, the films were cured in an oven for 1 h at either 60 °C (lo-bake, LB) or 120 °C (hi-bake, HB) at atmospheric pressure

and then stored at ambient conditions for at least 1 week before testing. Dry film thicknesses ranged from *ca*. 15-25 μm.

3.2.2.2. Property Characterization

The DSC measurements were performed on a TA Instruments Q2000 calorimeter with a TZero aluminum pan and lid used as the reference. Once a predetermined amount of each resin was placed in the pan, the pan was sealed and the resin was heated from □20 to 180 °C at a heating rate of 5 °C/min. The $T_g$ values reported here were calculated from the inflection point in the second heating cycle. Complementary DMA was conducted on a TA Instruments Q800 instrument operated in tensile mode. Only HB films were examined here due to the inherent brittleness of the LB films. Film samples were first cut into rectangles measuring approximately 15 mm x 6.35 mm and then loaded into the instrument. A pre-load force of 0.05 N was initiated to ensure constant tension, and force tracking with a minimum dynamic force of 0.05 N was implemented. A displacement of 50 μm at 1 Hz resided within the linear viscoelastic regime for the resins examined and was thus utilized for all dynamic measurements. Isochronal temperature ramps were performed from □20 to 180 °C at a heating rate of 3 °C/min. Measurements were performed in triplicate (DSC) and duplicate (DMA) to ensure reproducibility. Analysis of DSC and DMA data was performed with the TA Instruments Universal Analysis software package.

For NI testing, film samples cast on aluminum substrates were cut into approximately 1.5 mm x 1.5 mm squares, which were subsequently mounted onto magnetic stubs. Measurements were conducted under load control using a Hysitron Ubi-1 instrument outfitted with a diamond Berkovich tip. For each sample, three separate areas measuring 60 □m x 60 □m were scanned and six indents were generated in each area. The indentation procedure consisted of a 20 s load period, followed by a 60 s hold at the maximum indentation force and finally a 2 s unload period.

Data analysis was performed with the Triboscan software package. Molecular-level free volume of bulk films was measured at ambient temperature (~22°C) by PALS in the Department of Nuclear Engineering at North Carolina State University. Pieces of each Kapton-backed film were placed on either side of a $^{22}$Na positron source for ~12 h at ambient temperature. [Kapton was selected due to its known[32] inability to form *o*-positronium, in which case it does not contribute to measured annihilation events.] Measurements started with the birth of positrons, identified by emission of γ radiation at 1274 keV, and terminated with an annihilation event that coincided with γ emission at 511 keV. Due to the uniqueness of this measurement, analysis of the data is described in detail later.

## 3.3. Results and Discussion

### *3.3.1. Thermal Analysis*

Differential scanning calorimetry provides the $T_g$ of the neat resins before cross-linking, as well as the cross-linked films cured under both LB and HB conditions. Measured $T_g$ values are presented in **Figure 3.2a** and reveal two important features. The first is that $T_g$ consistently increases significantly with increasing TMCD content irrespective of thermal history. In the case of the neat resin, this increase translates to about 59 °C when the NPG is completely replaced by TMCD. The cross-linked resins display, albeit less pronounced, changes in $T_g$ (in °C): 43 (LB) and 49 (HB). The second noteworthy attribute of the data evident in **Figure 3.2a** is that $T_g$ increases systematically with increasing cure temperature. Differences in $T_g$ between the neat resin and the LB resins range from 14 to 33 °C, whereas those between the LB and HB resins are lower: 10 to 22 °C. Since the $T_g$ generally provides a metric of local segmental motion of polymer chains as they overcome thermal barriers associated with restricted motion in the glassy state, the results furnished in **Figure 3.2a** indicate that (*i*) substitution of TMCD for NPG

promotes chain rigidity in these polyester polyols and (*ii*) increasing the cure temperature increases chemical conversion within the system and densifies the network structure, yielding a further increase in $T_g$. The measured $T_g$ results acquired by DSC from the HB resins are also included in **Figure 3.2b** for direct comparison with our DMA findings, which are discussed in the following section.

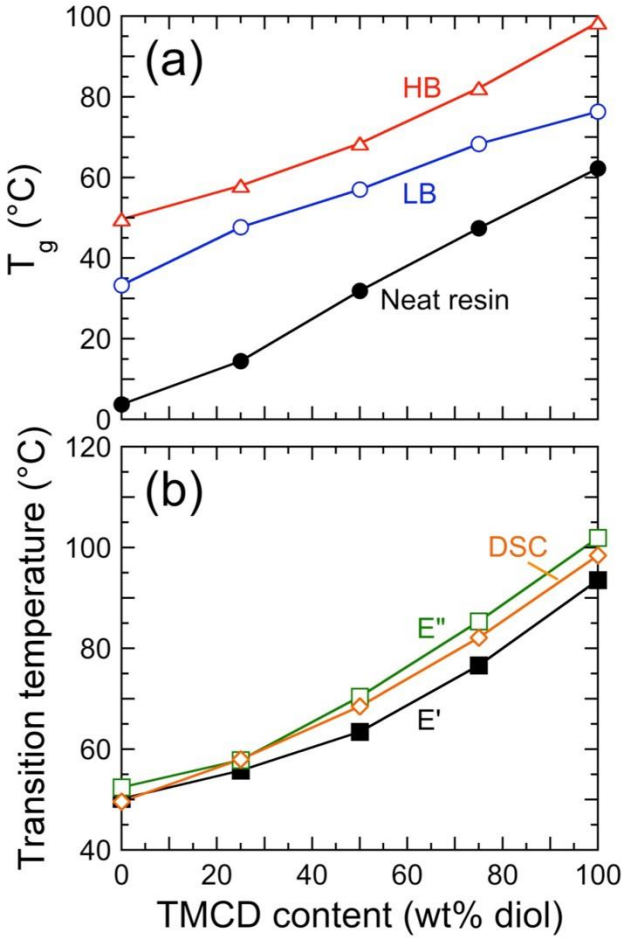


**Figure 0.14**. (a) Glass transition temperature ($T_g$) values of the neat resin and films cured at two temperatures (60 °C, LB; 120 °C, HB) presented as a function of TMCD content in polyester-polyol resins, as measured by DSC. (b) Comparison of transition temperatures of HB films as determined by DSC, the onset of the E' drop-off and the peak in E". The color-coded solid lines serve to connect the data.

*3.3.2. Mechanical Analysis*

The bulk mechanical properties of the five HB resins have been evaluated as a function of temperature by DMA (the LB resins are omitted since they form poor free-standing films). Results from these tests are shown in **Figure 3.3**, in which the temperature dependence of the dynamic storage and loss moduli (E' in **Figure 3.3a** and E'' in **Figure 3.3b**, respectively) is provided as a function of TMCD loading. All the HB resins possess a similar value of E' (≈2 GPa) in the glassy state (the minimum $T_g$ from DSC in **Figure 3.2** is ≈50 °C), which is expected[33–35] for thermosetting polymers of this nature. As the temperature is increased, each resin exhibits a precipitous reduction in E' as the specimen transitions from its glassy to rubbery state. It immediately follows that the onset of each abrupt plunge in E' corresponds roughly to $T_g$. As anticipated from the DSC results reported in **Figure 3.2**, the temperature at which this onset occurs is directly proportional to the fraction of TMCD incorporated into the resin backbone. That is, these DMA results corroborate that $T_g$ for these polyester polyols increases systematically with increasing TMCD content. Temperatures above $T_g$ correspond to the rubbery plateau, from which the cross-link density can typically be extracted. In the present resin systems, however, E' increases upon further heating (especially pronounced in TMCD-lean formulations), in which case a reliable cross-link density from each resin is indiscernible. While the precise reason for this behavior is unknown at this time, we posit that it likely reflects additional densification due to continued curing. Moreover, at these temperatures above $T_g$, values of E' are, for the most part, inversely proportional to the TMCD level in each resin, indicating that these rubbery resins generally become more flexible as the fraction of TMCD is increased.

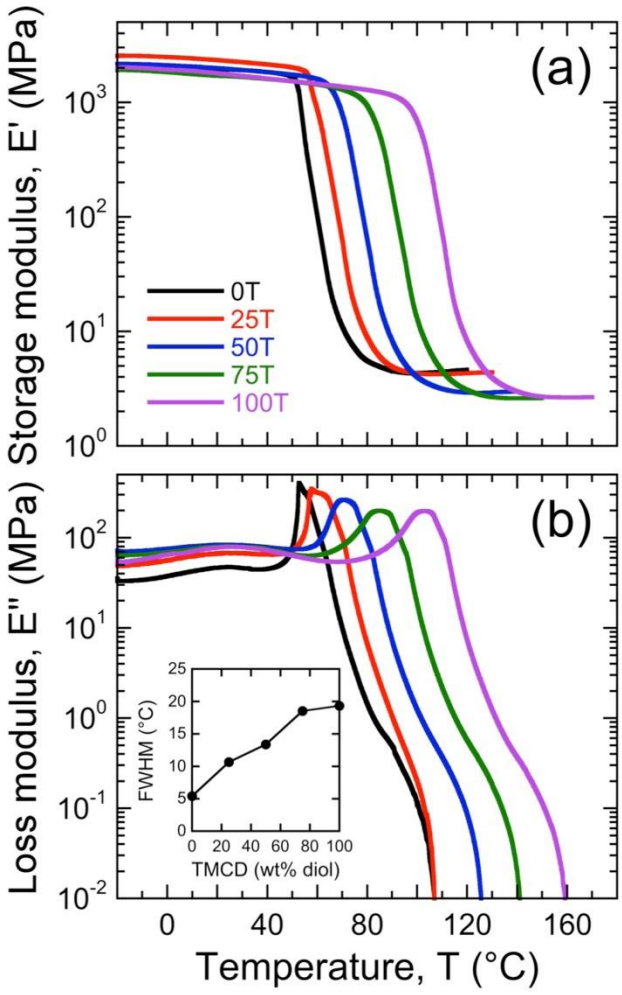


**Figure 0.15**. Temperature dependence of the dynamic (a) storage and (b) loss tensile moduli (E' and E", respectively) of the HB films (labeled and color-coded) from DMA. The inset in (b) displays the full-width at half-maximum (FWHM) of the E" peaks as a function of TMCD content.

The associated loss (E") moduli for the five HB resins are included as a function of temperature in **Figure 3.3b**. In the vicinity of 25 °C, all of these resins appear to exhibit a β-relaxation indicative of CHDA ring-flip, since this characteristic is independent of TMCD content. Similar phenomena have been previously reported[36] for polymers possessing main-chain aliphatic rings. At higher temperatures, each resin displays a well-defined E" peak at a composition-dependent temperature due to the presence of an □-relaxation, which directly

relates to $T_g$. As indicated from DSC in **Figure 3.2** and E' in **Figure 3.3a**, the locations of these peaks monotonically shift to higher temperatures as the TMCD level is increased. Values of $T_g$ ascertained from these three independent analyses compare favorably in **Figure 3.2b**, with a maximum difference (between $T_g$ values extracted from E' and E") of less than 9 °C. In fact, the maximum difference in $T_g$ evaluated from DSC and E" measurements is less than 4 °C, strongly suggesting that these thermal and mechanical features correspond to the same molecular phenomenon; that is, cooperative segmental motion of polymeric chains on a large scale.[37] Values of $T_g$ assessed at the precipitous onset of E', which is often attributed to the mechanical failure of films, is consistently the lowest of the three measurements. This value of $T_g$ is especially useful when evaluating materials for end-use applications, as it identifies the maximum operating temperature of a polymeric material that must remain glassy. At temperatures above the primary peak in the curves displayed in **Figure 3.3b**, E" for each resin (irrespective of TMCD content) undergoes an abrupt two-stage reduction to the level at which reliable measurement is not possible due to insufficiently low signal-to-noise.

Another noteworthy feature of **Figure 3.3b** is that the shapes of the □-relaxation peaks in E" likewise change with increasing TMCD content. For instance, the resin with no TMCD exhibits a large and sharp peak. As the TMCD content of the HB resins is increased, however, the peak not only decreases in magnitude but also broadens. This phenomenon can be explained by considering the network structure within these resins, as well as the nature of the measurement under consideration. A peak in E" corresponds to a maximum in energy dissipation by a specimen as a consequence of viscous losses. A spatially and chemically uniform network is expected to yield a single, sharp peak, indicating that segmental motion occurs throughout the bulk film at nearly the same time as chains, formerly in glassy "cages," become mobile and move

past nearest neighbors. As the TMCD content is increased, this peak decreases in magnitude and becomes broader, which implies that the network becomes increasingly more heterogeneous. The extent of this TMCD-induced peak broadening in HB resins, evaluated at the full-width at half maximum (FWHM), is evident from the results included in the inset of **Figure 3.3b**. This type of phenomenon has been previously reported[38,39] for fully-cured double-network epoxies and has been attributed to an increase in network heterogeneity.[40] This conclusion is also in qualitative agreement with our recent findings, which suggest that TMCD increases network heterogeneity in polyester-polyol systems as evidenced by gel point depression.[31]

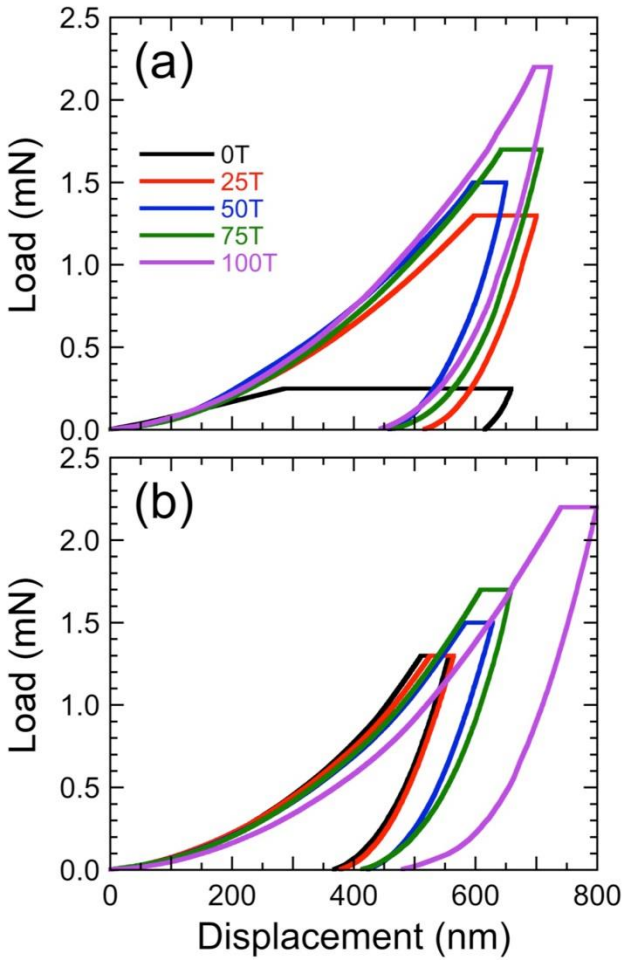


**Figure 0.16.** Load-displacement curves for (a) LB and (b) HB polyester-polyol films with different levels of TMCD (labeled and color-coded) from NI.

In addition to investigating the effect of TMCD on the bulk mechanical properties of polyester-polyol films, we have likewise interrogated the role of TMCD on the surface mechanical properties of LB and HB films with NI. In this case, the indentation loads listed in **Table 3.2** are necessarily varied to maintain a maximum indentation depth between *ca*. 500 and 800 nm. Representative load-displacement curves for films cured under LB and HB conditions are presented in **Figures 3.4a** and **3.4b**, respectively. Due to the nature of NI, contact mechanics

**Table 0.4.** Maximum indentation loads for LB and HB polyester-polyol films.

| Specimen designation | LB maximum indentation load (mN) | HB maximum indentation load (mN) |
|---|---|---|
| 0T | 0.25 | 1.30 |
| 25T | 1.30 | 1.30 |
| 50T | 1.50 | 1.50 |
| 75T | 1.70 | 1.70 |
| 100T | 2.20 | 2.20 |

must be employed to interpret the data. Analysis of the NI results has been performed in the context of the Oliver-Pharr theory.[41] According to this framework, the reduced modulus ($E_r$), which represents a composite modulus of two bodies in contact, is related to the slope of the unload curve ($S = dP/dh$, where $S$ constitutes stiffness, $P$ is the load and $h$ represents the indenter height) at the point of unloading, and is typically calculated by first fitting a power-law function to the unload curve. At the point of unloading, $E_r$ can be written in terms of $S$ as

$$E_r = \frac{\sqrt{\pi}}{2\beta}\frac{S}{\sqrt{A}} \tag{3.1}$$

where $\beta$ is a correction factor to account for the indenter geometry (~1.07 for a Berkovich indenter), and $A$ is the calculated contact area. Once $E_r$ is extracted from each load-displacement curve, the surface modulus of each film ($E_s$) is then computed from

$$\frac{1}{E_r} = \frac{(1-\nu^2)}{E_s} + \frac{(1-\nu_{tip}{}^2)}{E_{tip}} \tag{3.2}$$

where $E_{tip}$ is the modulus of the indenter tip, and $\nu$ and $\nu_{tip}$ correspond to Poisson's ratios of the specimen and indenter tip, respectively. For the diamond Berkovich tip employed in this study, the Poisson's ratio and modulus are 0.07 and 1140 GPa, respectively.[42] Previous studies[43] investigating similar thermosetting polymers have assumed $\nu$ = 0.4, in which case we have done the same with all the LB and HB films, recognizing that their mechanical properties vary.

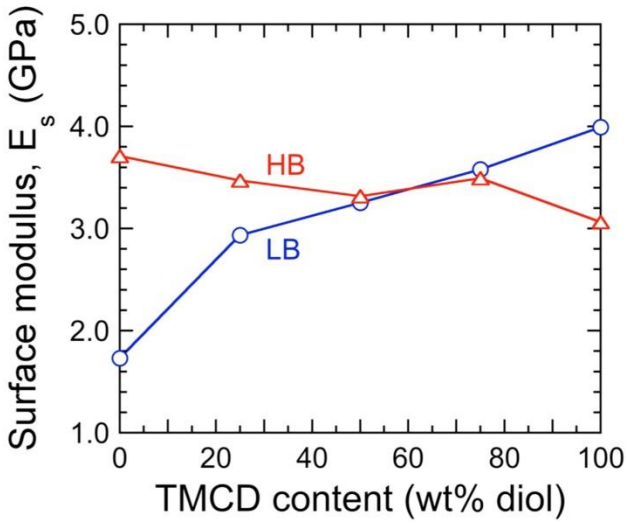


**Figure 0.17.** Surface modulus (Es) of polyester-polyol films cured under LB and HB conditions (labeled and color-coded) as calculated from NI measurements in conjunction with Eqs. 3.1 and 3.2 in the text.

Surface moduli calculated according to **Eq. 3.2** are provided in **Figure 3.5** for all specimens cured under both LB and HB conditions. In the case of the LB films, $E_s$ is strongly correlated

with the TMCD content in the polyester backbone, increasing by about 130% (up to 4.0 GPa) as the fraction of TMCD increases from 0 to 100 wt%. In marked contrast, however, $E_s$ is observed to fluctuate between 3.0 and 3.8 GPa over the entire composition range for HB films. This significant difference in surface properties suggests that, in addition to polymer network mechanics, additional effects not explicitly considered in the Oliver-Pharr analysis may play a role in the observed mechanical response. We return to discuss this topic further below. In addition to $E_s$, another parameter commonly referred to as the plasticity index ($\Psi$) is used to distinguish the plastic and elastic character of a material.[44,45] This parameter is calculated from the areas under specific parts of the load-displacement curves, as illustrated in **Figure 3.6a**. From these areas identifying elastic and plastic work, $\Psi$ can be determined from

$$\Psi = \frac{w_p}{w_p + w_e} \tag{3.3}$$

where $w_p$ is the plastic work done on the sample by the indenter tip, and $w_e$ is the elastic work done by the sample on the indenter tip. If $\Psi = 0$, the measured mechanical response is fully elastic, whereas $\Psi = 1$ corresponds to a fully plastic response. Values of $\Psi$ between 0 and 1 are indicative of viscoelasticity. In **Figure 3.6b**, the plasticity indices of the polyester-polyol films cured under LB and HB conditions are displayed as a function of TMCD content and reveal two interesting features. The first is that $\Psi$ calculated for the LB films monotonically decreases (from a nearly plastic response of the TMCD-free specimen) as the fraction of TMCD in the polyester backbone increases. Conversely, $\Psi$ for films subjected to HB cure conditions appears independent of TMCD content but generally lower than that for LB films (an interesting and unexpected outcome in **Figure 3.6b** is that $\Psi_{LB} \approx \Psi_{HB}$ when the diol is 100 wt% TMCD).

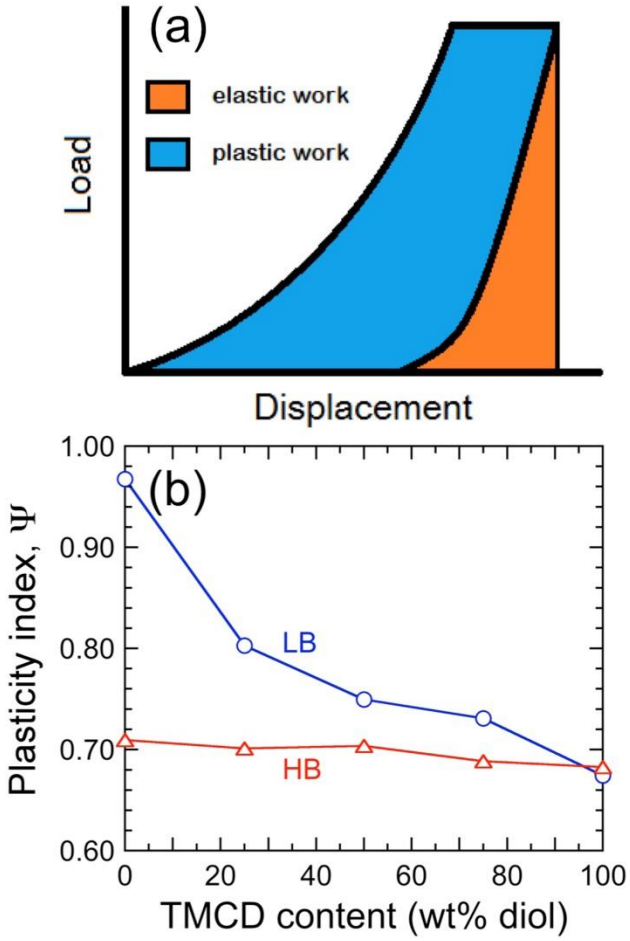


**Figure 0.18**. (a) Schematic depiction of the plastic and elastic work contributions from NI load-displacement curves used to ascertain the plasticity index (ψ). (b) Values of ψ determined for LB and HB specimens (labeled and color-coded) and presented as a function of TMCD content.

The data presented in **Figure 3.6b** for the LB films suggest that incorporation of TMCD reduces the extent of plastic work during NI. A recent study[31] of the cross-linking behavior of these same polyester-polyol systems has, however, revealed that increasing TMCD content substantially reduces resin reactivity and consequently increases gelation time. If this outcome is considered alongside the observation that films containing TMCD do not form a free-standing film after being cured under LB conditions (60 °C for 1 h), we question whether the corresponding NI results represent the true indentation response of the LB films or a different

phenomenon often encountered[46] with polymeric materials and known as "pile-up." Scanning probe microscopy (SPM) images acquired after the indentations yield line scans that bisect the triangular indent three ways. On one side of most of the line scans included in **Figure 3.7** (except for the LB TMCD-free film), a pile of rim material introduced during NI is evident. Pile-up areas for resins subjected to both cure conditions have been measured and compiled in **Figure 3.8**. From these data, the pile-up area increases with increasing TMCD content at constant cure temperature and decreasing cure temperature. While incomplete cross-linking at high TMCD levels likewise explains the inability of LB films to form free-standing films, HB cure conditions serve to lessen the effect of TMCD on not only pile-up in **Figure 3.8** but also $\Psi$ in **Figure 3.6b** and $E_s$ in **Figure 3.5**. Although this analysis is primarily qualitative, an increase in rim pile-up would increase the contact area of the indenter tip beyond that calculated, which would artificially increase $E_s$. A detailed, systematic examination of pile-up capable of affording additional insight into surface mechanics, is beyond the scope of this work.

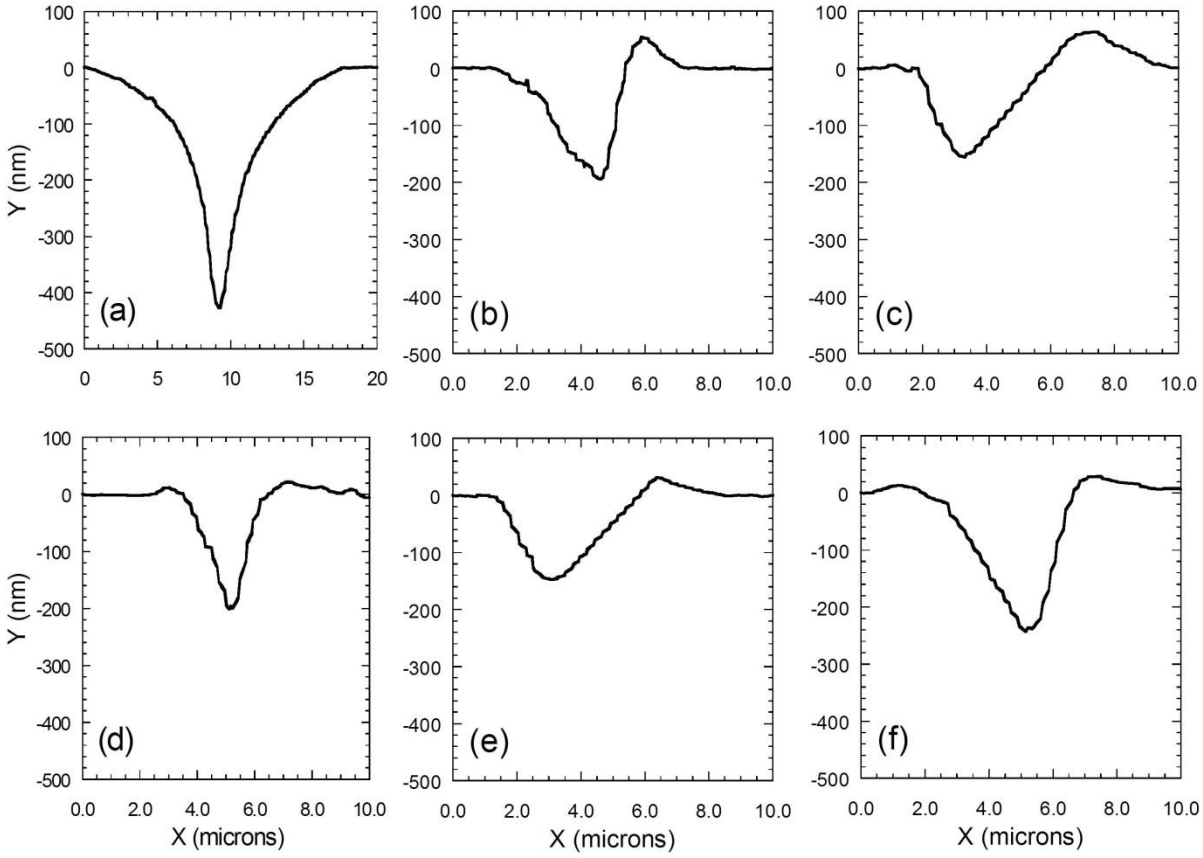


**Figure 0.19.** Line scans extracted from representative SPM topographical data of nanoindentations acquired from polyester-polyol films varying in TMCD content (in wt% diol) — (a,d) 0, (b,e) 50 and (c,f) 100 — under LB (top row) and HB (bottom row) cure conditions.

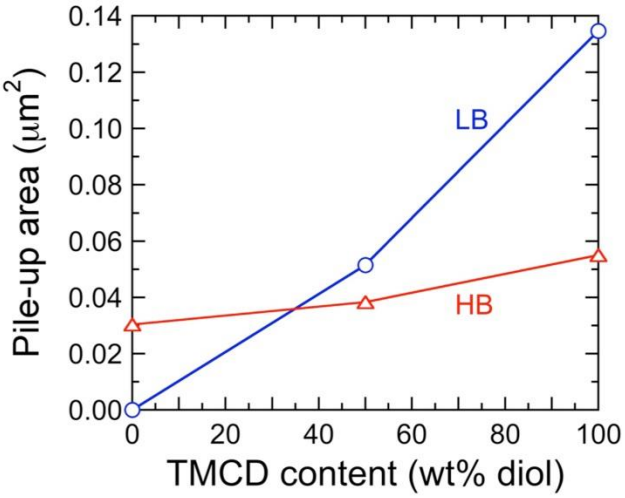


**Figure 0.20.** Rim pile-up areas calculated from the line scans provided in Figure 3.7 and displayed as a functions of cure condition (labeled and color-coded) and TMCD content.

*3.3.3. Free Volume Analysis*

One of the most useful techniques to directly probe the free-volume characteristics of polymeric materials is PALS.[47–49] Positrons from a radioactive source ($^{22}$Na in this study) bombard the specimen and localize in internal regions of low electron density. During PALS, three types of annihilation events produce detectable γ radiation. The positrons lose energy through inelastic collisions and undergo annihilation with surrounding electrons. They can also couple with electrons to form a metastable bound state, known as a positronium (Ps). Positronia can exist in two states on the basis of the relative spins of the positron and electron. If they are the same, they form the singlet-state *para*-positronium (*p*-Ps), whereas if they have opposite spins, they form the triplet-state *ortho*-positronium (*o*-Ps). Due to its relatively long lifetime (142 ns in vacuum[50]), *o*-Ps is more suitable to probe the size and population of free volume voids in polymers (the lifetime of *o*-Ps is substantially reduced in condensed matter due to a "pick-off" process[51]). Normalized intensity (*I*) results acquired by PALS are displayed as a function of detection time (*t*) in **Figure 3.9** for polyester-polyol films cured under LB and HB conditions

(**Figures 3.9a** and **3.9b**, respectively). These data are analyzed as a summation of at least three exponential decay terms according to

$$I(t) = \sum_{j=1}^{n} I_j \exp\left(-\frac{t}{\tau_j}\right) \tag{3.4}$$

where $I_j$ and $\tau_j$ denote the intensity (or number-density population) and characteristic lifetime, respectively, of the $j^{th}$ annihilation component.

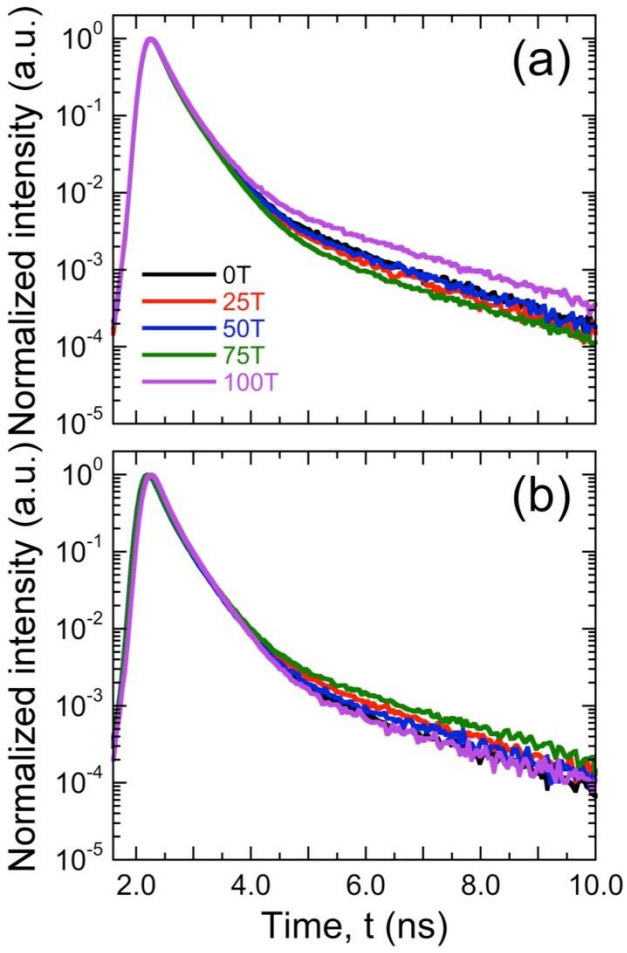


**Figure 0.21.** Normalized annihilation intensity as a function of o-Ps lifetime for (a) LB and (b) HB polyester-polyol resins differing in TMCD content (labeled and color-coded) and measured at ambient temperature.

The first two components correspond to short-lived events unsuitable to describe the nanoscale structure of polymers, but the third component corresponds to the annihilation of *o*-Ps

in polymeric media (in some cases a fourth component is introduced, but we only consider three components here). The characteristic lifetime associated with this component ($\tau_3$, in ns) directly relates to free-volume pore size by detailed theoretical formalisms such as the classic Tao-Eldrup model, which assumes spherical free-volume elements in the following form:[52,53]

$$\tau_3 = \frac{1}{2}\left(1 - \frac{r}{r+\Delta r} + \frac{1}{2\pi}\sin\left(\frac{2\pi r}{r+\Delta r}\right)\right)^{-1} \quad (3.5)$$

Here, $r$ is the radius of a free-volume element, and $\Delta r$ accounts for the polymer electron shell extending into the free volume void[54] (assigned an empirical value of 0.166 nm). Although this model accurately accounts for the physics underlying PALS and, for this reason and the simplifying assumption of spherical pores, remains a popular choice for quantifying free-volume elements in polymeric media, the free-volume void sizes reported here utilize a shape-free model, the details of which are discussed elsewhere.[55] The model, derived from quantum mechanics, does not have a closed analytical form. Calculated $\tau_3$ values and the average free-volume pore diameter ($D$) are presented in **Figures 3.10a** and **3.10b**, respectively, for the LB and HB films. Both $\tau_3$ and $D$ are observed to increase systematically with increasing TMCD content. The increase in average free-volume pore diameter for both LB and HB samples is not very large, about 9%, as the TMCD content increases from 0 to 100 wt%. Under these same conditions, however, the measured $T_g$ is likewise observed in **Figure 3.2a** to increase. Taken together, these results are contrary to established theories[56–59] that associate an increase in free volume with a reduction in $T_g$. The process of physical aging via sub-$T_g$ annealing is known to cause a reduction in the size of free volume elements in amorphous media, including crosslinked polymeric networks.[60] Due to the significant increase in glass transition temperature with increasing TMCD content, and the fact that the films were kept at room temperature, there may be an effect of physical aging in these films, whereby the low-$T_g$ films have densified to a greater

degree than the high-$T_g$ films. The effects of physical aging on these systems is beyond the scope of this work, however it could provide an interesting future topic of study.

Not included here (due to the relatively low recorded intensities), the composition-dependent product $I_3\tau_3$, which provides a measure of the total free volume, likewise increases monotonically with increasing TMCD content for both LB and HB specimens and is consistently higher for LB films. This latter feature can be explained by the higher extent of reaction and a denser network structure achieved under HB, compared to LB, cure conditions. A similarly important consideration especially for coating materials of this genre is that an increase in free-volume dimensions is anticipated[61] to be accompanied by enhanced permeability of small-molecule penetrants. While barrier performance constitutes an important and relevant property, measurement of molecular transport through the current films is, however, beyond the scope of this study.

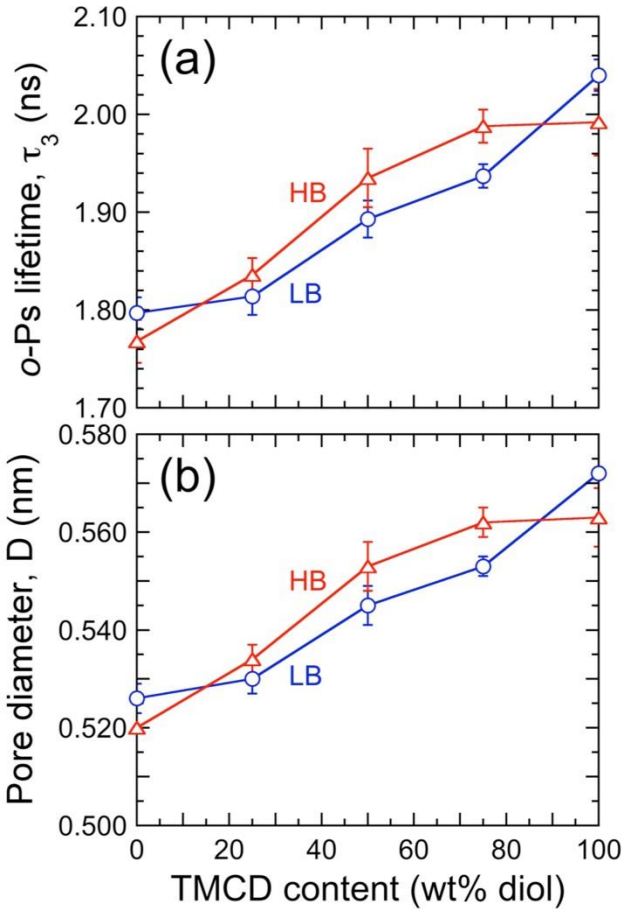


**Figure 0.22**. Values of (a) $\tau_3$ and (b) D extracted from the PALS data provided in Figure 3.9 for LB and HB films varying in TMCD content (labeled and color-coded). The pore diameter in (b) corresponds to the shape-free equivalent of the spherical free-volume elements calculated from the Tao-Eldrup model.

### 3.4. Conclusions

This work provides a systematic study of the effect of TMCD content on polyester-urethane films cured at two different conditions. The authors have shown that incorporating TMCD in a polyester-urethane backbone can significantly increase the $T_g$ of the cross-linked film, especially when cured at high temperatures. The incorporation of TMCD does not significantly affect the elastic modulus of films at temperatures below the glass transition, however it does increase the operating temperature range of films with increased levels of

TMCD by delaying the E' onset to higher temperatures. As TMCD content is increased, the width of the glass transition (as measured by a peak in E'') increases, suggesting heterogeneity in the cross-linked network, which is in agreement with previous works. It also corresponds with a large increase in observed surface modulus for LB films, however this relationship is muted for HB films. It is shown that the "pile-up" phenomenon is occurring non-uniformly for samples cured under different conditions and containing varying levels of TMCD, suggesting artificial inflation of measured surface moduli values. The average free volume hole size of films also increases proportionally with TMCD content and does not strongly depend on cure conditions. As such, it can be seen that a film's thermomechanical properties can be tailored by incorporating different levels of TMCD in the polyester backbone.

### 3.5. Acknowledgements

This work was supported by the Eastman Center of Excellence at NC State University. This work was performed in part at the Analytical Instrumentation Facility (AIF) at North Carolina State University, which is supported by the State of North Carolina and the National Science Foundation (award number ECCS-1542015). The AIF is a member of the North Carolina Research Triangle Nanotechnology Network (RTNN), a site in the National Nanotechnology Coordinated Infrastructure (NNCI). The authors thank Mr. Phillip Strader for his assistance with the NI measurements. We also thank Dr. Andrew Detwiler of Eastman Chemical Company for his guidance with this work and for the many helpful discussions regarding its technical content.

### 3.6. References


(1) Garcés, J. M.; Moll, D. J.; Bicerano, J.; Fibiger, R.; McLeod, D. G. *Adv. Mater.* **2000**, *12*, 1835–1839.

(2) Yang, Y.; Yu, G.; Cha, J. J.; Wu, H.; Vosgueritchian, M.; Yao, Y.; Bao, Z.; Cui, Y. *ACS Nano* **2011**, *5*, 9187–9193.

(3) Twite, R. L.; Bierwagen, G. P. *Prog. Org. Coatings* **1998**, *33*, 91–100.

(4) Arora, A.; Padua, G. W. *J. Food Sci.* **2010**, *75*, R43–R49.

(5) Panchireddy, S.; Grignard, B.; Thomassin, J.-M.; Jerome, C.; Detrembleur, C. *ACS Sustain. Chem. Eng.* **2018**, *6* (11), 14936–14944.

(6) Cornille, A.; Michaud, G.; Simon, F.; Fouquay, S.; Auvergne, R.; Boutevin, B.; Caillol, S. *Eur. Polym. J.* **2016**, *84*, 404–420.

(7) Dolci, E.; Michaud, G.; Simon, F.; Boutevin, B.; Fouquay, S.; Caillol, S. *Polym. Chem.* **2015**, *6* (45), 7851–7861.

(8) Kausar, A. *Am. J. Polym. Sci. Eng.* **2017**, *5* (1), 1–12.

(9) Lee, S. H.; Kim, S. W.; Kang, B. S.; Chang, P.-S.; Kwak, M. K. *Soft Matter* **2018**, *14* (14), 2586–2593.

(10) Chattopadhyay, D. K.; Raju, K. V. S. N. *Prog. Polym. Sci.* **2007**, *32* (3), 352–418.

(11) Raquez, J.-M.; Deléglise, M.; Lacrampe, M.-F.; Krawczak, P. *Prog. Polym. Sci.* **2010**, *35*, 487–509.

(12) Bajat, J. B.; Mišković-Stanković, V. B. *Prog. Org. Coatings* **2004**, *49*, 183–196.

(13) Sørensen, P. A.; Kiil, S.; Dam-Johansen, K.; Weinell, C. E. *J. Coatings Technol. Res.*

**2009**, *6*, 135–176.

(14) Ghosh, B.; Gogoi, S.; Thakur, S.; Karak, N. *Prog. Org. Coatings* **2016**, *90*, 324–330.

(15) Cao, S.; Li, S.; Li, M.; Xu, L.; Ding, H.; Xia, J.; Zhang, M.; Huang, K. *Polym. J.* **2017**, *49* (11), 775–781.

(16) Sultan, M.; Atta, S.; Bhatti, H. N.; Islam, A.; Jamil, T.; Bibi, I.; Gull, N. *Polym. Plast. Technol. Eng.* **2017**, *56* (15), 1608–1618.

(17) Griffini, G.; Passoni, V.; Suriano, R.; Levi, M.; Turri, S. *ACS Sustain. Chem. Eng.* **2015**, *3* (6), 1145–1154.

(18) Gogoi, G.; Karak, N. *Polym. Degrad. Stab.* **2017**, *143*, 155–163.

(19) Panda, S. S.; Panda, B. P.; Nayak, S. K.; Mohanty, S. *Polym. Plast. Technol. Eng.* **2018**, *57* (6), 500–522.

(20) Sharmin, E.; Zafar, F.; Akram, D.; Alam, M.; Ahmad, S. *Ind. Crops Prod.* **2015**, *76*, 215–229.

(21) Cornille, A.; Auvergne, R.; Figovsky, O.; Boutevin, B.; Caillol, S. *Eur. Polym. J.* **2017**, *87*, 535–552.

(22) Weiss, K. D. *Prog. Polym. Sci.* **1997**, *22*, 203–245.

(23) Goldberg, M.; Mahon, K.; Anderson, D. *Adv. Drug Deliv. Rev.* **2008**, *60* (9), 971–978.

(24) Xue, H.; Zhao, Y.; Wu, H.; Wang, Z.; Yang, B.; Wei, Y.; Wang, Z.; Tao, L. *J. Am. Chem. Soc.* **2016**, *138* (28), 8690–8693.

(25) Chianella, I.; Lotierzo, M.; Piletsky, S. A.; Tothill, I. E.; Chen, B.; Karim, K.; Turner, A. P. F. *Anal. Chem.* **2002**, *74*, 1288–1293.

(26) Lakshmi, D.; Akbulut, M.; Ivanova-Mitseva, P. K.; Whitcombe, M. J.; Piletska, E. V.; Karim, K.; Güven, O.; Piletsky, S. A. *Ind. Eng. Chem. Res.* **2013**, *52* (39), 13910–13916.

(27) Pervaje, A. K.; Tilly, J. C.; Inglefield, D. L.; Spontak, R. J.; Khan, S. A.; Santiso, E. E. *Macromolecules* **2018**, *51* (23), 9526–9537.

(28) Marsh, S. In *The Waterborne Symposium : Proc. 39th Ann.Int. Waterborne, High-Solids, Powder Coatings Symp.*; DEStech Publications: Lancaster Penn., 2012; pp 263–276.

(29) Kelsey, D. R.; Scardino, B. M.; Grebowicz, J. S.; Chuah, H. H. *Macromolecules* **2000**, *33*, 5810–5818.

(30) Hoppens, N. C.; Hudnall, T. W.; Foster, A.; Booth, C. J. *J. Polym. Sci. A Polym. Chem.* **2004**, *42*, 3473–3478.

(31) Tilly, J. C.; Pervaje, A. K.; Inglefield, D. L.; Santiso, E. E.; Spontak, R. J.; Khan, S. A. *ACS Omega* **2019**, *4* (1), 932–939.

(32) Monge, M. A.; del Rio, J. *J. Phys. Condens. Matter* **1994**, *6* (13), 2643–2646.

(33) Mishra, A. K.; Narayan, R.; Raju, K. V. S. N. *Prog. Org. Coatings* **2012**, *74* (3), 491–501.

(34) Xu, W.; Zhou, L.; Sun, W.; Zhang, J.; Tu, W. *J. Appl. Polym. Sci.* **2015**, *132* (2), n/a-n/a.

(35) Zhang, J.; Tu, W.; Dai, Z. *J. Coatings Technol. Res.* **2013**, *10* (6), 887–895.

(36) Li, X.; Yee, A. F. *Macromolecules* **2003**, *36*, 9411–9420.

(37) Sun, Y.; Zhang, Z.; Moon, K.-S.; Wong, C. P. *J. Polym. Sci. Part B Polym. Phys.* **2004**, *42* (21), 3849–3858.

(38) de Nograro, F. F.; Llano-Ponte, R.; Mondragon, I. *Polymer (Guildf).* **1996**, *37* (9), 1589–1600.

(39) Detwiler, A. T.; Lesser, A. J. *J. Mater. Sci.* **2012**, *47* (8), 3493–3503.

(40) Cook, W. D.; Scott, T. F.; Quay-Thevenon, S.; Forsythe, J. S. *J. Appl. Polym. Sci.* **2004**, *93* (3), 1348–1359.

(41) Oliver, W. C.; Pharr, G. M. *J. Mater. Res.* **1992**, *7* (06), 1564–1583.

(42) Chowdhury, S.; de Barra, E.; Laugier, M. T. *Surf. Coatings Technol.* **2005**, *193*, 200–205.

(43) Skaja, A.; Fernando, D.; Croll, S. *J. Coatings Technol. Res.* **2006**, *3*, 41–51.

(44) Ghermezcheshme, H.; Mohseni, M.; Yahyaei, H. *Tribol. Int.* **2015**, *88*, 66–75.

(45) Du, B.; Tsui, O. K. C.; Zhang, Q.; He, T. *Langmuir* **2001**, *17*, 3286–3291.

(46) Hardiman, M.; Vaughan, T. J.; McCarthy, C. T. *Polym. Test.* **2016**, *52*, 157–166.

(47) Torstensen, J. Ø.; Liu, M.; Jin, S.-A.; Deng, L.; Hawari, A. I.; Syverud, K.; Spontak, R. J.; Gregersen, Ø. W. *Biomacromolecules* **2018**, *19* (3), 1016–1025.

(48) Dong, A. W.; Fong, C.; Waddington, L. J.; Hill, A. J.; Boyd, B. J.; Drummond, C. J. *Phys. Chem. Chem. Phys.* **2015**, *17* (3), 1705–1715.

(49) Sharma, S. K.; Pujari, P. K. *Prog. Polym. Sci.* **2017**, *75*, 31–47.

(50) Lepage, G. P. *Atomic Physics, Vol. 7*; Plenum Press: New York, N.Y., 1981.

(51) Yoshinori, K.; Kenji, H.; Yoshinori, K.; Shigeru, H. *Bull. Chem. Soc. Jpn.* **1992**, *65* (1), 160–163.

(52) Tao, S. J. *J. Chem. Phys.* **1972**, *56* (11), 5499–5510.

(53) Eldrup, M.; Lightbody, D.; Sherwood, J. N. *Chem. Phys.* **1981**, *63* (1–2), 51–58.

(54) Goworek, T.; Jasińska, B.; Wawryszczuk, J.; Zaleski, R.; Suzuki, T. *Chem. Phys.* **2002**, *280* (3), 295–307.

(55) Wada, K.; Hyodo, T. *J. Phys. Conf. Ser.* **2013**, *443*, 012003.

(56) Williams, M. L.; Landel, R. F.; Ferry, J. D. *J. Am. Chem. Soc.* **1955**, *77* (14), 3701–3707.

(57) Vogel, H. *Phys. Z.* **1921**, *22*, 645–646.

(58) Fulcher, G. S. *J. Am. Ceram. Soc.* **1925**, *8* (6), 339–355.

(59) Tammann, G.; Hesse, W. *Z. Anorg. Allg. Chem.* **1926**, *156* (4), 245–257.

(60) Odegard, G. M.; Bandyopadhyay, A. *J. Polym. Sci. Part B Polym. Phys.* **2011**, *49* (24), 1695–1716.

(61) Xie, W.; Ju, H.; Geise, G. M.; Freeman, B. D.; Mardel, J. I.; Hill, A. J.; McGrath, J. E. *Macromolecules* **2011**, *44* (11), 4428–4438.

# CHAPTER 4: RHEOLOGY OF UV-CROSSLINKABLE POLYMER NANOCOMPOSITES BASED ON POLY(DIMETHYL SILOXANE) AND ZIRCONIA NANOPARTICLES: ROLE OF REACTIVE VS. PASSIVE FILLERS

## 4.1. Introduction

Network polymers are an interesting subset of polymeric materials due to their densely cross-linked structure, which makes them attractive for a number of different applications. One conventional way to form these network polymers is via thermosetting, whereby the network polymer is formed in the presence of heat. Induction of network formation through application of ultraviolet radiation, or UV crosslinking, is another method of forming network polymers that has garnered significant research interest in recent years[1–5]. The properties of network polymers, including UV-cross-linkable polymers, can be enhanced or altered by including fillers within the polymeric matrix to form polymer nanocomposites.[6] Previous works have investigated filler materials such as carbonaceous nanomaterials[7,8], cellulosics[9,10], organoclays[11,12] and inorganic materials[13–16]. The size, structure and chemical nature of these fillers can have a profound impact on how well they can be incorporated within the polymeric matrix[17]. Zirconia nanoparticles in particular have found uses in UV- and thermally-crosslinked nanocomposites for coatings and electronics applications[18–25].

The crosslinking behavior of UV-crosslinkable systems has been studied previously using two popular techniques: photo-DSC[26–29] and infrared spectroscopy[30–33]. While these techniques can give valuable insight into the thermal and chemical nature of the crosslinking process, they do not explicitly provide information regarding the mechanical property and structural development as these systems undergo UV-crosslinking. Dynamic rheology is a powerful tool by which we can probe a sample's microstructural evolution as it proceeds along a UV-induced

reaction coordinate, as well as evaulate the final microstructure dynamic moduli[34–38]. A few recent studies have explored dynamic rheology as a tool by which to interrogate the effect of filler on UV-induced crosslinking behavior in nanocomposite systems for a number of different applications, from inkjet printer ink[39] to dental materials[40]. In this study, we utilize dynamic rheology to examine the effects of two different zirconia nanoparticles, one reactive and one passive, at various loadings, as well as the effect of irradiation intensity, on the crosslinking behavior of solvent-swollen UV-curable PDMS nanocomposites. We also examine the turbidity of the resulting swollen films and determine how well each type of zirconia is retained within the network upon swelling, This is then correlated with morphological behavior observed in cross-sectional scanning electron micrographs in order to gain an understanding of how zirconia nanoparticle loading and functionality affect cure and ultimate film properties.

## 4.2. Experimental

### *4.2.1. Materials*

Methacryloxypropyl-terminated poly(dimethylsiloxane) (PDMS) (Mn ~500) was purchased from Gelest and used without further purification. Meta-cresol (MC) was purchased from Fisher Scientific and used as received. The photoinitiator 2,2-dimethoxy-2-phenylacetophenone (DMPA) was purchased from Sigma Aldrich and was used without further purification. The chemical structure of methacryloxypropyl-terminated PDMS, DMPA and MC are shown in **Figure 4.1.** Two grades of ethyl acetate- dispersed functionalized zirconia nanoparticles (50 wt%) were purchased from Pixelligent (PCPB-2-50-ETA and PCPG-2-50-ETA) and the solvent was removed via vacuum oven (80°C, 24 hours) to yield dry powdered nanoparticles which were stored in a dark cabinet until use. The nanoparticles have an average diameter of 5 nm (from manufacturer's specifications). Although the exact nature of the

nanoparticle functionality is proprietary, it is known that PCPB is reactive under UV radiation, whereas PCPG is not.

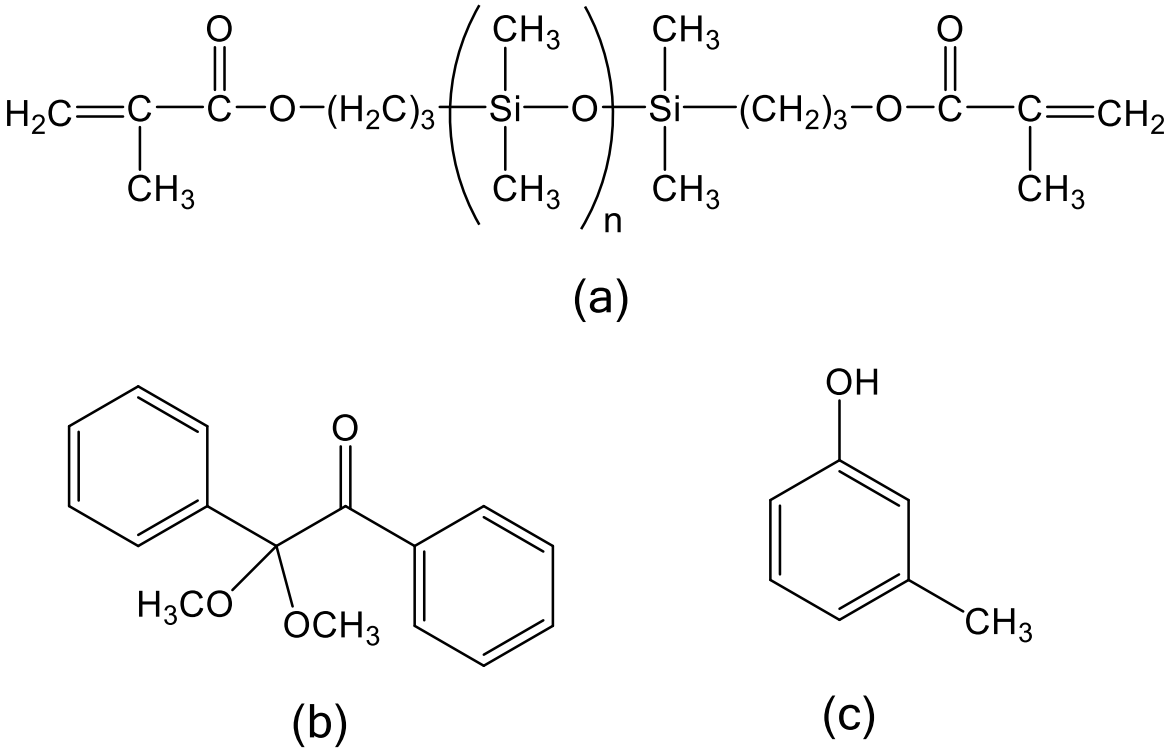


**Figure 4.1.** Chemical structures of (a) methacryloxypropyl-terminated PDMS; (b) DMPA photoinitiator, and (c) m-cresol, the solvent used in this study.

The overlaid transmission FTIR spectra for both reactive and passive NPs were analyzed but are not shown. From the full spectra it is difficult to discern any major differences between the two particle grades, suggesting that the functionalities are fairly similar. There is, however, a peak in the reactive spectrum at ~1720 $cm^{-1}$ that is not present in the passive NP's spectrum. We believe this peak corresponds to the C=O stretch of an acrylate group, which suggests that the reactive nanoparticle (NP) contains a surface acrylate moiety that allows it to react under UV radiation. A corresponding shoulder at ~1630 $cm^{-1}$ lends further evidence that the reactive NP has acrylate functionality, as this peak typically accompanies the C=O stretch and corresponds to

the C=C stretch in an acrylate functional group. The FTIR spectrum for the passive NPs lacks both of these features, suggesting that its surface functionality includes photo-stable organic compounds that will not interact with the cross-linking PDMS.

### *4.2.2. Methods*

#### 4.2.2.1. Specimen Preparation

Both grades of powdered NPs were isolated as described above and dispersed at 50 wt% in MC via sonication for 2 hours, resulting in clear colloidal solutions. Prescribed amounts of the NP/MC colloidal solutions and PDMS, along with additional MC, were added to a 10mL scintillation vial and a 5 wt% solution of DMPA in MC was then added such that the final photoinitiator concentration was 0.25 wt% of the total solution mass. Samples were prepared in 1.6g quantities and stored in a refrigerator for no more than one week before use. The nomenclature that is utilized for formulations studied in this work can be generalized to X#, where X is a letter and # is a number designating the loading of zirconia (in wt%) of the solids content. A "P" designation indicates that the zirconia in the system is passive and an "R" indicates that the zirconia in the system is reactive (i.e. R25 refers to a formulation with reactive zirconia at a loading of 25 wt% of solids content (or 12.5 wt% of total mass).

#### 4.2.2.2. Rheological Analysis

Dynamic oscillatory shear rheology was conducted to monitor the cross-linking reaction of each formulation. Frequency sweeps (0.1-10 rad/s) on formulations before crosslinking were conducted at room temperature on a TA Instruments Discovery Series Hybrid Rheometer HR-3 outfitted with a Peltier plate and a 40mm upper aluminum plate. A fixed gap of 400μm and strain amplitude of 50% (within samples' linear viscoelastic regime) was used for these measurements.

All crosslinking and post-crosslinking rheological measurements were performed on the same rheometer, equipped with the 365nm UV LED accessory. A 20mm quartz bottom plate was utilized in order to allow light to pass vertically upward into the sample, and a 20mm upper aluminum plate was used. All measurements were conducted at a gap size of 180μm. Samples were removed from the refrigerator and allowed to equilibrate at room temperature for 5 minutes before being loaded onto the rheometer. Reaction progress was followed *in situ* as a function of time at a fixed strain amplitude of 10%, which is within the linear viscoelastic regime of the sample at an angular frequency of 5 rad/s. The UV intensity was varied between 0.5-5 $mW/cm^2$, and the functionality and loading of zirconia were all varied as well. Frequency sweeps were conducted after thirty minutes of curing samples at 1 $mW/cm^2$ in order to determine the effect of zirconia functionality and loading on final gel modulus.

#### 4.2.2.3. UV-Vis Spectrophotometry

UV-Vis measurements were carried out on a Thermo Fisher GENESYS 10S UV-Vis spectrophotometer. In order to determine the ability of cured film samples to retain zirconia NPs, samples that had been cured for 30 minutes on the rheometer (containing a known amount of zirconia) were weighed and placed into 10mL scintillation vials. The vials were filled with a known amount of MC and were left in solvent for three days and agitated daily for ~60s. After the 3 day equilibration period, ~2.5mL of supernatant was extracted and placed in a 2.5 mL cuvette for UV-Vis analysis and the wt% of dissolved zirconia was calculated based on the maximum intensity of the absorbance peak between 302-204 nm weighted against a calibration curve. There were no differences in absorbance between the two types of zirconia NPs, so the passive NPs were dissolved in MC and diluted to different concentrations to generate this calibration curve. Samples were tested between 200 and 800nm wavelength.

Films with a fixed path length (180μm in thickness) were cured for 30 minutes at 1 $mW/cm^2$ on the same rheometer described above and then placed on glass slides for UV-Vis spectroscopy. The PDMS/MC/$ZrO_2$-coated glass slides were then placed in the spectrophotometer and scanned from 400-700nm. Turbidity was determined using the samples' absorbances at 600nm.

#### 4.2.2.4. Scanning Electron Microscopy (SEM)

Four samples used for UV-Vis measurements (25 and 75 wt% reactive and passive zirconia loading) were cryo-fractured in liquid nitrogen and mounted onto a stub such that the cross-sectioned surface was facing upwards. Measurements were carried out using a FEI Verios field emission SEM. Signals were collected using a through the lens (TLD) detector at magnifications of 1500x, 10000x and 25000x in order to visualize the observed morphologies at various lengthscales.

## 4.3. Results and Discussion

### *4.3.1. Dynamic Rheology*

The kinetics of microstructural evolution are followed through *in situ* monitoring of the two dynamic moduli; G', the storage or elastic modulus, and G'', the loss or viscous modulus via dynamic rheology. Before exposure to UV radiation, these samples are Newtonian solutions whose behavior is characterized by their complex viscosity being independent of frequency, as shown for select samples in **Figure 4.2.** An increase in the nanoparticle loading of both reactive and passive zirconia results in an increase in initial solution complex viscosity which almost certainly affects the time required to achieve a modulus crossover. Furthermore, both types of particles behave the same with regard to particle concentration and do not show shear-thinning

behavior which is typical of agglomerated particle systems, as has been reported previously in various concentrated nanoparticle systems[41].

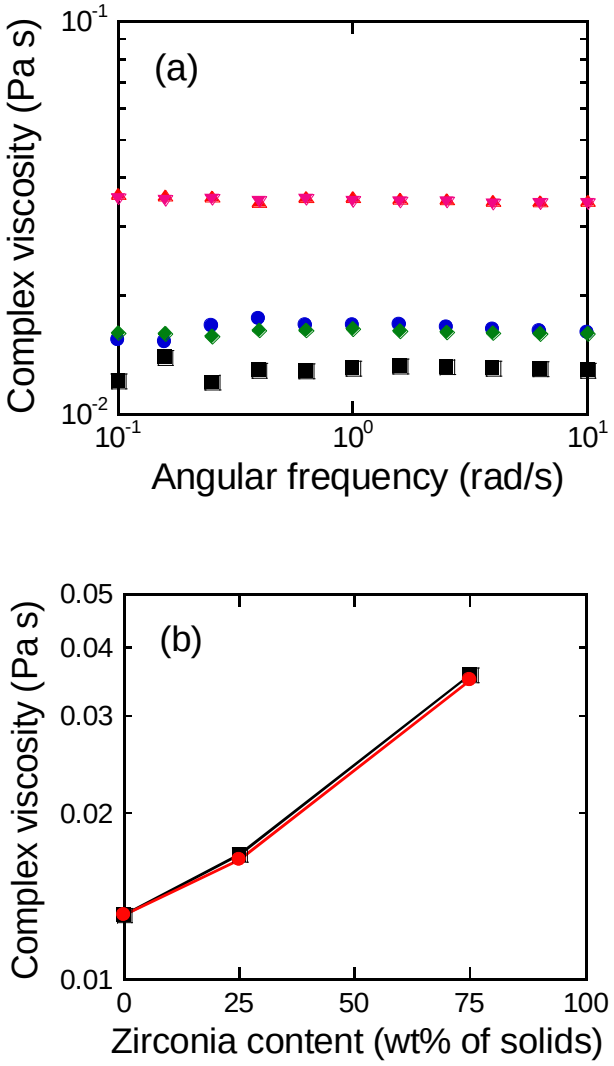


**Figure 4.2.** (a) Representative complex viscosity vs. angular frequency curves for select formulations prior to exposure to UV irradiation. Symbols represent: neat PDMS with 0.5 wt. % DMPA (black squares); R25 (blue diamonds); R75 (red triangles); P25 (green diamonds); P75 (pink inverted triangles). Complex viscosity (at 1 rad/s) vs. zirconia content for both unreacted formulations containing reactive (black squares) and passive (red circles) zirconia are given in (b).

As the reaction proceeds and a microstructure begins to develop, G' begins to increase and ultimately dominate over G". A true gel point, as defined by the Winter-Chambon Criterion[42,43], was not determined for these systems. Instead, we are using the modulus crossover as an estimate of the gel point, as in our recent work[44] and a previous study on a similar system by Nguyen et al.[45]. The modulus crossover times at three different frequencies were found to be very close to one-another for the first two formulations that we tested, so we therefore believe that even though a true gel point is not identified, the modulus crossover will provide a good estimate (data not shown).

#### 4.3.1.1. Effect of Zirconia Loading and Functionality at a Single UV Intensity

**Figure 4.3** shows the evolution of dynamic moduli of systems with different loadings of both reactive and passive nanoparticles cured at 1mW/cm$^2$. In the case of both nanoparticles, it is clear that increasing the loading of zirconia in the formulation increases the time required to achieve a modulus crossover. In most cases, the time required to reach the modulus crossover under constant 1mW/cm$^2$ UV irradiation is very similar for both the reactive and passive zirconia particles at a given loading. This is an interesting observation, since intuition might dictate that the systems with a reactive filler would react faster with the zirconia particles functioning as nano-scale cross-linking agents, but this is not what we observe. There is little that distinguishes the reactive from the passive filler in terms of rheological property development up to the modulus crossover at 1 mW/cm$^2$, however the two fillers begin to differentiate themselves slightly more when the nanocomposites are fully cured for 30 minutes, as discussed in the subsequent paragraphs regarding the ultimate film properties. The full cure is not depicted here due to the ~ 6 orders of magnitude increase in G'; therefore, the 10% strain and 5 rad/s angular frequency required to reliably identify a crossover in modulus lies outside the linear viscoelastic

regime of the fully cured systems.

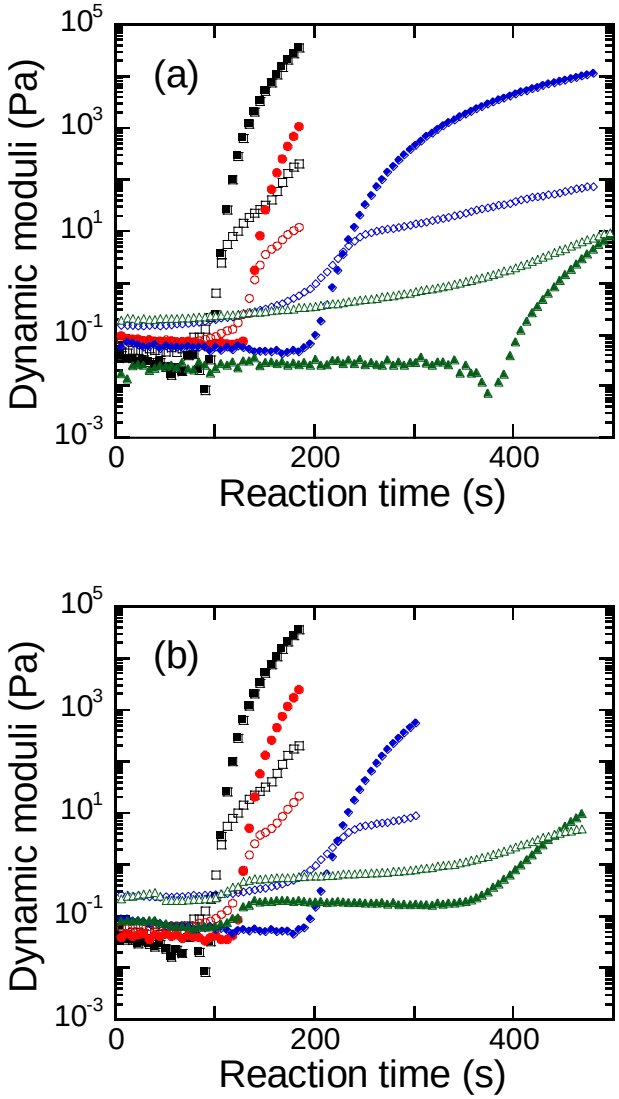


**Figure 4.3.** Evolution of G' and G'' as measured by dynamic rheology as the nanocomposites cure with various loadings of either (a) reactive or (b) passive zirconia as a filler. In the plots, G' is marked by closed shapes and G'' is marked by open ones. In both plots, 0% zirconia is given by black squares; 25% is given by red circles; 75% is given by blue diamonds; and 85% is given by green triangles.

The frequency-dependent behavior of these systems after 30 minutes of exposure to 1 $mW/cm^2$ UV irradiation can be found in **Figure 4.4**. Frequency sweep data was not able to be

obtained for fully crosslinked nanocomposites containing less than 50% zirconia content as the materials had too high a modulus (>$10^7$ Pa) to reasonably probe with our experimental setup. At 50 wt% zirconia filler of solids content (black squares in **Fig. 3**), the storage modulus is near $10^6$ Pa for the passive zirconia and is only slightly lower for the reactive zirconia. As zirconia content is increased in both the reactive and passive filled systems, the storage moduli decrease. The storage moduli for all examined specimens do, however, maintain their frequency-independent behavior over the temperature range examined, which suggests that they are all strong gels after 30 minutes of exposure to 1 mW/cm$^2$ UV radiation. One interesting observation is that, for both reactive and passive zirconia, the ultimate gel storage modulus decreases with increasing filler content, which runs counter to conventional understanding of high-modulus filler effects on network mechanical properties. This phenomenon has been previously observed in systems containing carbon nanotubes, graphite and zinc oxide nanoparticles.[46–48] As the PDMS is the primary network former in these systems, the increase in zirconia content (and resultant decrease in PDMS content) leads to a dilution effect, which increases the number of network defects and lowers the effective crosslink density throughout the film. Another observation is that, as zirconia content is increased to 75% and beyond, the nanocomposite materials containing the reactive zirconia tend to have slightly higher ultimate gel moduli than those containing passive zirconia. This suggests that the reactive zirconia are being incorporated into the network via covalent bonding with the PDMS. This topic will be discussed further in a following section.

**Figure 4.4.** Frequency sweeps of fully-cured nanocomposite materials containing varied levels of either (a) reactive zirconia, or (b) passive zirconia. Storage moduli values are given by closed shapes while representative loss moduli curves are given by open shapes. In both plots, 50% zirconia is given by black squares; 75% is given by red circles; 80% is given by blue diamonds; and 85% is given by green triangles. Storage moduli values measured at 1 rad/s are given as a function of zirconia loading of solids content in (c) for both reactive (black squares) and passive (red circles).

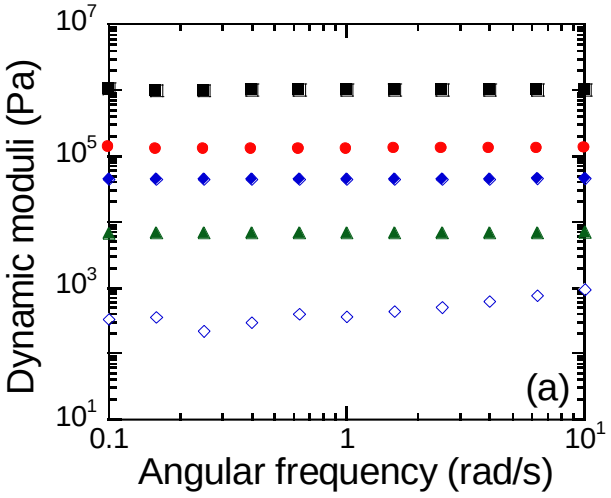
Dynamic moduli (Pa)
$10^7$
$10^5$
$10^3$
$10^1$
0.1
1
$10^1$
Angular frequency (rad/s)
(a)

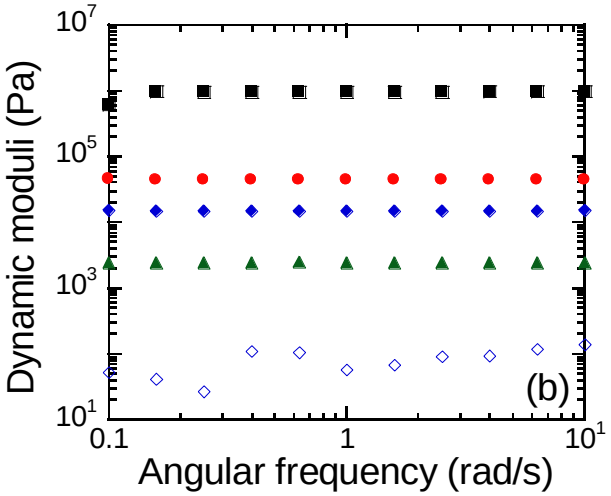
Dynamic moduli (Pa)
$10^7$
$10^5$
$10^3$
$10^1$
0.1
1
$10^1$
Angular frequency (rad/s)
(b)

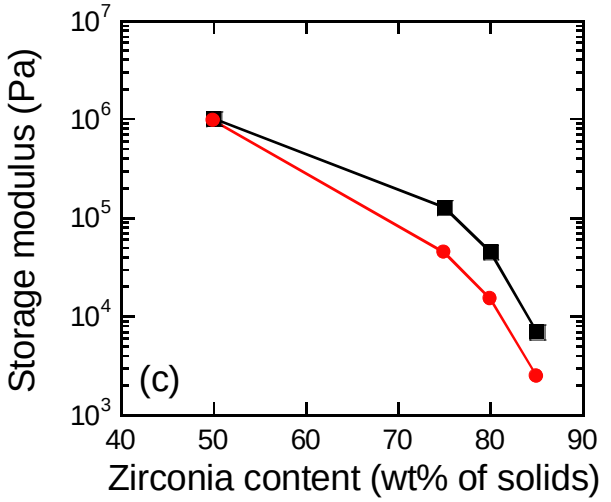
Storage modulus (Pa)
$10^7$
$10^6$
$10^5$
$10^4$
$10^3$
40
50
60
70
80
90
Zirconia content (wt% of solids)
(c)

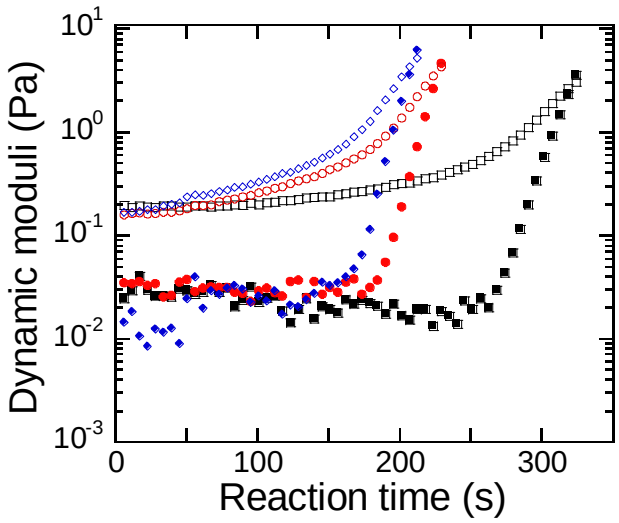


**Figure 4.5.** Representative sample data (P80 formulation) used to determine time to modulus crossover and the modulus value at the crossover for three of the intensities studied. Storage moduli are given by closed shapes and loss moduli values are given by open ones. The intensities studied are given by: 0.5 mW/cm$^2$ (black squares), 2 mW/cm$^2$ (red circles), and 4 mW/cm$^2$ (blue diamonds).

#### 4.3.1.2. Effect of UV Irradiation Intensity and Zirconia Loading and Type on Modulus Crossover

Both types of zirconia-filled systems and unfilled PDMS in MC were subjected to ultraviolet irradiation intensities of 0.5, 1, 2, 3, 4 and 5 mW/cm$^2$ to ascertain the effect of irradiation intensity on cure behavior up the modulus crossover time, at which point (or shortly thereafter) the experiments were stopped. **Figure 4.5** depicts the evolution of G' and G" over time for a representative formulation (P80) at all irradiation intensities examined. As the UV intensity increases, the time required for G' to dominate the mechanical response decreases. The modulus crossover times are displayed in **Figure 4.6** as functions of both zirconia type and loading, as well as UV intensity. There is an inverse relationship between UV intensity for crosslinking and the time required for modulus crossover, which is relatively intuitive; a higher energy flux into the system will cause a system to more rapidly crosslink. **Figure 4.6** reveals a

power-law relationship between UV intensity and crossover time. This behavior has been observed previously in thiol-ene UV-curable polymer systems[45,49], as well as an acrylate-based system[50]. We do find it interesting that the passive system achieves a modulus crossover more quickly than the reactive system when zirconia content exceeds 80 wt%. This could be due to a greater degree of particle aggregation in the passive system, which would increase the storage modulus, whereas in the reactive system the particles are able to be incorporated into the network and stay fairly well dispersed. The subject of particle aggregation and its consequences will be discussed in the following section.

**Figure 4.7** contains the power law exponents for formulations containing both the functional and non-functional zirconia as a function of filler loading, and the scaling relationships are similar for both types of NPs. This similarity suggests that the mechanism of gelation is similar for both reactive and passive zirconia fillers, as the time required to achieve a modulus crossover shows the same dependence on UV intensity for both fillers. We hypothesize that this is due to faster reaction kinetics for the methacryloxypropyl groups on the PDMS than the reactive groups on the zirconia nanoparticles. Differences in reactivity between different types of acrylate functionalities have been previously documented[52,53], which could explain the similarity in reaction mechanism up to the gel point for all loadings of zirconia and the ability for reactive zirconia retention within the matrix structure, which is discussed in the following section. Therefore, the PDMS plays a larger role in the network formation at shorter times and the reactive zirconia is incorporated more slowly in the network.

**Figure 4.6.** Time required to achieve modulus crossover for (a) formulations without any fillers (i.e. PDMS in MC), (b) formulations containing reactive zirconia, and (c) formulations containing passive zirconia. In (a), the symbols represent: PDMS with 0.5 wt% DMPA (black squares), 50 wt% PDMS in MC (blue circles), 37.5 wt% PDMS in MC (red triangles) and 25 wt% PDMS in MC (green diamonds). In both (b) and (c), the symbols represent: 25 wt% zirconia of total solids (black squares), 50 wt% zirconia of total solids (blue circles), 75 wt% zirconia of total solids (red triangles), 80 wt% zirconia of total solids (green diamonds) and 85 wt% zirconia of total solids (pink inverted triangles). Modulus crossover times show power-law dependence (solid lines) on UV intensity.

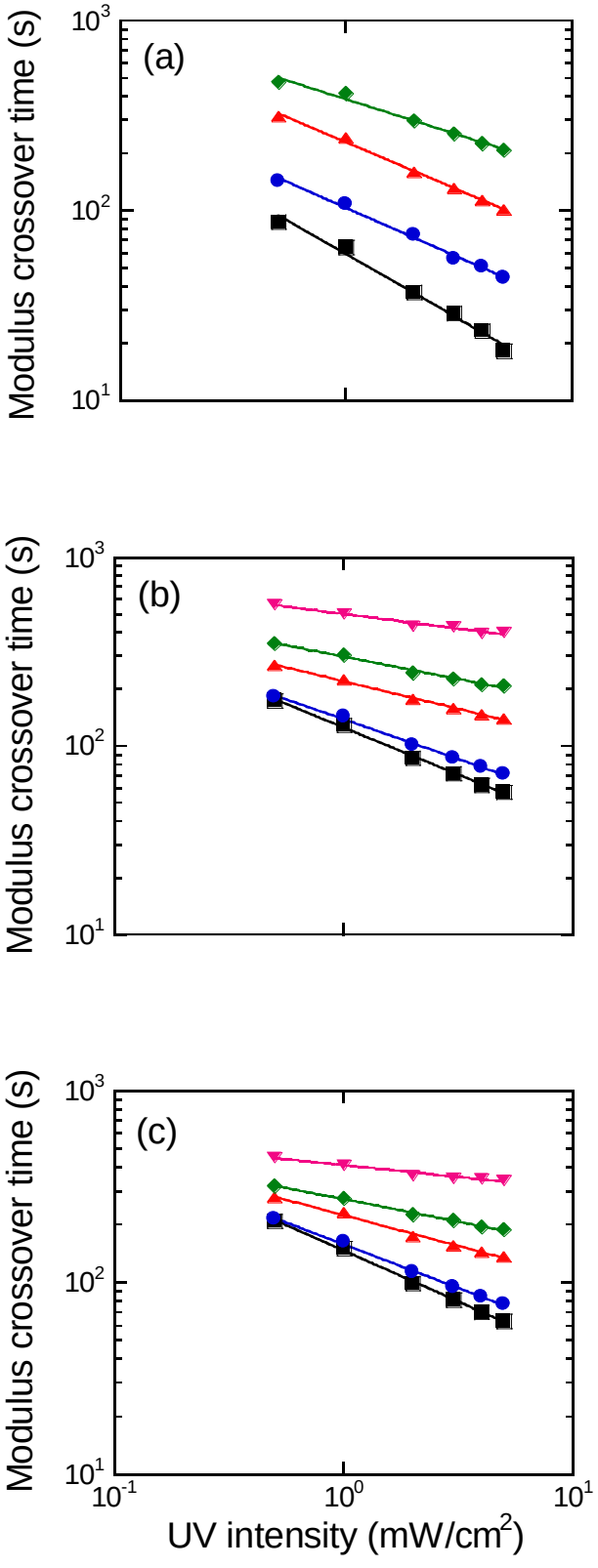
(a)
(b)
(c)
Modulus crossover time (s)
Modulus crossover time (s)
Modulus crossover time (s)
$10^3$
$10^2$
$10^1$
$10^{-1}$
$10^0$
$10^1$
UV intensity (mW/cm$^2$)

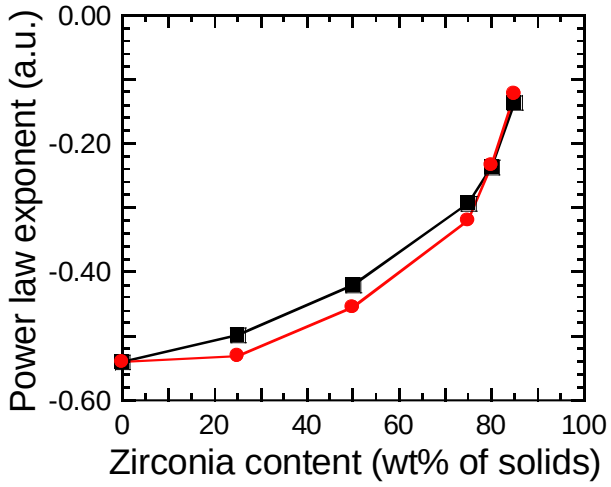


**Figure 4.7.** Calculated power-law exponents from linear regressions in Figure 4.7 (b) and (c). The reactive (black squares) and passive (red circles) zirconia appear to have similar power-law behavior as it pertains to modulus crossover time vs. UV intensity for different loadings of zirconia.

The time required to achieve an observed crossover in modulus is not the only material property that is affected by the inclusion of zirconia NPs; the value of the moduli at the crossover point also has a dependence on the zirconia loading and UV intensity. This relationship is demonstrated in **Figure 4.8** for both reactive and passive zirconia-containing formulations at 0.5 and 5 mW/cm$^2$, respectively. In the case of both reactive and passive particles, the systems cured at 5 mW/cm$^2$ have a higher crossover modulus at all zirconia loadings compared to their counterparts cured at 0.5 mW/cm$^2$. In the case of the passive NPs, the modulus values increase from about 0.8 Pa to 4 Pa (0.5 mW/cm$^2$) and 2 Pa to 6 Pa (5 mW/cm$^2$) as zirconia content is increased from 25 to 85% of solids content. This amounts to less than an order of magnitude change in both of these cases. In contrast, systems containing the reactive zirconia particles (PCPB) show moduli increases from about 0.5 Pa to 9 Pa (0.5 mW/cm$^2$) and 2 Pa to 20 Pa (5 mW/cm$^2$) over the same zirconia content range. Both of these increases are by at least a factor of 10 in magnitude, which suggests that the reactive zirconia is not only acting as a filler but is also participating in the crosslinking reaction under UV exposure.

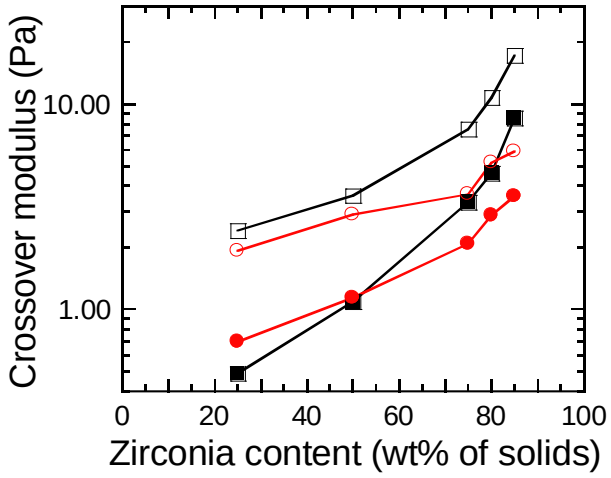


**Figure 4.8.** Observed magnitude of dynamic moduli at crossover for both reactive and passive zirconia. Filled symbols in the plot represent systems cured at 0.5 mW/cm$^2$, and open symbols represent systems cured at 5 mW/cm$^2$. Formulations containing reactive zirconia are given by black squares, whereas the passive zirconia systems are given by red circles.

*4.3.2. Optical Properties and Zirconia Retention in Nanocomposites*

The PDMS/zirconia nanocomposites swollen in MC that are studied herein have shown the ability to form gelled systems up to 85 wt% for both reactive and passive forms of zirconia, however ultra-high loadings of nanoparticles in polymeric matrices often lead to opaque materials, which limits potential application areas. Furthermore, it could be favorable if the zirconia in the nanocomposite is able to be retained within the system, even after washing or swelling the nanocomposite material. **Figure 4.9** depicts the fraction of zirconia retained in the film for systems containing both reactive and passive zirconia after swelling in MC for 3 days with periodic agitation. The films containing reactive zirconia appear to retain almost all of the zirconia after being left in solvent for 72 hours, although there is a slight decrease in retained zirconia at the highest loading. In contrast, the passive zirconia is retained to a significantly lower degree. This provides further evidence that the reactive zirconia NPs are being covalently

incorporated into the matrix structure, whereas the passive NPs are occupying free volume around the PDMS network structure.

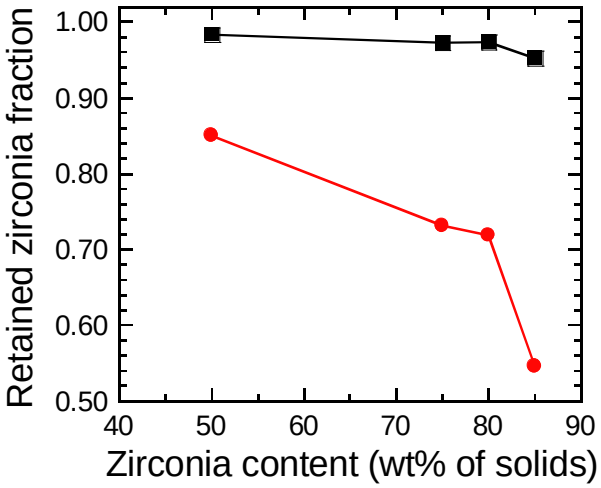


**Figure 4.9.** Calculated fraction of zirconia retained by the films after 72 hours of soaking in MC; reactive zirconia-containing systems are given by black squares and passive zirconia-containing systems are given by red circles.

As the network develops and the reactive zirconia is incorporated into its structure, it is able to remain in a well-dispersed state, whereas the passive zirconia particles are excluded from the network formation and form aggregate structures which increase the observed opacity of the films. This is evidenced by turbidity measurements made using UV-Vis spectrophotometry of films containing varied loadings of both reactive and passive zirconia particles (0-75 wt% passive zirconia, 0-80% reactive zirconia), shown in **Figure 4.10.a.** Turbidity can be calculated from the absorbance at a single wavelength, in our case at 600 nm, via the following equation:

$$turbidity = \frac{\ln(10) * A}{L},$$

where $A$ is the absorbance at a specific wavelength and $L$ is the optical path length. In our case, $L$ is constant at 180μm for all samples, and the absorbance can be extracted at a specific

wavelength from the UV-Vis absorbance curves. This method of determining turbidity from UV-Vis absorbance data has been undertaken previously[54,55]. The turbidity is very similar for both the reactive and passive systems up to 25 wt% NPs, however above this level the turbidity continues to increase exponentially for the passive system, while it levels off in the reactive system. **Figure 4.10.b.** provides visual evidence of the increasing turbidity and its effect on the observed optical clarity of films with differing levels of reactive and passive zirconia. The turbidity of the film containing 75 wt% passive zirconia is apparent to the naked eye, whereas the films containing reactive zirconia appear transparent up to 85 wt% zirconia. Scanning electron micrographs of cryo-fractured cross-sections of both reactive and passive zirconia at 25 and 75 wt% (of solids content) are depicted in **Figure 4.11**. A well-dispersed morphology is observed at a loading of 25 wt% for both reactive and passive zirconia, which corresponds to optically clear films found in **Figure 4.10.b.** The cross-sections observed with SEM appear similar for both types of filler, and the measured turbidity for both is low and the observed optical clarity is high. When the loading of reactive zirconia increased to 75 wt% of solids, the dispersed morphology is maintained, but the inclusions become slightly larger. This slight coarsening of the microstructure leads to a slight increase in the measured turbidity value, but does not manifest itself as a decrease in apparent optical clarity. In stark contrast, the film with 75 wt% passive zirconia exhibits a significantly coarsened microstructure, which gives a higher measured turbidity. This coarsened microstructure leads to an optically opaque material, as seen in the top-right photo in **Figure 4.10.b.**

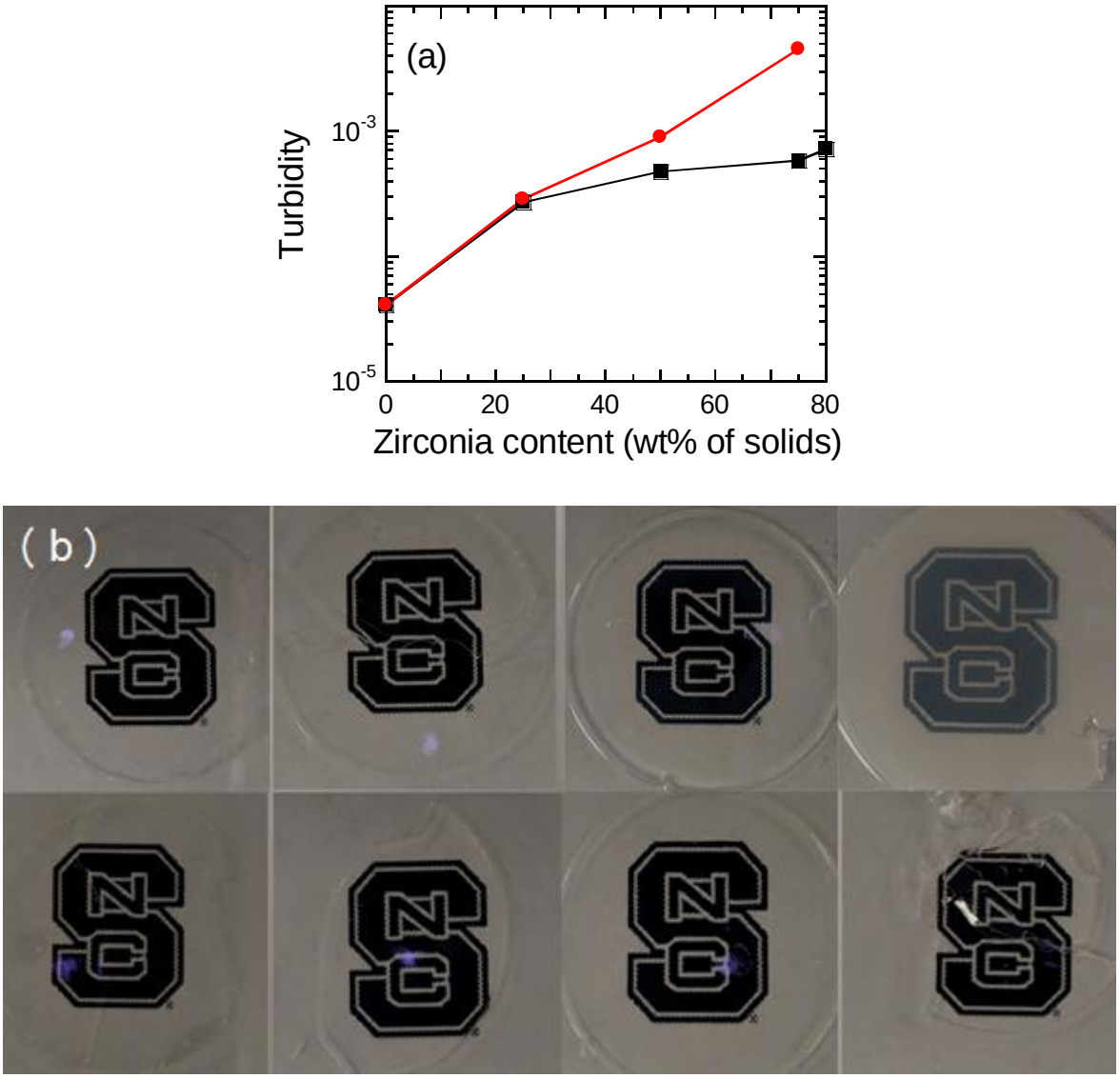


**Figure 4.10. (a)** Calculated turbidity values from UV-Vis spectrophotometry at a wavelength of 600nm. Reactive zirconia-containing systems are given by black squares, while passive zirconia-containing systems are given by red circles. (b) Images of 180μm-thick films on glass slides above NCSU logo. Top row, left to right: 50 wt% PDMS in MC, P25, P50, P75. Bottom row, left to right: R25, R50, R75, R80.

**Figure 4.11.** Micrographs obtained from SEM of uncoated PDMS/zirconia nanocomposite materials containing reactive and passive zirconia loadings of 25 and 75 wt% of solids content. Larger-scale features and significant coarsening of microstructure can be observed in the case of passive zirconia loaded into a PDMS matrix at 75 wt%.

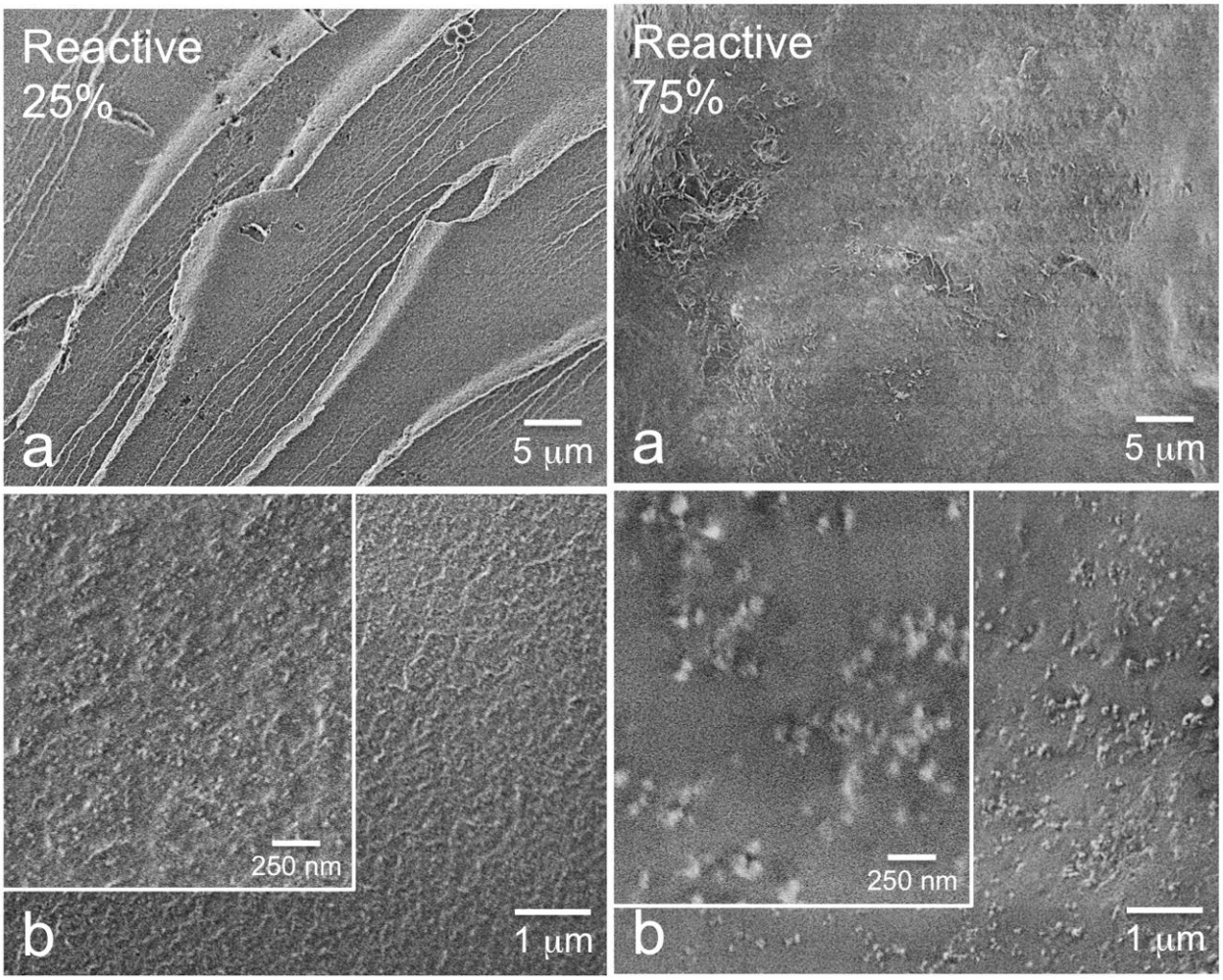
Reactive
25%
a
5 μm
Reactive
75%
a
5 μm
250 nm
b
1 μm
250 nm
b
1 μm

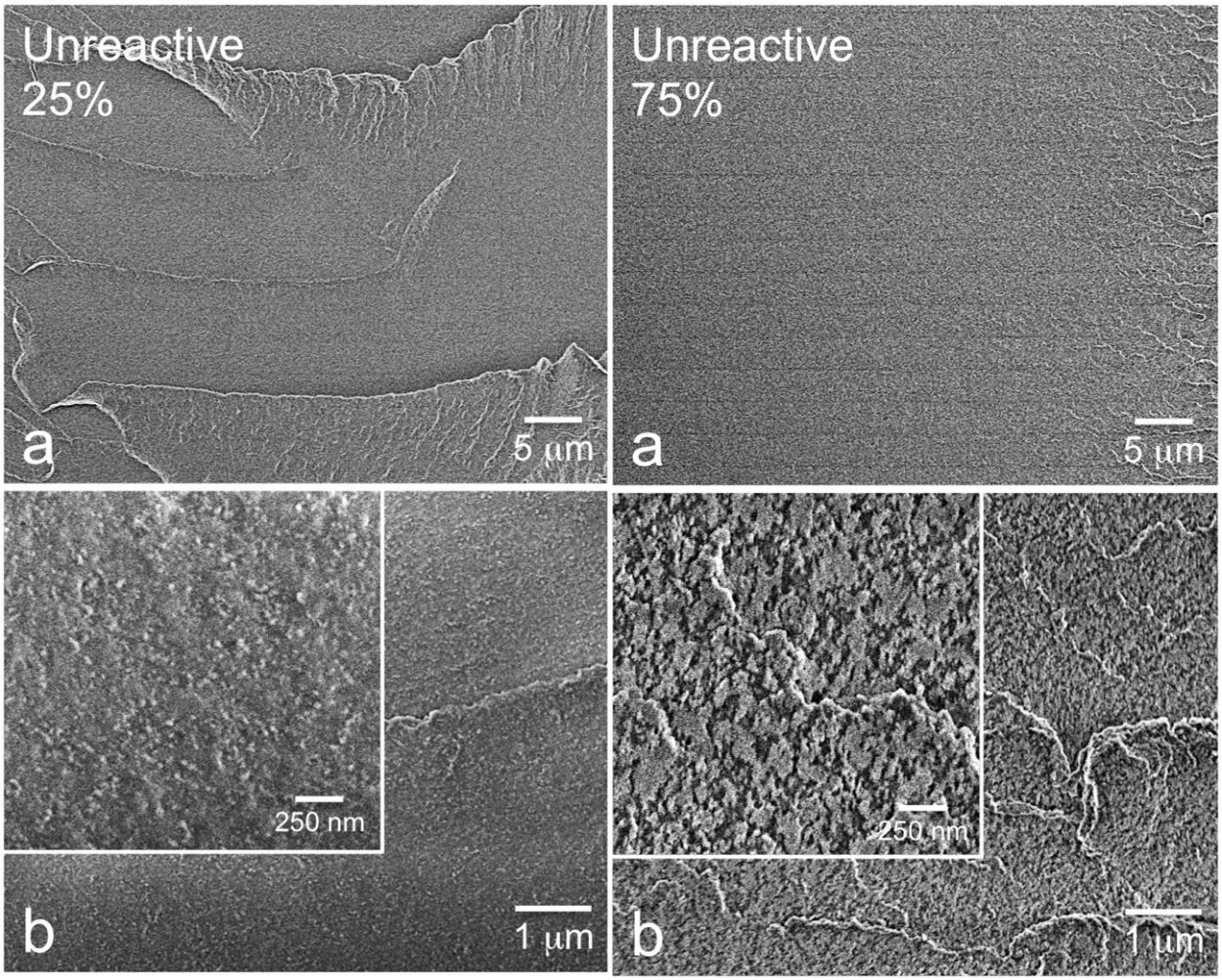
Unreactive
25%
a
5 μm
Unreactive
75%
a
5 μm
250 nm
b
1 μm
250 nm
b
1 μm

## 4.4. Conclusions

In this work, the UV cross-linking behavior of methacryloxypropyl-terminated PDMS is examined in m-cresol, and the effect of two commercially available surface functionalized zirconia nanoparticles are investigated in terms of rheological property development and optical properties of these nanocomposite systems. Both the reactive and passive zirconia nanoparticle-based systems were able to form cross-linked networks in systems containing up to 85 wt% zirconia of solids content (50% solids content overall), and a power law scaling relationship was found between UV irradiation intensity and time required to achieve a crossover in dynamic moduli for different loadings of zirconia. The magnitude of the modulus crossover value also had a positive dependence on zirconia content, which was stronger for the reactive than the passive zirconia. UV-Vis measurements showed that reactive zirconia was retained within the nanocomposite much more strongly than the passive zirconia upon swelling, suggesting covalent incorporation within the network. Turbidity measurements carried out in UV-Vis show a significant increase in turbidity in the passive zirconia systems with NP loadings above 50 wt%, while the reactive system's turbidity increases only slightly at the same loadings. Micrographs obtained from SEM of cryo-fractured cross-sectioned surfaces of samples containing both reactive and passive loadings of 25 and 75 wt% (of solids) zirconia suggest that large-scale aggregation of the NPs plays a role in the observed turbidity increase in films containing high levels of passive zirconia.

## 4.5. Acknowledgements

This work was supported by the Eastman Center of Excellence at NC State University. This work was performed in part at the Analytical Instrumentation Facility (AIF) at North Carolina State University, which is supported by the State of North Carolina and the National

Science Foundation (award number ECCS-1542015). The AIF is a member of the North Carolina Research Triangle Nanotechnology Network (RTNN), a site in the National Nanotechnology Coordinated Infrastructure (NNCI).

## 4.6. References


(1) Patel, D. K.; Sakhaei, A. H.; Layani, M.; Zhang, B.; Ge, Q.; Magdassi, S. *Adv. Mater.* **2017**, *29* (15), 1606000.

(2) Layani, M.; Cooperstein, I.; Magdassi, S. *J. Mater. Chem. C* **2013**, *1* (19), 3244–3249.

(3) Decker, C.; Masson, F.; Schwalm, R. *Macromol. Mater. Eng.* **2003**, *288*, 17–28.

(4) Xu, H.; Qiu, F.; Wang, Y.; Wu, W.; Yang, D.; Guo, Q. *Prog. Org. Coatings* **2012**, *73*, 47–53.

(5) Gestos, A.; Whitten, P. G.; Spinks, G. M.; Wallace, G. G. *Soft Matter* **2010**, *6* (5), 1045.

(6) Balazs, A. C.; Emrick, T.; Russell, T. P. *Science (80-. ).* **2006**, *314* (5802), 1107–1110.

(7) Miculescu, M.; Thakur, V. K.; Miculescu, F.; Voicu, S. I. *Polym. Adv. Technol.* **2016**, *27* (7), 844–859.

(8) Navarro-Pardo, F.; Martinez-Hernandez, A. L.; Velasco-Santos, C. *J. Nanomater.* **2016**, *2016*, 1–16.

(9) Oksman, K.; Aitomäki, Y.; Mathew, A. P.; Siqueira, G.; Zhou, Q.; Butylina, S.; Tanpichai, S.; Zhou, X.; Hooshmand, S. *Compos. Part A Appl. Sci. Manuf.* **2016**, *83*, 2–18.

(10) Thakur, V. K.; Voicu, S. I. *Carbohydr. Polym.* **2016**, *146*, 148–165.

(11) Zabihi, O.; Ahmadi, M.; Nikafshar, S.; Chandrakumar Preyeswary, K.; Naebe, M. *Compos. Part B Eng.* **2018**, *135*, 1–24.

(12) Salam, H.; Dong, Y.; Davies, I. *Fill. Reinf. Adv. Nanocomposites* **2015**, 101–132.

(13) Chiou, B.-S.; Raghavan, S. R.; Khan, S. A. **2001**.

(14) Kim, D. J.; Jo, M. J.; Nam, S. Y. *J. Ind. Eng. Chem.* **2015**, *21*, 36–52.

(15) Kaushik, A.; Kumar, R.; Arya, S. K.; Nair, M.; Malhotra, B. D.; Bhansali, S. *Chem. Rev.* **2015**, *115* (11), 4571–4606.

(16) Adnan, M.; Dalod, A.; Balci, M.; Glaum, J.; Einarsrud, M.-A. *Polymers (Basel)*. **2018**, *10* (10), 1129.

(17) Xiong, S.; Yin, S.; Wang, Y.; Kong, Z.; Lan, J.; Zhang, R.; Gong, M.; Wu, B.; Chu, J.; Wang, X. *Mater. Sci. Eng. B* **2017**, *221*, 41–53.

(18) Luo, K.; Zhou, S.; Wu, L. *Thin Solid Films* **2009**, *517* (21), 5974–5980.

(19) Xu, K.; Zhou, S.; Wu, L. *Prog. Org. Coatings* **2010**, *67* (3), 302–310.

(20) Luo, K.; Zhou, S.; Wu, L.; You, B. *Thin Solid Films* **2010**, *518* (23), 6804–6810.

(21) Xu, K.; Hu, Y. *Chinese J. Polym. Sci.* **2010**, *28* (1), 13–20.

(22) Liu, C.; Hajagos, T. J.; Chen, D.; Chen, Y.; Kishpaugh, D.; Pei, Q. *ACS Appl. Mater. Interfaces* **2016**, *8* (7), 4795–4802.

(23) Xu, K.; Zhou, S.; Wu, L. *J. Mater. Sci.* **2009**, *44* (6), 1613–1621.

(24) Reyes-Acosta, M. A.; Torres-Huerta, A. M.; Domínguez-Crespo, M. A.; Flores-Vela, A. I.; Dorantes-Rosales, H. J.; Ramírez-Meneses, E. *J. Alloys Compd.* **2015**, *643*, S150–S158.

(25) Lee, S.; Shin, H.-J.; Yoon, S.-M.; Yi, D. K.; Choi, J.-Y.; Paik, U. *J. Mater. Chem.* **2008**, *18* (15), 1751.

(26) Ha, H.; Kim, S. C.; Ha, K. *Macromol. Res.* **2010**, *18* (7), 674–679.

(27) Mohseni, M.; Bastani, S.; Jannesari, A. *Prog. Org. Coatings* **2014**, *77* (7), 1191–1199.

(28) Sadej, M.; Gojzewski, H.; Andrzejewska, E. *J. Polym. Res.* **2016**, *23* (6), 116.

(29) Ingrosso, C.; Esposito Corcione, C.; Striani, R.; Comparelli, R.; Striccoli, M.; Agostiano, A.; Curri, M. L.; Frigione, M. *ACS Appl. Mater. Interfaces* **2015**, *7* (28), 15494–15505.

(30) Sharif, M.; Pourabbas, B.; Sangermano, M.; Sadeghi Moghadam, F.; Mohammadi, M.; Roppolo, I.; Fazli, A. *Polym. Int.* **2017**, *66* (3), 405–417.

(31) Lee, S.-W.; Park, J.-W.; Park, C.-H.; Kwon, Y.-E.; Kim, H.-J.; Kim, E.-A.; Woo, H.-S.; Schwartz, S.; Rafailovich, M.; Sokolov, J. *Int. J. Adhes. Adhes.* **2013**, *44*, 200–208.

(32) Lee, S.-W.; Park, J.-W.; Kwon, Y.-E.; Kim, S.; Kim, H.-J.; Kim, E.-A.; Woo, H.-S.; Swiderska, J. *Int. J. Adhes. Adhes.* **2012**, *38*, 5–10.

(33) Zhang, Q.; Huang, C.; Wang, H.; Hu, M.; Li, H.; Liu, X. *RSC Adv.* **2016**, *6* (109), 107942–107950.

(34) Bonino, C. A.; Samorezov, J. E.; Jeon, O.; Alsberg, E.; Khan, S. A. *Soft Matter* **2011**, *7*, 11510.

(35) Chiou, B.-S.; Khan, S. A. **1997**, *30* (23), 7322–7328.

(36) Higham, A. K.; Garber, L. A.; Latshaw, D. C.; Hall, C. K.; Pojman, J. A.; Khan, S. A. *Macromolecules* **2014**, *47*, 821–829.

(37) Khan, S. A.; Plitz, I. M.; Frantz, R. A. *Rheol. Acta* **1992**, *31* (2), 151–160.

(38) Lucio, B.; de la Fuente, J. L. *Thermochim. Acta* **2014**, *596*, 6–13.

(39) Jafarifard, S.; Bastani, S.; Soleimani-Gorgani, A.; Sari, M. G. *Prog. Org. Coatings* **2016**, *90*, 399–406.

(40) Bacchi, A.; Pfeifer, C. S. *Dent. Mater.* **2016**, *32* (8), 978–986.

(41) Yang, Y.; Oztekin, A.; Neti, S.; Mohapatra, S. *J. Nanoparticle Res.* **2012**, *14* (5), 852–

861.

(42) Chambon, F.; Winter, H. H. *J. Rheol. (N. Y. N. Y).* **1987**, *31*, 683–697.

(43) Winter, H. H.; Chambon, F. *J. Rheol. (N. Y. N. Y).* **1986**, *30*, 367–382.

(44) Tilly, J. C.; Pervaje, A. K.; Inglefield, D. L.; Santiso, E. E.; Spontak, R. J.; Khan, S. A. *ACS Omega* **2019**, *4* (1), 932–939.

(45) Nguyen, K. D. Q.; Megone, W. V.; Kong, D.; Gautrot, J. E. *Polym. Chem.* **2016**, *7* (33), 5281–5293.

(46) Hassouneh, S. S.; Daugaard, A. E.; Skov, A. L. *Macromol. Mater. Eng.* **2015**, *300* (5), 542–550.

(47) Yu, L.; Skov, A. L. *RSC Adv.* **2017**, *7* (72), 45784–45791.

(48) Goswami, K.; Daugaard, A. E.; Skov, A. L. *RSC Adv.* **2015**, *5* (17), 12792–12799.

(49) Higham, A. K.; Bonino, C. A.; Raghavan, S. R.; Khan, S. A. *Soft Matter* **2014**, *10* (27), 4990–5002.

(50) Sun, G.; Huang, Y.; Li, D.; Chen, E.; Zhong, Y.; Fan, Q.; Shao, J. *Ind. Eng. Chem. Res.* **2019**, *58* (22), 9266–9275.

(51) Lin, T.-S.; Wang, R.; Johnson, J. A.; Olsen, B. D. *Macromolecules* **2018**, *51*, 1224–1231.

(52) Barner-Kowollik, C.; Beuermann, S.; Buback, M.; Castignolles, P.; Charleux, B.; Coote, M. L.; Hutchinson, R. A.; Junkers, T.; Lacík, I.; Russell, G. T.; Stach, M.; van Herk, A. M. *Polym. Chem.* **2014**, *5* (1), 204–212.

(53) Beuermann, S.; Buback, M.; Davis, T. P.; Gilbert, R. G.; Hutchinson, R. A.; Kajiwara, A.; Klumperman, B.; Russell, G. T. *Macromol. Chem. Phys.* **2000**, *201* (12), 1355–1364.

(54) Contreras-Cáceres, R.; Sánchez-Iglesias, A.; Karg, M.; Pastoriza-Santos, I.; Pérez-Juste, J.; Pacifico, J.; Hellweg, T.; Fernández-Barbero, A.; Liz-Marzán, L. M. *Adv. Mater.* **2008**, *20* (9), 1666–1670.

(55) Lemieux, V.; Adams, P. H. H. M.; van Hest, J. C. M. *Chem. Commun.* **2010**, *46* (18), 3071.

# CHAPTER 5: CONCLUSIONS AND FUTURE WORK

In this body of work, we have examined the formation and ultimate film properties of network polymers created through thermally- and UV irradiation-induced crosslinking processes. These types of materials have the potential to find applications in fields such as protective and optical coatings, as well as standalone optical devices. Specifically, we have examined the effects of temperature and polymer backbone composition on the thermal crosslinking of TMCD-based polymers with a polymerized aliphatic isocyanate crosslinking agent from both a chemical and mechanical standpoint. We also studied the ultimate film thermomechanical and free volume properties of these same resin systems after being cured at two industrially relevant temperatures for one hour. Finally, we investigated the UV radiation-induced crosslinking of an unfilled PDMS system, as well as with both reactive and passive nanofillers at different concentrations. The specific conclusions for each chapter of this dissertation, along with recommendations for future work, are given below.

## 5.1. Analysis of Crosslinking Behavior in Model Polyester Polyol-based Systems

The crosslinking behavior of a series of model polyester polyol resins with a trifunctional isocyanate crosslinking agent is examined as a function of reaction temperature and polymer backbone composition up to the sol-gel transition (as defined by the crossover in dynamic moduli). This crosslinking analysis was undertaken from both a mechanical and a chemical perspective. The techniques utilized to study the crosslinking behavior from these two standpoints are dynamic rheology and variable temperature FTIR, respectively. Results from the analysis indicate that increasing temperature decreases the time required to achieve the sol-gel transition for all resin systems examined. It can also be concluded that increasing TMCD content (and by extension, statistical secondary hydroxyl content) not only increases the amount of time

required for modulus crossover, but also increases the critical conversion required to achieve the crossover. The apparent activation energies for gelation (rheology) and apparent kinetic activation energies (VT-FTIR) also increase slightly with increasing secondary hydroxyl content, but mostly remain similar when comparing the two techniques. This suggests that the conversion of the isocyanate group is directly related to the growing microstructure of the systems.

As statistical secondary hydroxyl content is increased above 25%, the critical extent of conversion also begins to deviate significantly from classical theories. A conceptual model is proposed which agrees with previous works in the literature and illustrates a phenomenon known as gel point suppression. In this model localized crosslinking occurs, creating network fluctuations. The formation of topological defects is prominent in the form of loops which do not contribute to the overall elasticity of the network, which agrees with previously reported results.

An interesting future direction for this work could be to incorporate solvent evaporation into the mechanical and chemical characterization of the systems during cure. During the curing process of protective coatings, solvent evaporation plays a key role in the evolution of the mechanical and chemical characteristics of the system. In the system evaluated herein, solvent was retained within the system to gain a fundamental understanding of polymer crosslinking, but a comprehensive study of the mechanical property evolution in a scenario which is more representative of those encountered in product application might further enhance understanding of the relationship between polymer backbone architecture, cure temperature and mechanically observed curing.

### 5.2. Role of TMCD Content and Crosslinking Conditions in the Final Film Thermomechanical and Free Volume Properties of Model Coating Systems

The ultimate thermomechanical and free volume properties of 5 polymer resin systems containing differing levels of TMCD in their backbone are examined to elucidate the effect of TMCD content and cure condition on the ultimate film properties. Regardless of TMCD content, increasing the cure temperature of the films cured for 1h increased the glass transition temperature (as measured by DSC for HB and LB films, and DMTA for HB films). For all HB films, DMTA results indicate that below the films' respective glass transition temperature, there is no significant difference in the mechanical properties. For LB films, the observed surface modulus increases monotonically with increasing TMCD content, however the HB films show a very slight negative correlation in observed surface modulus as a function of TMCD content. This is attributed to an observed phenomenon referred to as pile-up, wherein the surface modulus in artificially increased due to limitations in the analysis of nanoindentation data. Finally, the average free volume pore size is shown to increase with increasing TMCD content, and for all levels of TMCD content the average hole size is similar between the LB and HB samples.

One interesting route for a future study is to thoroughly examine the effect of pile-up for films containing varied levels of TMCD and cured at both HB and LB conditions, as well as perform scratch testing on the various films in order to gain a more thorough understanding of how the surface responds to stresses. Another potential path for future study is a more in-depth examination of the free volume properties at different temperatures. One final recommendation is to examine the barrier properties of these materials, not only to gases but also to water. These experiments could be performed within a permeation cell and would give insight into how the free volume within the samples affects transport of penetrant molecules through the films.

## 5.3. Rheology and Ultimate Films Properties of UV-crosslinkable Polymer Nanocomposites Based on Poly(dimethyl siloxane) and Zirconia Nanoparticles: Role of Reactive vs. Passive Fillers

The UV radiation-induced crosslinking behavior of a linear short-chain PDMS with UV-reactive end groups in solvent, both with with and without various loadings of commercially available reactive and passive zirconia nanofillers, is examined. By maintaining a constant solids content of 50 wt% for the filled systems and varying it slightly for some of the unfilled systems, the effect of zirconia filler loading, type and irradiation strength could be analyzed. For all systems examined, a higher UV intensity decreased the time required to achieve a crossover in dynamic moduli, but also increased the magnitude of the modulus crossover. As zirconia content (for filled systems) or PDMS content (for unfilled systems) is varied, a power law relationship between the time required to achieve a modulus crossover and UV intensity is observed. For the filled systems at all loadings of zirconia, the power law scaling exponent is very similar for both the reactive and passive fillers. This suggests a similar mechanical mechanism to achieve a modulus crossover. The ultimate network strength, as measured by dynamic rheology frequency sweeps, decreases with increasing filler loading for both reactive and passive zirconia.

The ultimate film optical properties are characterized with UV-Vis spectroscopy. From swelling/solubility measurements on films cured at 1 $mW/cm^2$ for 30 minutes, it is found that the films containing reactive zirconia are able to retain above 90 wt% of their zirconia for up to 85 wt% zirconia loading, whereas the passive filled systems lose a substantial amount of filler above 50 wt% on solids. The turbidity, as measured by absorbance in UV-Vis, increases in a semi-logarithmic fashion for the passive zirconia up to 75 wt% on solids loading, whereas the reactive zirconia shows significantly less turbidity than its passive counterpart above 25 wt%.

Cryo-fractured SEM micrographs show significant morphological changes between reactive and nonreactive zirconia-filled systems at 75 wt% solids loading. These findings suggest that reactive zirconia could prove to be a good filler for UV-curable optical applications.

This work provides the potential building blocks for a much larger study on filled PDMS matrices cured under UV irradiation. One promising future direction is to investigate the specific type of UV-reactive end group, of the PDMS, such as methacrylate vs. methacryloxypropyl, as well as the molecular weight of the PDMS chains. By changing the end capping it may be possible to better incorporate the reactive zirconia into the polymeric matrix, and increasing the molecular weight of the PDMS might improve the elastomeric nature of the nanocomposite. It might also be interesting to examine the ultimate film mechanical and optical properties after the solvent has been removed.